UNIVERSITY OF THE WITWATERSRAND

Exploring the 95 GeV Excess with Extended Scalar Models

Author:
ANZA-TSHILIDZI
MULAUDZI

Supervisor(s):
Prof. BRUCE MELLADO
Dr. MUKESH KUMAR

A thesis submitted in fulfillment of the requirements
for the degree of Master of Science
in the School of Physics
for the Institute for Collider Particle Physics

Declaration of Authorship

I, ANZA-TSHILIDZI MULAUDZI, certify that the work presented in this thesis is my own. It is being submitted to University of the Witwatersrand for the degree of Master of Science. It has not been turned in for a test or degree at any other academic institution.

List of Publications and talks

Journals:

1. K. Mosala, **A. T. Mulaudzi**, T. Mathaha, P. Sharma, M. Kumar, B. Mellado and M. Ruan, The Observation of a 95 GeV Scalar at Future Electron-Positron Colliders, arXiv:2407.16806 [hep-ph].

2. A. Ahriche, M. L. Bellilet, M. O. Khojali, M. Kumar, **A. T. Mulaudzi**, The scale invariant scotogenic model: CDF-II W-boson mass and the 95 GeV excesses, Phys. Rev. D **110** (2024) no.1, 015025, doi:10.1103/PhysRevD.110.015025, arXiv:2311.08297 [hep-ph].

3. S. Ashanujjaman, S. Banik, G. Coloretti, A. Crivellin, B. Mellado, **A. T. Mulaudzi**, $SU(2)_L$ triplet scalar as the origin of the 95 GeV excess?, PSI-PR-23-20, ZU-TH 28/23, ICPP-71, Phys. Rev. D 108 (2023) 09, doi:10.1103/PhysRev D.108.L091704.

Proceedings:

1. **A. T. Mulaudzi**, M. Kumar, B. Mellado, A.K. Swain, Studying the Production of a Singlet Scalar at future e^+e^- Colliders with Deep Neural Networks, in The Proceedings of SAIP2022, the 66th Annual Conference of the South African Institute of Physics, edited by Prof. Aletta Prinsloo, (UJ), pp. 168-174. ISBN: 978-0-6397-4426-1, pp 168-174. Available online at https://events.saip.org.za.

2. **A. T. Mulaudzi**, M. Kumar, B. Mellado, A.K. Swain, Studying the Production of a Singlet Scalar at future e^+e^- Colliders with Deep Neural Networks, at The First Pan-African Astro-Particle and Collider Physics Workshop (PAC2022) (submitted).

Abstract

This thesis focuses on three interconnected studies investigating the presence of an additional scalar particle, S, of mass around $m_S \approx 95\,\text{GeV}$. In the initial study, we explore the notion that an $SU(2)_L$ triplet scalar, characterised by a hypercharge $Y = 0$, could be the origin of the observed 95 GeV di-photon ($\gamma\gamma$) excesses seen at ATLAS and CMS. By thoroughly examining its properties, particularly the neutral component, and considering a small mixing angle with the Standard Model Higgs boson, we uncover that this scalar naturally exhibits a substantial branching ratio to $\gamma\gamma$. Additionally, we find that its Drell-Yan production via $pp \to W^* \to HH^\pm$ adequately accounts for the observed excess. The second study examines how recent measurements of the W bosons's mass by experiments such as ATLAS and CDF affect the theoretical predictions of the Two Higgs Doublet Model augmented with a Singlet Scalar (2HDM+S) model. It addresses how this model's parameter space is further constrained by the inclusion of vector-like leptons, focusing on their impact on the muon $g-2$ measurements. The third study involves exploring the potential discovery of the aforementioned scalar at future electron-positron colliders. Employing several methodologies, including the recoil mass method in e^+e^- collisions ($e^+e^- \to ZS$, where $Z \to \mu^+\mu^-$ and $S \to b\bar{b}$), we leverage a Deep Neural Network to refine the differentiation between the Standard Model background and the targeted signal. The outcomes not only reinforce the potential for detecting the proposed scalar, but also enhance the scientific argument for the establishment of future electron-positron colliders like CEPC, FCC-*ee* or ILC. Together, these studies contribute valuable insights into the evolving landscape of particle physics.

Acknowledgements

I am profoundly grateful to my two supervisors, Professor Bruce Mellado and Dr. Mukesh Kumar, for their exceptional guidance, unwavering support, and invaluable mentorship throughout my Master's degree. Their expertise has been instrumental in shaping the trajectory of my academic pursuits. A heartfelt thank you goes to the collaborators who worked alongside me on our projects. Your dedication and teamwork have enriched my learning experience, and I am grateful for the shared insights and collective effort. I extend my sincere appreciation to the SA-CERN programme for their generous support, which has been instrumental in making my Master's degree journey possible. The opportunities and resources provided have been crucial to my academic and professional development. In memory of my late father and grandmother, who sadly passed away during my Master's degree, I would like to dedicate this acknowledgement. Their wisdom, guidance, and unwavering belief in my abilities continue to inspire me. Their memory will forever be a guiding light in my academic and personal endeavours. Lastly, I want to express my gratitude to my friends and family for their unyielding support, encouragement, and understanding throughout this journey. Your presence and encouragement have been a source of strength, and I am truly fortunate to have you by my side. Thank you, from the depths of my heart.

Contents

List of Figures

List of Tables

List of Abbreviations

ALFA **A**bsolute **L**uminosity **F**or **A**TLAS
ATLAS **A** **T**oroidal **LHC** Apparatu**S**
BSM **B**eyond the **S**tandard **M**odel
CDF **C**ollider **D**etector at **F**ermilab
CEPC **C**ircular **E**lectron **P**ositron **C**ollider
CLIC **C**ompact **L**inear **C**ollider
CERN European Organization for Nuclear Research
CMS **C**ompact **M**uon **S**olenoid
FCC **F**uture **C**ircular **C**ollider
HL-LHC **H**igh **L**uminosity-**LHC**
HTM **H**iggs **T**riplet **M**odel
ICPP **I**nstitute for **C**ollider **P**article **P**hysics
LEP **L**arge **E**lectron **P**ositron collider
LHC **L**arge **H**adron Collider
LHCb **L**arge **H**adron Collider beauty
LINAC 2 **Lin**ear **AC**celerator 2
LO **L**eading **O**rder
NLO **N**ext to **L**eading **O**rder
QCD **Q**uantum **C**hromo **D**ynamics
QED **Q**uantum **E**lectro **D**ynamics
SM **S**tandard **M**odel
2HDM **T**wo **H**iggs **D**oublet **M**odel

Chapter 1

Introduction

Our universe consists of baryonic matter and an invisible component known as dark matter. Photons, neutrons, electrons, and other building blocks in everyday objects are examples of baryonic matter. Dark matter, on the other hand, remains mysterious and is yet to be directly observed. To understand the universe's fundamental building blocks and how they interact, physicists developed the Standard Model (SM). This theoretical framework serves as a comprehensive explanation for elementary particles and the forces that govern their interactions.

The constituents of the SM include Leptons, which are fundamental particles like electrons, muons, and taus, and quarks, which are the building blocks of protons, neutrons, and other hadrons. Finally, force carriers mediate the fundamental forces, including photons (electromagnetism), W and Z bosons (weak nuclear force), and gluons (strong nuclear force) [1]. For several decades, scientists have constructed increasingly powerful particle accelerators to test the predictions of the SM with exceptional accuracy. These experiments have repeatedly confirmed the strength and viability of the model. The discovery of the Higgs boson by the CMS [2, 3] and ATLAS [4] collaborations at CERN's Large Hadron Collider (LHC) marked a significant milestone in this ongoing quest. This elusive particle, independently predicted by Peter Higgs [5] and Robert Brout and François Englert [6], played a crucial role in explaining how elementary particles acquire mass.

While the SM has successfully described known particles and their interactions, some mysteries remain. The model needs help explaining certain aspects of the universe, such as the hierarchy problem, dark matter and quantum gravity. The hierarchy problem discusses why some particles have vastly different masses from others [7]. The surprising part is that the Higgs field, according to the theory itself, should create a very "sticky" environment (large mass for the field), yet some particles (like the Higgs boson itself) experience it as much less sticky (relatively small mass). This discrepancy between the predicted "stickiness" and the observed masses is the crux of the hierarchy problem. The SM does not encompass dark matter, which is thought to constitute a significant portion of the universe's mass [8]. The description of quantum gravity remains elusive within the framework of the SM [9]. These limitations have fueled extensive research into physics beyond the SM (BSM) [10]. High-energy collider experiments [11], neutrino physics investigations [12], and astronomical observations [13] are vital in this ongoing pursuit. Collectively, these efforts aim to address the shortcomings of the SM and provide a more complete picture of the universe's underlying principles.

This intriguing situation presents two possibilities: the SM needs to be expanded to include an as-yet-unknown realm of new physics valid within a particular energy

frontier, and a more comprehensive theory governs nature beyond that boundary. Particle colliders play a pivotal role in our quest to unravel these mysteries by enabling us to explore elementary particles [14] at previously uncharted energies. These colliders generate vast datasets, harnessing the potential to harbour crucial insights into new physics phenomena that lie beyond the scope of the SM. In this way, they offer us a unique window of opportunity to better understand the universe's inner workings.

The LHC's utilisation of superconducting magnets to rotate two counter-rotating bunches of protons results in four collisions taking place at the ring's location. To measure and identify particles resulting from the collisions, many particle detectors are strategically positioned around these collision points: these include the Compact Muon Solenoid (CMS) [2, 3] and the A Toroidal LHC Apparatus (ATLAS) [4]. When two particles collide with enough energy, a heavier particle can be created. One method for studying some of the heaviest and most novel particles in the SM and possibly beyond the SM (BSM) particles is to use the LHC, the world's highest-intensity proton collider. The goal of ATLAS and CMS collaborations is to shed light on the nature of the cosmos and find a new particle that the SM does not predict. There are increasing indications of new physics. An increasing number of excesses at specific mass ranges have been seen when examining the ATLAS and CMS databases, which is encouraging for the BSM particles.

Conversely, existing and upcoming electron-positron (e^+e^-) colliders present an opportunity for investigating BSM particles, such as extra scalar bosons. Accelerators such as the Large Electron-Positron Collider (LEP) [15] and the Circular Electron-Positron Collider (CEPC) [16, 17] (which is a future project) offer key advantages when searching for BSM particles. They provide a clean experimental environment in the sense that the collision between electrons and positrons produces relatively simple final states. This simplicity allows for precise measurements and a better understanding of the underlying physics. The e^+e^- colliders enable precision measurements of fundamental parameters in the SM, and these include measurements of the masses, lifetimes, and couplings of particles like the Brout-Englert-Higgs boson, W and Z bosons, and the top quark. The fact that e^+e^- colliders are especially useful for researching the characteristics of the Higgs boson gives them an advantage over proton-proton colliders. A clean experimental environment allows for exact measurements of the Higgs boson's interactions with other particles, revealing its properties in greater detail. Furthermore, these colliders have adjustable collision energies, enabling experimentation at various energy scales and, consequently, the study of weak interactions at these accelerators. These investigations advance our knowledge of electroweak symmetry breaking [18].

In an attempt to shed light on new and mysterious phenomena discovered at particle colliders, this thesis explores the exciting world of particle physics beyond the SM [10], as more and more searches employ the BSM models. Even though the SM has been incredibly effective in explaining elementary particle interactions, fascinating oddities continue to entice us to investigate new areas. BSM models are proposed to account for scientific anomalies not explained by SM, such as Dark matter candidates, which can be explained by Supersymmetry [19] and Weakly Interacting Massive Particles (WIMPs) [20], which is incorporated into the SM's extension, the Minimal Supersymmetric Standard Model (MSSM) [21], Grand Unified Theories

(GUTs) [22], and Axions [23].

1.0.1

The phenomenological investigation of additional scalar bosons seen in experiments is the focus of this thesis. A brief review of the SM of particles is given in section 1.1, which also presents a BSM framework, the Two Higgs Doublet with an Additional Scalar model (2HDM+S). These hypotheses account for the experimentally observed 95 GeV excess. The Higgs Triplet Model with hypercharge of 0 ($Y = 0$) and its functions in explaining the 95 GeV di-photon excess is introduced in chapter 2. Chapter 3 discusses the muon g-2 and W boson mass observations in the context of the 2HDM+S parameter space, including the contributions from Vector-Like leptons [24]. The possibility of finding the 95 GeV scalar boson at future e^+e^- colliders is discussed in Chapter 4. Chapter 5 serves as the thesis's conclusion, highlighting the application of complex phenomenological analyses and sophisticated theoretical frameworks to unlock nature's mysteries and expand our knowledge of the universe's basic components.

1.1 The Standard Model of Particle Physics

The Standard Model of particle physics provides an extensive explanation of the behaviours of known particles. Developed in the 1970s, this model has consistently proven effective in accurately predicting phenomena, demonstrating resilience through rigorous high-precision testing [5, 6, 25–27]. This model is framed within quantum field theory, primarily through constructing a Lagrangian. The development of the theory hinges on establishing a set of symmetries, leading to the creation of a detailed, renormalisable Lagrangian, which is in accordance with the symmetries and the particle configuration inherent in the model.

The SM exhibits inherent symmetries independent of the reference frame chosen for observation. These encompass spacetime symmetries, which consist of translational symmetry (unchanged under spatial translations), rotational symmetry (unchanged under rotations) and Lorentz boosts (unchanged under changes in reference frame velocity). Gauge symmetries are described by the group structure $SU(3)_C \times SU(2)_L \times U(1)_Y$ [28]. In particle physics, C, L and, Y correspond to colour-charge, which is responsible for the strong force acting on quarks [29], left-handed helicity, which describes the handedness of fundamental particles [30] and hypercharge (Y), which is a combination of electric charge and baryon number. The charm (C) is a quantum number associated with the weak interaction and refers to the "charm" of a particle. The lepton number (L) is a quantum number that is associated with the weak interaction and lepton number conservation. Each symmetry within this group is associated with a fundamental force due to its invariance under gauge transformations. A key feature of the SM is the unified electroweak theory. This theory arises from the requirement of gauge invariance under the combined $SU(2)_L \times U(1)_Y$ gauge. It unifies the weak force and electromagnetism, showcasing an elegant aspect of the SM.

The electroweak theory achieves gauge invariance through the $SU(2)_L \times U(1)_Y$ gauge group, unifying the weak and electromagnetic forces. The abelian $U(1)$ group,

represented by hypercharge (Y), gives rise to a single gauge field, B_μ. The non-abelian $SU(2)_Y$ group defines the theory's chirality structure. Chiral projection operators are used to describe these chiral properties[1]. Chirality refers to the handedness of fundamental particles, a key concept in the electroweak theory. The chiral projections are defined as:

$$P_L = \frac{1}{2}(1-\gamma^5),\ P_R = \frac{1}{2}(1+\gamma^5), \tag{1.1}$$

where the four-component Dirac spinors can be projected onto the chiral states that are left- and right-handed. The electroweak theory interacts differently with left-handed and right-handed particles, a phenomenon known as parity violation. The Dirac spinors, which describe fundamental particles, can be separated into left-handed (LH) and right-handed (RH) states using chiral projection operators. The gauge fields in the electroweak theory interact only with doublets of LH fermion fields. For example, the electron and its corresponding electron neutrino (both left-handed) form a doublet.

Similarly, left-handed up-and-down quarks form another doublet. On the other hand, the right-handed fermion fields don't participate in these interactions and remain singlets under the $SU(2)_L$ symmetry. The $SU(2)_L$ group, with its three generators often represented by Pauli matrices, leads to the existence of three gauge boson fields, denoted as W^a_μ.

The electroweak theory describes the force carriers, or gauge bosons, through the $SU(2)_L \times U(1)_Y$ gauge group. However, the physical observable bosons are the photon (A_μ), the neutral Z boson (Z^0_μ), and the charged W bosons ($W^\pm_\mu$). These physical bosons are related to the initial four gauge fields from the symmetry group via the electroweak symmetry breaking mechanism and characterised by a parameter known as the Weinberg angle (θ_W). The Weinberg angle, also referred to as the weak mixing angle, is defined by the ratio of two coupling constants (g_1 and g_2, which are related to the $SU(2)$ and $U(1)$ gauge groups, respectively) as $\tan\theta_W = g_1/g_2$ [31]. The gauge fields are described by the following equations:

$$A_\mu = \sin\theta_W W^3_\mu + \cos\theta_W B_\mu, \tag{1.2}$$

$$Z^0_\mu = \cos\theta_W W^3_\mu - \sin\theta_W B_\mu, \tag{1.3}$$

$$W^\pm_\mu = \frac{1}{\sqrt{2}}(W^1_\mu \mp i W^2_\mu). \tag{1.4}$$

This theory incorporates interactions between gauge bosons themselves, fermions (matter particles) and charged W and Z bosons (charged and neutral current interactions), and charged fermions and photon field (electromagnetic interactions).

In the Standard Model (SM), explicit mass terms for bosons and fermions are forbidden by gauge invariance. This raises the question of how particles acquire mass while maintaining gauge symmetry. The solution lies in the mechanism of Electroweak Symmetry Breaking (EWSB), achieved by introducing a complex scalar field to the theory. EWSB occurs when the scalar field, called the Higgs field, acquires a nonzero vacuum expectation value (vev), spontaneously breaking the electroweak

[1] In this notation one defines $\gamma^5 = i\gamma^0\gamma^1\gamma^2\gamma^3$

symmetry. This process generates mass terms for particles while preserving gauge invariance for the remaining forces.

This idea, developed independently by Peter Higgs [5], Robert Brout, and Francois Englert [6] in 1964, is central to explaining how particles gain mass. The scalar field, denoted as ϕ, is charged under the $U(1)_Y$ gauge group and represented as a doublet under the $SU(2)_L$ gauge group. Through EWSB, the SM maintains gauge invariance while allowing particles to acquire mass, solving one of the fundamental challenges in particle physics.

The scalar field, ϕ, interacts with the $U(1)_Y$ and $SU(2)_L$ gauge groups. The Lagrangian for this field, $\mathcal{L}_\phi$, is described by the following equation:

$$\mathcal{L}_\phi = (\partial^\mu \phi)^\dagger (\partial_\mu \phi) - V(\phi), \tag{1.5}$$

where

$$V(\phi) = -\frac{1}{2}\mu^2 \phi^\dagger \phi + \frac{1}{4}\lambda(\phi^\dagger \phi)^2. \tag{1.6}$$

where the first term in the potential is the mass term, μ is a parameter with dimensions of mass squared. The negative sign in front of μ^2 is crucial because it makes the potential unstable at the origin ($\phi = 0$), leading to spontaneous symmetry breaking. If $\mu^2 > 0$, the potential has a minimum away from zero, causing the Higgs field to acquire a non-zero vev, which breaks the electroweak symmetry. The second term is the self-interaction term, where λ is a dimensionless parameter determining the strength of the scalar field's self-interaction. This term ensures that the potential is bounded from below, preventing the Higgs field from running off to infinity and making the potential stable at large values of ϕ. The minimum of the potential is at a non-zero value of ϕ, driving spontaneous symmetry breaking.

The key to EWSB lies in the potential energy term ($V(\phi)$) of the scalar field Lagrangian. This term has a specific structure that leads to a non-zero vacuum expectation value (vev) for ϕ, which has been experimentally measured. By expanding the field around its minimum value, we can express ϕ in terms of its components. This expansion reveals four degrees of freedom associated with the field. EWSB breaks the initial $SU(2)_L \times U(1)_Y$ gauge symmetry down to electromagnetic (EM) $U(1)_{EM}$ symmetry. This symmetry violation, however, is compatible with the principle of gauge invariance through the introduction of covariant derivatives. As a consequence of EWSB and non-zero vev, the SM bosons ($W^\pm$ and Z^0) acquire mass. The relationship between their masses and the coupling constants of the theory is described by the following equation:

$$\phi = -\frac{1}{\sqrt{2}} \begin{pmatrix} 0 \\ v \end{pmatrix} + \begin{pmatrix} \phi^1 + i\phi^2 \\ h^0 + ia^0 \end{pmatrix}. \tag{1.7}$$

Three of the initial four scalar field components transform into the longitudinal components of the massive W and Z bosons. These components, known as Goldstone bosons, are not directly observable as physical particles due to the Higgs mechanism in the SM since they are massless. The Higgs mechanism removes the Goldstone bosons associated with the broken symmetry, and these excluded Goldstone bosons become part of the longitudinal components of the massive W and Z bosons. The remaining degree of freedom corresponds to the physical Higgs boson (h^0). The

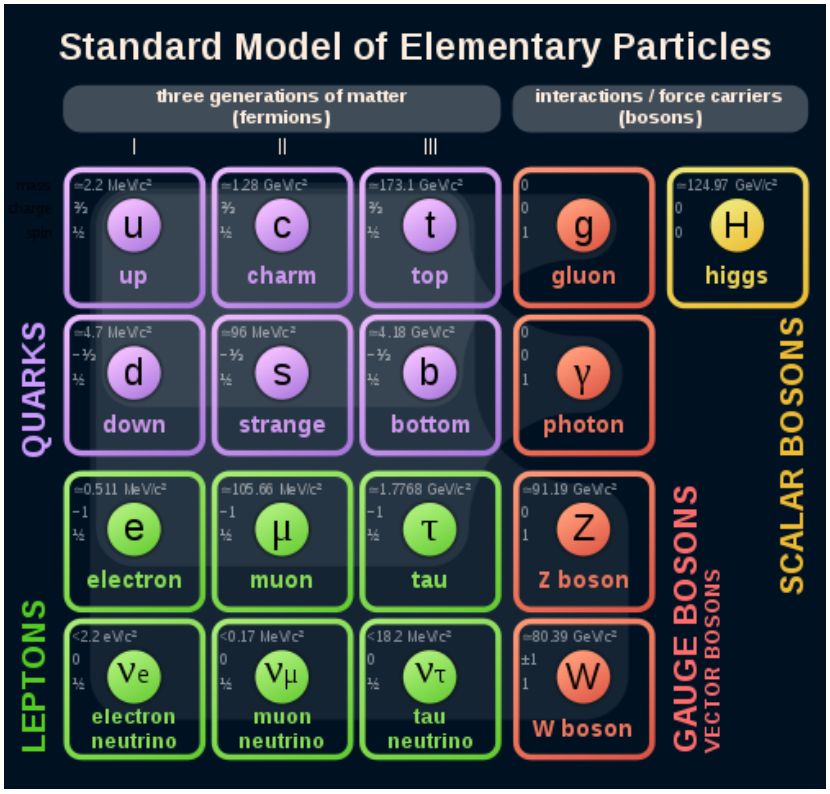

FIGURE 1.1: Representation of the Standard Model particles [33].

unbroken $U(1)_{EM}$ symmetry ensures that the photon (γ) remains massless. Additionally, since the scalar field doesn't interact with the strong force mediated by gluons, they, too, remain massless. The final step in generating fermion masses involves Yukawa interactions. These interactions are introduced between fermions and the scalar field in the Lagrangian:

$$\mathcal{L}_{Yuk} = \lambda_d^{ij} \bar{q}_L^{-i} \phi d_R^j - \lambda_u^{ij} \bar{q}_L^{-i} \tilde{\phi} u_R^j - \lambda_\ell^{ij} \bar{\ell}_L^{-i} \phi e_R^j. \tag{1.8}$$

The coupling strengths associated with these interactions determine the masses of the fermions. In summary, the SM incorporates two fundamental building blocks: fermions and bosons [32]. Fermions are matter particles with half-integer spin, while bosons (including the spin-0 Higgs boson) are force carriers with integer spin. The Higgs mechanism, arising from EWSB, plays a crucial role in explaining how these particles acquire mass within the framework of the SM.

This segment delves into the foundational components of the SM, encompassing leptons, quarks, gauge bosons, and the fundamental interactions in which they engage. Despite the considerable success of the SM, it is widely recognised as incomplete. This serves as a catalyst for continuous investigations into physics beyond the SM (BSM), aiming to elucidate phenomena that remain unexplained within the existing model.

Fermions					
Leptons			Quarks		
Particle	Charge	Mass [GeV/c^2]	Particle	Charge	Mass [GeV/c^2]
tau	-1	1.78	top	$+2/3$	173 ± 0.30
τ neutrino	0	$< 10^{-9}$	bottom	$-1/3$	4.2 ± 0.03
muon	-1	0.106	charm	$+2/3$	1.2 ± 0.025
μ neutrino	0	$< 10^{-9}$	strange	$-1/3$	0.095 ± 0.0005
electron	-1	5.11×10^{-4}	up	$+2/3$	$2 \times 10^{-3} \pm 0.00026$
e neutrino	0	$< 10^{-9}$	down	$-1/3$	$5 \times 10^{-3} \pm 0.00056$

TABLE 1.1: SM Fermion Overview: Leptons and Quarks (charges in q_e units) with approximate masses from Ref. [35]).

1.1.1 Fermions

Within the structure of the SM, there exist three varieties of electrically charged leptons: the muon (μ), the electron (e), and the tau (τ) [34]. These particles are ordered by ascending mass and are matched to their respective mass eigenstates. Each type of charged lepton bears a negative electromagnetic charge, and there is a corresponding antiparticle for each lepton with a positive charge. These charged leptons are known to engage in interactions governed by electromagnetic and weak forces [35]. Some leptons, termed neutrinos, do not carry an electric charge. Distinct from their charged counterparts, neutrinos have neutral charges, and their flavour eigenstates are not aligned straightforwardly with their mass eigenstates [36]. This discrepancy leads to the phenomenon where neutrinos oscillate among different flavour states during their journey through the cosmos. Neutrinos are elusive to detection because they interact almost exclusively via the weak force.

Like leptons, the SM also categorises quarks into three families, each partaking in strong and weak force interactions and possessing an electric charge. Quarks of the *up-type* hold a charge that is $+2/3$ of the elementary charge (q_e), whereas *down-type* quarks have a charge equal to $-1/3$ of q_e [37]. There are six distinct flavours of quarks: up, down, charm, strange, top, and bottom. Each quark is also associated with a colour charge, labelled as either blue, green, or red, and their corresponding antiparticles carry complementary anti-colours. Figure 1.1 shows an overview of the SM particles and their respective properties.

Observations in nature do not reveal isolated quarks, a phenomenon ascribed to colour confinement; quarks are perpetually found in groups. Consequently, stable particles within the Standard Model exhibit no net colour charge. Composite particles of quarks that result in a colour-neutral state are termed hadrons. Those hadronic states composed of a quark and an antipark of contrasting colour charges are identified as mesons, while baryons are made up of three quarks, each a different colour, culminating in a neutral colour combination. A detailed enumeration of the fermions in the Standard Model, including their respective electric charges and masses, can be found in Table 1.1 provided in the subsequent section.

A fascinating aspect of the SM is the concept of antiparticles, which posits that for every SM fermion, there exists an antiparticle that mirrors all of its characteristics but carries an opposite electric charge [38]. Yet, the nature of neutrinos remains an

enigma. The debate revolves around whether neutrinos are similar to quarks and charged leptons, classified as Dirac fermions, or whether they are Majorana fermions, distinct in that they would be identical to their own antiparticles. This subject remains an area of active research and discussion (for further details, see ref. [39]). The idea of antiparticles has its roots in the Dirac equation, a pivotal element in particle physics that maintains compatibility with the principles of Lorentz invariance:

$$(i\gamma^\mu \partial_\mu - m)\psi(x) = 0. \tag{1.9}$$

Within this framework, the field corresponding to Dirac fermions is symbolised by $\psi(x)$, while the collection of gamma matrices, represented by γ^μ where μ varies from 0 to 3, embodies the Lorentz algebra. The term ∂_μ represents the spacetime derivatives, including temporal and spatial components. Those interested in a deeper understanding of how particle fields are described within quantum field theory should refer to subsection 1.1.2. The gamma matrices are structured as 4×4 entities to ensure the equation upholds Lorentz covariance. The field $\psi(x)$ is conceptualised as a four-component spinor that characterises spin-1/2 particles, with two components depicting positive energy states and two for negative energy states, which correlate to the particles and their corresponding antiparticles, respectively.

Initially, the negative energy solutions from the Dirac equation were considered non-physical. However, their true physical interpretation was eventually realised within quantum field theory, where they are understood to denote antiparticles. The Dirac equation is a relativistic wave equation that incorporates special relativity into quantum mechanics. In quantum field theory, we introduce the concept of the Dirac sea which is a filled state of negative energy electrons that permeates all of spacetime and by the Puali exclusion principle, the negative energy states will be already filled. Therefore, when we observe an electron in a positive energy state, it's not a particle created from nothing. Instead, it's a vacancy, or "hole", in the filled Dirac sea. This hole behaves like a positively charged particle with the same properties as an electron (except for charge) and is called a positron. The historical detection of the positron in 1932 [40] marked the first identification of an antiparticle. It was distinguished by its unique path in a bubble chamber that curved in the opposite direction to that of an electron under a magnetic field, signifying a opposite electric charge. Present-day particle accelerators routinely generate antiparticles, and advanced experiments are dedicated to examining the attributes of antimatter, probing for subtle discrepancies in the behaviour of antimatter relative to its matter counterparts.

1.1.2 Gauge Bosons

The SM categorises the fundamental particles that make up our universe and describes the forces governing their interactions. These forces arise from the requirement of consistency with various symmetries within the SM Lagrangian. While observed as distinct, the electromagnetic and weak forces stem from a unified electroweak force. The process of EWSB separates this unified force into the familiar electromagnetism and weak interaction. Mediated by the massless photon, this force interacts with electrically charged particles and is well-described by Quantum Electrodynamics (QED) due to its long-range nature. Carried by the gauge bosons (Z and W), the weak force acts on all fermions (fundamental particles with half-integer spin).

The Z boson interacts with both left-handed and right-handed fermions, while the W boson interacts specifically with left-handed fermions. Notably, the W boson has an electric charge, allowing it to interact with photons. The masses of these bosons have been experimentally determined: 80.357 GeV for the W and 91.188 GeV for the Z boson [41].

The strong force responsible for the interactions between quarks is governed by Quantum Chromodynamics (QCD). This force is mediated by gluons (g), unique particles that carry colour charge. Unlike electric charge, which comes in positive and negative, colour charge comes in three types (red, green, blue) and their anti-colour counterparts. This combination leads to eight possible gluon configurations. A crucial feature of the strong force is its dependence on distance. Unlike electromagnetism, a force known as confinement explains why quarks are never found isolated but rather bound together in composite particles like protons and neutrons. The strength of the strong force is described by the coupling constant, α_s, which increases with decreasing energy according to the equation:

$$\alpha_s(\mu) = \frac{12\pi}{(32 - 2n_f)ln(\frac{\mu^2}{\Lambda^2_{QCD}})}, \tag{1.10}$$

where n_f is number of active quarks at the scale μ, and Λ^2_{QCD} is experimentally determined cutoff scale (usually ≈ 0.2 GeV). The number of active quarks determines the strong coupling at a given scale, denoted by n_f, and the experimentally determined cutoff scale, Λ^2_{QCD}, usually around 0.2 GeV. This coupling arises from two features of the strong force: colour confinement and asymptotic freedom. Stable particles must have a neutral colour charge in colour confinement because the coupling constant increases with distance. For example, consider a quark-antiquark pair in a meson. As the distance between the two quarks increases, more energy is required to continue the separation. Eventually, producing a second quark-antiquark pair becomes more energetically favourable, resulting in two neutral-charged hadrons. In asymptotic freedom, the strength of the coupling constant decreases at minimal distances. Quarks within hadrons reach a state where they do not experience any resistance from the strong force, allowing them to move freely. Table 1.2 provides an overview of the forces, their associated bosons, and their respective characteristics. It's important to note that the interaction of a particle with a particular force depends on the values of specific charges or quantum numbers, which vary among different particle types within the Standard Model.

The coupling constant becomes small at high energies, allowing QCD predictions to be made through perturbation theory. Conversely, processes become non-perturbative when the coupling constant is large. The energy region that separates these two is known as the Λ_{QCD}. When determining a cross-section for an LHC process, we divide the calculation into perturbative and non-perturbative processes. For instance, QCD can be used to describe the behaviour of high-energy quarks and gluons. However, the process of quarks and gluons forming colourless composite particles, known as hadronisation, is non-perturbative. During high-energy collisions at the LHC, quarks and gluons are produced, radiating coloured particles through a phenomenon known as fragmentation or parton showering. This process

Bosons			
Force	Particle	Charge	Mass [GeV/c^2]
Strong	gluons (g)	0	0
Electromagnetic	photon (γ)	0	0
Weak	W boson ($W^{\pm}$)	±1	80.357$\pm$0.012
Weak	Z boson (Z)	0	91.188$\pm$0.0021
Gravitational*	graviton?	?	?

TABLE 1.2: The Standard Model describes subatomic forces and predicts particle masses [35], but excludes gravity$*$, explained by general relativity.

continues until energies reach approximately 1 GeV, and the resulting spray of particles produces colourless composite particles known as jets. Instead of detecting the constituents (quarks and gluons), the ATLAS detector detects these jets.

1.1.3 Brout-Englert-Higgs Mechanism

The Higgs mechanism explains how particles acquire mass through their interaction with a field called the Higgs field [5, 6]. Initially, in the very hot early universe, the Higgs field is symmetric, and particles are massless. As the universe cools and undergoes a phase transition, the Higgs field adopts a specific non-symmetrical configuration, breaking the electroweak symmetry. This non-symmetrical state, described mathematically as a doublet in SU_L isospin symmetry, can be pictured as the Higgs field acquiring a non-zero vev. Here's the equation representing the Higgs field doublet:

$$\phi = \frac{1}{\sqrt{2}} \begin{pmatrix} \phi^+ \\ \phi^0 \end{pmatrix}_L . \tag{1.11}$$

The Lagrangian of the SM before electroweak symmetry breaking is the sum of two terms: the Lagrangian for leptons (fundamental particles like electrons and neutrinos) and the Lagrangian for gauge bosons (force carrier particles). After the EWSB, an additional term is added to the Lagrangian specifically for the Higgs field:

$$\mathcal{L}_{Higgs} = (D_\mu \phi)^\dagger (D^\mu \phi) - \mu^2 (\phi^\dagger \phi) + \lambda (\phi^\dagger \phi)^2, \tag{1.12}$$

where $D_\mu = \partial_\mu - (ig/2) W_\mu^a \sigma^a - (ig'/2) B_\mu Y$. The term D_μ represents a covariant derivative. This mathematical tool ensures that under a gauge transformation, the result maintains the gauge symmetry when you take a derivative of a field (like the spinor field ψ_μ here). The partial derivative (∂_μ) is modified by the gauge field (W_μ^a that is associated with the $SU(2)$ gauge group, with $a = 1, 2, 3$ and σ^a being the generators of the $SU(2)$ gauge group. B_μ is associated with the $U(1)$ group, and Y is the hypercharge operator (that is related to the electric charge of the field). g and g' are the coupling constants associated with the $SU(2)$ and $U(1)$ gauge groups, respectively.

This term consists of two parts: A kinetic energy term that ensures the Higgs field interacts with the other particles in a way that respects the principles of gauge invariance. A potential energy term, often visualised as a "Mexican hat" due to its

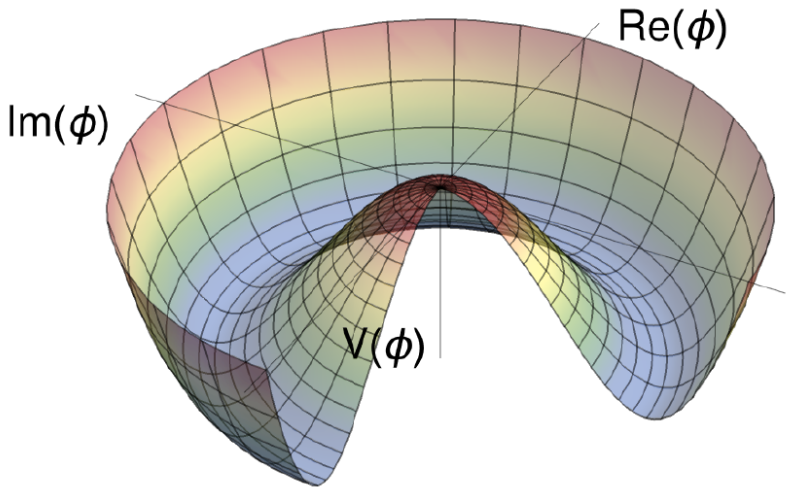

FIGURE 1.2: This graph depicts the Higgs Potential as a function of ϕ in both the real and imaginary planes when $\mu^2 < 0$. Its characteristic shape bears resemblance to a well-known analogy often referred to as a "Mexican hat" [42].

shape, which has a key role in mass generation (Figure 1.2). Imagine a ball placed exactly at the peak of the Mexican hat. This represents the state of the electroweak force before symmetry breaking. In this high-energy state, the W and Z bosons, mediators of the weak force, have no mass. Due to the unstable nature of the peak, the ball (representing the Higgs field) "rolls down" the potential towards the lower energy minimum. There are many possible directions to roll down within the ring-shaped minimum. This "rolling down" process is called spontaneous symmetry breaking. As the Higgs field settles at a specific point within the minimum, it acquires a non-zero value. This breaks the initial symmetry of the electroweak force. The interaction of the W and Z bosons with the Higgs field, now having a non-zero value, gives these bosons mass. This explains why the weak force is much weaker than the electromagnetic force at low energies. The W and Z bosons, unlike the massless photon of electromagnetism, need to "interact" with the Higgs field to move, effectively giving them mass.

The LHC experiments, CMS [2, 3] and ATLAS [4], marked a significant milestone with the uncovering of the Higgs boson. This particle, with a mass around 125 GeV, is a cornerstone of the Higgs mechanism. Run 2 data from the LHC provided strong validation for the SM's predictions regarding the Higgs boson. The SM portrays electroweak interactions through $SU(2)_L \times U(1)_Y$ gauge theory. The Higgs mechanism, involving a Higgs field doublet, plays a crucial role in assigning mass W and Z bosons, the carriers of the weak force. This mechanism gives rise to the Higgs boson itself. Measurements from the LHC experiments place the Higgs boson mass at approximately $125.09 \pm 0.21(stat) \pm 0.11(syst)$ GeV.

The Higgs field interacts with other particles through Yukawa couplings. This interaction, along with EWSB, is responsible for giving mass to fermions. The Higgs boson also interacts with itself and gauge bosons, with the strength of these

interactions depending on the mass of the particles involved:

$$g_{hVV} = \frac{2m_V^2}{v}, \quad g_{hhVV} = \frac{2m_V^2}{v^2}, \quad g_{hff} = \frac{m_f}{v}, \tag{1.13}$$

$$g_{hhh} = \frac{3m_h^2}{v}, \quad g_{hhhh} = \frac{3m_h^2}{v^2}. \tag{1.14}$$

Equation 1.13 and Equation 1.14 are the couplings of the SM Higgs boson with gauge bosons and fermions, where $V = W, Z$, $f = e,\ \mu, \tau$ and m_V is the mass of the gauge bosons. The vacuum expectation value is represented as v, and m_f is the fermion mass.

Production Modes of the SM Higgs

Gluon-gluon fusion is the dominant mechanism for Higgs boson production, responsible for roughly 65% of Higgs creation events at the Tevatron. This process is represented by the $gg \to H$ (Figure 1.3 A) [43]. Vector boson fusion is another significant Higgs production method. Here, two quarks annihilate ($q\bar{q} \to qq$) to produce a pair of vector bosons (VV), which then radiate a Higgs boson ($qa \to qqH$). Vector boson fusion contributes about 10-15% to the total-cross-section, depending on the specific Higgs mass (Figure 1.3 B) [44].

For lighter Higgs bosons (below 135 GeV), Higgstrahlung becomes more important. In this process, a Higgs boson is produced alongside a massive vector boson (V) through the process $q\bar{q} \to V^* \to VH$ (Figure 1.3 C). This mechanism is similar to how an electron emits a photon during bremsstrahlung radiation. The Higgs boson can also be created alongside a pair of top quarks ($t\bar{t}$) through a process such as $q\bar{q}$ or $gg \to t\bar{t}H$ (Figure 1.3 D) [45].

SM Higgs decays

The strength of the Higgs boson's interaction with other particles, called gauge bosons, is proportional to the masses of those gauge bosons squared. Due to its own mass, the Higgs boson predominantly decays into bottom quarks, accounting for roughly 58% of all decay events. These decays can also occur through intermediate, short-lived W and Z bosons (off-shell). In a much smaller fraction of cases (around 0.23%), the Higgs boson can decay into photons, either directly through quark interactions or indirectly through virtual W boson loops. A comprehensive breakdown of the Higgs boson's decay modes can be found in Figure 1.4.

1.2 The Two Higgs Doublet Model with an Additional Scalar

The Two Higgs Doublet with an additional Scalar (2HDM+S) extends the SM by introducing a new scalar particle, a singlet denoted by (S). This model builds on the existing CP-conserving 2HDM, but with a key difference. The 2HDM+S relaxes a specific symmetry constraint, allowing for a wider range of theoretical possibilities and potential observable effects. The crucial addition is the singlet field (ϕ_S). This

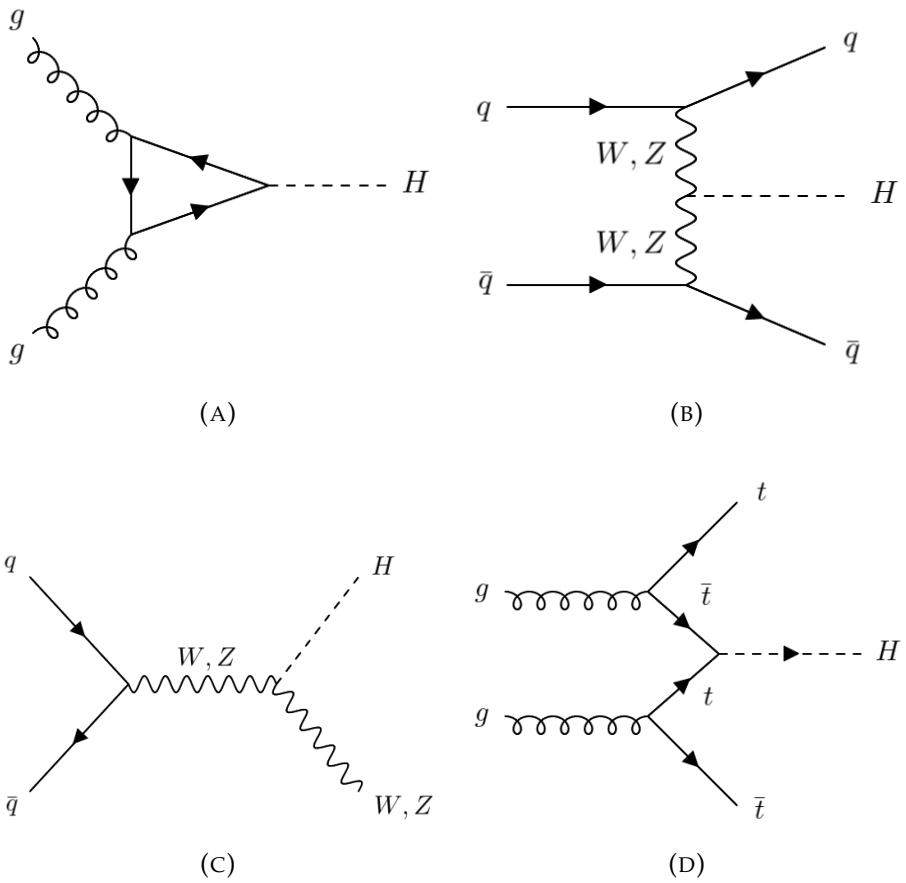

FIGURE 1.3: Production modes of the Higgs boson [46].

field is a real scalar, meaning it has no complex component, and it doesn't acquire a vev. This property makes it a strong candidate for dark matter particles, which are theorised to exist but haven't been directly observed yet.

While previous studies explored scenarios where the singlet field in the 2HDM+S model has a non-zero vev, they often relied on simplifying assumptions. For instance, they might have neglected the possibility of the singlet contributing to the properties of the recently discovered 125 GeV Higgs boson. This work takes a different approach. It avoids such limitations and considers the full potential of the 2HDM+S model. This model is described by two Higgs doublets (ϕ_1 and ϕ_2) and the singlet field (ϕ_S), as detailed in the equation [47, 48]:

$$\begin{aligned} V(\Phi_1,\Phi_2,\Phi_S) = {} & m_{11}^2|\Phi_1|^2 - m_{22}^2|\Phi_2|^2 - m_{12}^2(\Phi_1^\dagger\Phi_2 + h.c.) + \frac{\lambda_1}{2}(\Phi_1^\dagger\Phi_1)^2 \\ & + \frac{\lambda_2}{2}(\Phi_2^\dagger\Phi_2)^2 + \lambda_3(\Phi_1^\dagger\Phi_1)(\Phi_2^\dagger\Phi_2) + \lambda_4(\Phi_1^\dagger\Phi_2)(\Phi_2^\dagger\Phi_1) \\ & + \frac{\lambda_5}{2}[(\Phi_1^\dagger\Phi_2)^2 + \text{h.c.}] + \frac{1}{2}m_S^2\Phi_S^2 + \frac{\lambda_6}{2}\Phi_S^4 + \frac{\lambda_7}{2}(\Phi_1^\dagger\Phi_1)\Phi_S^2 \\ & + \frac{\lambda_8}{2}(\Phi_2^\dagger\Phi_2)\Phi_S^2. \end{aligned} \tag{1.15}$$

The 2HDM+S model introduces a softly broken symmetry term (m_{12}^2) to prevent

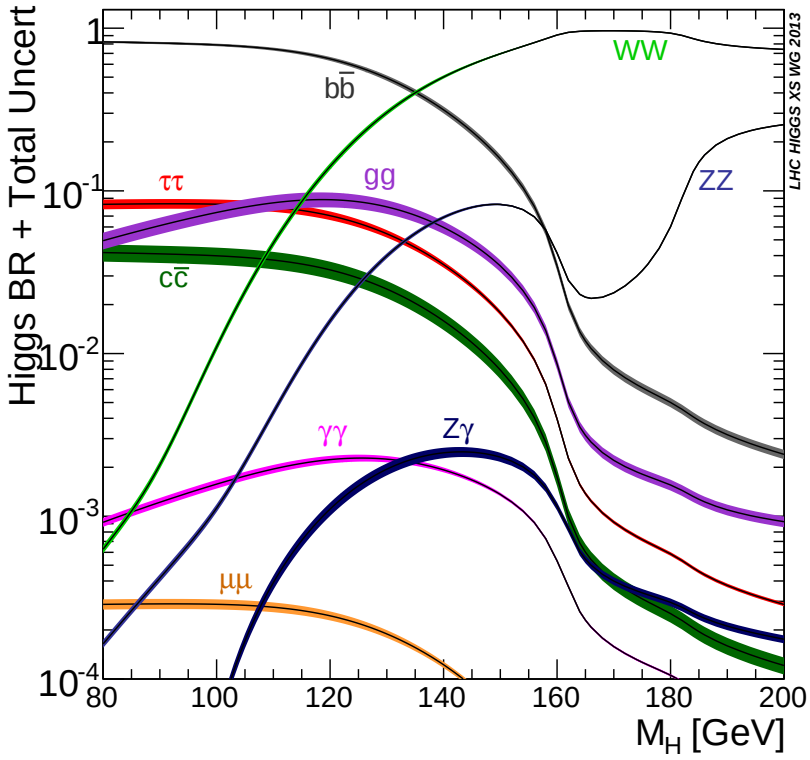

FIGURE 1.4: This graph depicts the SM Higgs boson decay branching ratios and total decay width [41].

unwanted interactions at the fundamental particle level. This symmetry can further be extended to the sector responsible for fermion masses (Yukawa sector) to ensure specific interactions don't occur at the tree level. The model incorporates two key symmetries, $\mathbb{Z}_2$ and $\mathbb{Z}_2'$. These symmetries dictate how the Higgs doublets and singlet scalar transform. One symmetry transforms ϕ_1 and ϕ_2 in opposite directions while leaving ϕ_S unchanged. The other transforms them identically but flips the sign of ϕ_S.

The second symmetry is spontaneously broken, meaning it's not enforced by the underlying physics. This breaking, along with the presence of the singlet field, modifies the properties of neutral particles compared to standard 2HDM. Instead of a 2×2 matrix describing the masses of these neutral particles, the 2HDM+S uses a 3×3 matrix due to the additional singlet field. This matrix considers various parameters that influence the masses and interactions of the particles.

A rotation matrix is applied to this matrix to arrive at the physical mass eigenstates, which are the actual particles observed in experiments. These eigenstates are denoted as H_1, H_2 and H_3, with masses increasing from H_1 to H_3. The model treats m_{12}^2 parameter as independent, resulting in a set of parameters that define the properties of the particles in this scenario. This set includes properties like masses, mixing angles, and vevs:

$$\tan_\beta, v, v_S, \alpha_1, \alpha_2, \alpha_3, m_{H_{1,2,3}}, m_A, m_{H^\pm}, m_{12}^2. \tag{1.16}$$

where t_β is the ratio of the vacuum expectation values of the doublets, v and v_S is

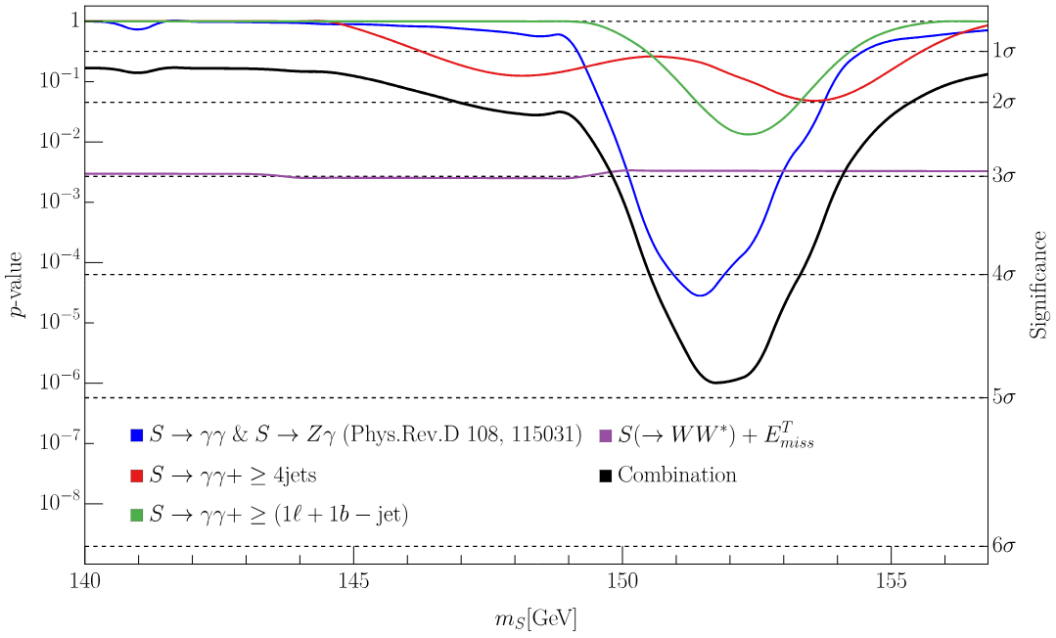

FIGURE 1.5: The p-values of the individual high-mass channels, as well as their combination, are shown as a function of m_S [58].

the SM and singlet vev, respectively, α_1, α_2, α_3 are the mixing angles, $m_{H_{1,2,3}}$ are the masses of the doublets, m_A is the mass of the pseudoscalar, $m_{H^\pm}$ is the mass of the charged scalar and m^2_{12} is the soft $\mathbb{Z}_2$ breaking parameter.

1.3 Multi-lepton anomalies at the LHC

The anomalies involving multiple leptons (electrons and muons) observed at the LHC pertain to distinct processes marked by their outcome, which includes two or more charged leptons [24, 49–56]. These processes may or may not involve the presence of hadronic b-jets, giving rise to topologies reminiscent of Higgs boson decays. Instances like these stand out significantly because they exhibit notable deviations from the SM predictions [52, 54–56]. Furthermore, this theoretical framework identifies a potential unique candidate, designated as S [52]. When coupled with a candidate Dark Matter [57], this model offers valuable perspectives on numerous astrophysical anomalies.

The detection of the Higgs boson at the LHC by the CMS [2, 3] and ATLAS [4] experiments has ushered in a new era in particle physics. With measurements placing the Higgs mass at 125 GeV and aligning with SM predictions, the possibility of additional or Higgs-like scalar bosons is considered, emphasising the need for minimal mixing with the SM. Multi-lepton anomaly final states at the LHC, as detailed in refs. [50, 52], are investigated within a Two-Higgs doublet model with an additional singlet scalar. In this model, the CP-even scalars h, S, H have masses of 125, 150 [52], and 270 GeV [49, 57], respectively. The primary anticipated decays involve $H \to Sh$, SS^*, SS', prompting a search for scalar resonances related to $S \to \gamma\gamma$, $Z\gamma$ in conjunction with missing transverse energy, light- and b-jets. The coupling details between scalar S and vector boson pairs are established through

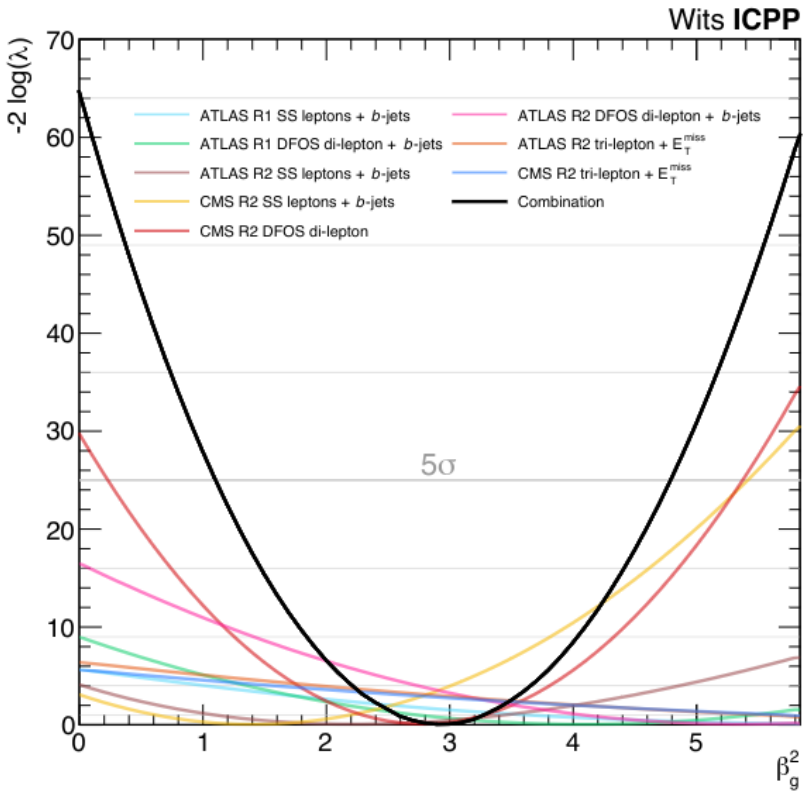

FIGURE 1.6: Profile likelihood ratio for the individual fits [54].

observed decays of S in channels such as WW, ZZ, $Z\gamma$, or $\gamma\gamma$. The first prediction of the mass of S was determined to be $m_S = 150 \pm 5\,\text{GeV}$ [52]. The predictions were confirmed in later studies on narrow resonances and di-lepton searches [57–60].

In recent times, there has been a notable emergence of what is referred to as "multi-lepton anomalies". These anomalies are characterised by several discrepancies observed in channels involving multiple electrons and/or muons in the final states. These disparities exhibit a significant level of statistical significance and suggest the potential existence of new scalar particles at the electroweak scale [50, 52, 54, 55, 61]. The 2HDM+S model under examination raised several important concerns. It demonstrates the ability to effectively account for the observed excesses in data using just one parameter, β_g^2. A study [54] involved simultaneous fitting for all measurements depicted in Figure 1.6. The most favourable fit resulted in a combination of all measurements with $\beta_g^2 = 2.92 \pm 0.35$, achieving a corresponding significance value of 8.04σ.The detailed characteristics of these anomalies are outlined in Table 1.3.

Previous research has suggested the possibility of an anomaly in high-energy proton-proton collisions. This anomaly involves the production of multiple leptons at a rate that isn't fully explained by the SM of particle physics. One potential explanation for this anomaly is the existence of a new heavy boson with a mass in the range of the electroweak force. This hypothetical boson would primarily decay into a known Higgs boson from the SM and a theorised singlet scalar particle. A study (Ref. [24]) investigated the long-standing discrepancy in the muon's anomalous magnetic moment. They explored a theoretical framework called the Two Higgs Doublet model with an additional singlet scalar (2HDM+S to see if it could explain

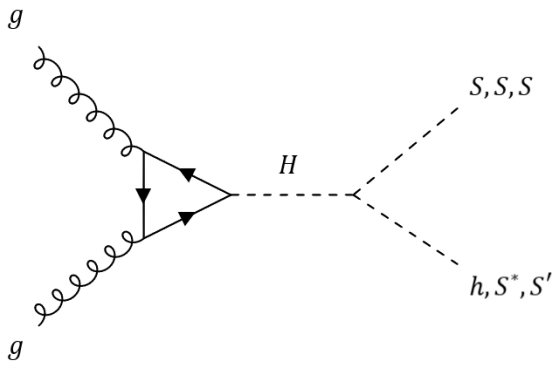

FIGURE 1.7: This is a representative Feynman diagram of the **ggF** production of H [54].

Final State	SM background	Significance
$\ell^+\ell^-$ + b-jets[54, 60, 62]	$t\bar{t} + Wt$	$> 5\sigma$
$\ell^\pm\ell^\pm$, $\ell^\pm\ell^\pm\ell$ (no b-jets)[55, 63, 64]	$W^\pm h(125), WWW$	$> 4\sigma$
$\ell^+\ell^-$+(no b-jets)[52, 65]	W^+W^-	$\approx 3\sigma$
$\ell^\pm\ell^\pm$, $\ell^\pm\ell^\pm\ell$+b-jets[56, 66, 67]	$t\bar{t}W^\pm, t\bar{t}t\bar{t}$	$> 3\sigma$
$Z(\rightarrow \ell\ell)\ell$(no b-jets)[54, 68]	$ZW^\pm$	$> 3\sigma$

TABLE 1.3: Anatomy of the multi-lepton final states [69].

this anomaly. However, their findings suggested that the contribution from the 2HDM+S was insufficient. The study then introduced the concept of Vector-Like Leptons as an alternative explanation for the observed discrepancy.

Specifically, these multi-lepton anomalies align with the hypothesis of direct production of a scalar particle, denoted as H, with an approximate mass of $\approx$ 270 GeV. This particle predominantly undergoes decay into a pair of lighter scalar particles, denoted as S. In Figure 1.7, the production of H is depicted. For the case where $H \rightarrow Sh$, we are able to produce a SM Higgs boson h and a singlet scalar [52]. In this configuration, S can be considered to be Higgs-like, with a mass $\approx$ 150 GeV and can decay into multi-lepton final states. This was the first instance of a potential 151.5 GeV scalar, and various resonant searches have been made.

Scientists recently conducted a search for a theorised particle called the singlet scalar (S). This particle is predicted to be produced alongside SM gauge bosons, specifically through the combined channels of $\gamma\gamma$ and $Z\gamma$. The analysis [57], favoured a simplified model with a new scalar particle around 151.5 GeV mass. This finding held a local significance of 4.3σ and a global significance of 3.9σ, suggesting a strong possibility of a new scalar resonance (S'). This particle, decaying into photons with associated missing energy, could be connected to the mystery of dark matter. The search also explored a mass window between 90 and 200 GeV. Around 95 GeV, researchers observed a preference for a new scalar decaying into a pair of W bosons through leptonic interactions. This finding reached a significance of 2.5σ. This suggests that a hypothetical heavy boson (H) could potentially decay into two scalar bosons ($S'S^*$), with S' being $\approx$95 GeV and S^* being the off-shell scalar at 151.5 GeV. The scalar S^* decays into a W boson pair (W^+W^-), while the scalar S' decays into a

Experiment	Final state	Significance (σ)
CMS	$\gamma\gamma$	2.9σ
ATLAS	$\gamma\gamma$	1.7σ
CMS	$\tau\tau$	2.8σ

TABLE 1.4: Local significance of the 95 GeV scalar at different final states.

bottom quark-antibottom quark pair ($b\bar{b}$) [59].

1.3.1 The 95 GeV Scalar Candidate

Particle physics experiments, especially those conducted at the LHC , are increasingly focused on a potential new light scalar particle with a mass around 95 GeV. This interest is driven by several observations of unexplained excesses in particle collisions at this energy range. The Large Electron-Positron (LEP) experiment reported an excess of events around 90-100 GeV with a statistical significance of 2.3σ. This excess was observed using a specific process called Higgstrahlung at centre-of-mass energies from 91 to 210 GeV [70]. During Run 2, the CMS experiment observed a localised excess of events with a significance of 2.9σ at a di-photon invariant mass of 95.4 GeV. Their analysis focused on searching for a SM-like Higgs boson decaying into two photons within a mass range of 70-110 GeV [71, 72]. Similar to CMS, the ATLAS experiment also conducted a search for resonances in the di-photon region using their Run 2 data. They found a slight excess with a significance of 1.7σ in the broader mass range of 66-110 GeV [73].

Analysing the tau lepton (τ) final states, CMS identified an excess of 2.8σ at 95.3 GeV, aligning with their previous di-photon findings [72]. This excess wasn't observed by ATLAS. A local excess of 2.5σ was reported by CMS in the W^+W^- final state decaying into electron or muon pairs, during their search for new scalar particles around 95 GeV and 151 GeV [59]. A combined analysis by CMS and ATLAS of the SM Higgs decaying into W bosons within the 90-200 GeV mass region is ongoing. The Table 1.4 summarises the observed excesses around 95 GeV from various LHC searches.

Currently, a local (global) significance of the excess at 95 GeV is evaluated to be 4.1σ (3.8σ) [58], illustrated in Figure 1.8. The ATLAS and CMS $\gamma\gamma$ data were merged under the assumption of equal signal sensitivity, and this combined result was subsequently integrated with the $\tau\tau$ and $S \to WW^*$ signals using Fischer's combined probability test [74] with three degrees of freedom. It's important to consider the possibility that the 95 GeV scalar might originate from the decay of H in the presence of multi-lepton anomalies observed at the LHC [50, 52, 54, 55]. In such a scenario, the decay pathway is $H \to SS'$, S could be responsible for lepton production and S' for the generation of b-quarks. The lack of an $S \to ZZ^* \to 4\ell$ signal also hints at S potentially being the neutral component of an $SU(2)$ triplet with $Y = 0$.

New findings from the CMS experiment hint at the existence of a new scalar particle around 95 GeV [71, 72]. While previous ATLAS studies didn't definitively exclude this possibility, their latest results show a weaker limit on the presence of such a particle at this mass compared to earlier expectations. Additionally, earlier

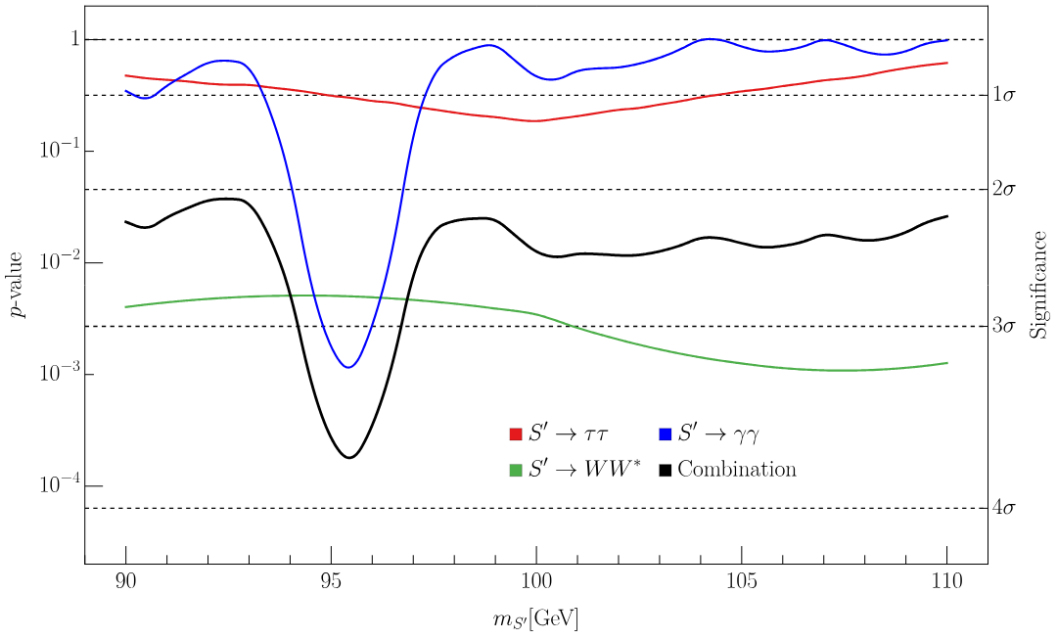

FIGURE 1.8: The p-value is shown as a function of $m_{S'}$ for the low-mass channels m_S [58].

LEP data suggested a process involving the production of a similar particle (S') through electron-positron collisions, followed by its decay into a Z boson and a pair of bottom quarks. Interestingly, CMS also observed a possible signal for the resonant production of tau lepton pairs at a similar mass.

Initial hints of a particle around 150 GeV came from studies of di-photon excesses [52]. The first evidence for a narrow resonance in this region was published elsewhere [57]. A recent combined analysis of ATLAS and CMS data explored the possibility of scalar resonances at the electroweak scale [58]. This analysis found consistent evidence for excesses around 96 GeV (denoted as S') and 152 GeV (denoted as S). The 95 GeV particle (S') appears to have a stronger presence compared to SM predictions, with a significance of 3.8σ. A simplified model interpretation of the 152 GeV excess suggests it could be due to the resonant pair production of the S particle via a new, heavier scalar particle H (with a mass of about 270 GeV). This scenario would result in a global significance of around 4.7σ (Figure 1.5). In this model, the S particle would be produced through the decay of the heavier H boson, potentially explaining the observed multi-lepton anomalies at the LHC. The production mechanism could involve processes like $pp \to H \to SS^*$ or $H \to SS'$, where S decays further into a pair of W bosons or a lighter scalar particle S'. The associated production of the S particle could be a link to the observed multi-lepton anomalies at the LHC.

Chapter 2

Investigation of a Triplet Scalar in $SU(2)_L$ as the Source of the 95 GeV Excess

The recent detection of an excess around 95 GeV in the di-photon channel at the LHC has sparked excitement in the physics community. This excess hints at the existence of a new scalar particle not predicted by the SM. Scientists are actively exploring possible explanations for this anomaly.

One intriguing possibility involves an $SU(2)_L$ triplet scalar with zero hypercharge ($Y = 0$). This type of scalar, when mixed slightly with the SM Higgs boson, could naturally have a significant decay rate into two photons. This characteristic allows it to be produced abundantly through the Drell-Yan process ($pp \to W^* \to HH^{\pm}$) at the LHC, where $H^{\pm}$ represents the charged component of the triplet, potentially explaining the observed signal strength as proposed in Ref. [75].

The discovery of the SM Higgs boson marked a milestone, but the possibility of other scalar particles remains open, especially if they play a more subtle role in EWSB and have weaker production cross-sections compared to the SM Higgs. The basic structure of the SM Higgs sector, consisting of a single $SU(2)_L$ doublet scalar, lacks strong theoretical justification. Many alternative models have been proposed, including models with additional singlets, doublets, and triplets of scalars [76, 77]. The 95 GeV excess has become a major focus of research due to its potential to reveal new physics beyond the SM. While the findings are still preliminary, they have opened exciting avenues for exploring the fundamental nature of the universe and our understanding of particle physics.

The CMS experiment has reported strong evidence for a neutral scalar (H) decaying into two photons at 95 GeV [71, 72]. These findings align with recent ATLAS regarding Z-strahlung with H decaying into b-quarks at LEP [70] as well as searches for the particle decaying into tau leptons $\tau\tau$ [78] and W bosons (WW) [79] by CMS. A combined analysis of these channels, detailed in chapter 1, suggests a global significance of 3.8σ. Previous studies have explored explanations for the 95 GeV excess using models with additional singlets and doublets. For example, the natural Next-to-Minimal Supersymmetric Standard Model (NMSSM) predicts a CP-even Higgs boson with a mass less than 120 GeV that could explain the di-photon excess within 1σ limits without violating known constraints [80]. Similarly, the Type I Yukawa Two Higgs Doublet Model has been proposed as a framework capable of explaining the excess [81]. This model achieves this by introducing a moderately-to-strongly fermiophobic CP-even Higgs boson (h) primarily produced through vector boson fusion or

through cascade decays in processes like top quark-antiquark ($t\bar{t}$) production.

However, there are constraints on the properties of new scalar particles. The measured value of a parameter called the ρ-parameter restricts the vev of any new scalar with higher dimensional representations under $SU(2)_L$ to be less than about 1 GeV [82]. This constraint excludes most other triplets with $Y = 0$, and the presence of multiple charged scalars at the same mass scale would make them difficult to detect at the LHC. The $SU(2)_L$ triplet is known to introduce a positive shift in the predicted mass of the W boson compared to the SM. This deviation is being investigated in light of the current global electroweak fit results [83, 84]. Similar deviations are expected for other types of new particles, including electroweak triplets (scalar or vector), singlet Z' bosons, and heavy neutral leptons. A recent result from the CDF II experiment reporting a 7σ deviation [85] in the W boson mass from the SM prediction also motivates this exploration. This work examines the possibility of the $Y = 0$ triplet as an alternative explanation for the observed hint of a scalar particle around 95 GeV.

2.1 Higgs Triplet Model with $Y_\Delta = 0$

We extend the SM by introducing a new scalar field, denoted by Δ. This scalar field transforms as a triplet under the weak isospin gauge group ($SU(2)_L$) and carries zero hypercharge ($Y = 0$) [86]. The Lagrangian for this extended scalar sector can be expressed as follows:

$$\mathscr{L} = (D_\mu \mathcal{H})^\dagger (D^\mu \mathcal{H}) + Tr(D_\mu \Delta)^\dagger (D^\mu \Delta) - V(\mathcal{H}, \Delta) + \mathscr{L}_{Yukawa}. \tag{2.1}$$

The covariant derivatives for the Higgs doublet ($\mathcal{H}$) and the Higgs triplet (Δ) are given by:

$$D_\mu \mathcal{H} = \partial_\mu \mathcal{H} + igT^\alpha W_\mu^\alpha \mathcal{H} + i\frac{g'}{2} B_\mu \mathcal{H}, \tag{2.2}$$

$$D_\mu \Delta = \partial_\mu \Delta + ig[T^\alpha W_\mu^\alpha, \Delta]. \tag{2.3}$$

The gauge bosons associated with the weak isospin ($SU(2)_L$) and hypercharge $U(1)_Y$ symmetries are denoted by W_μ^α and B_μ, respectively. Their couplings are represented by T^α, which are related by the Pauli matrices (σ_a). The scalar potential, $V(\mathcal{H}, \Delta)$, incorporating the newly introduced Higgs triplet (Δ), can be expressed as:

$$\begin{aligned} V(\mathcal{H}, \Delta) = -m_{\mathcal{H}}^2 \mathcal{H}^\dagger \mathcal{H} + \frac{\lambda}{4}(\mathcal{H}^\dagger \mathcal{H})^2 + m_\Delta^2 Tr(\Delta^\dagger \Delta) + \mu \mathcal{H}^\dagger \Delta \mathcal{H}) \\ +\lambda_1 (\mathcal{H}^\dagger \mathcal{H}) Tr(\Delta^\dagger \Delta) + \lambda_2 Tr(\Delta^\dagger \Delta)^2 + \lambda_3 Tr(\Delta^\dagger \Delta)^2 + \lambda_4 \mathcal{H}^\dagger \Delta^\dagger \Delta \mathcal{H}, \end{aligned} \tag{2.4}$$

where the Tr denotes the trace of a matrix, $\mathcal{H}^\dagger$ represents the Hermitian conjugate of the Higgs doublet (H) and $\Delta^\dagger$ represents the Hermitian conjugate of the Higgs triplet (Δ). The Yukawa Lagrangian ($\mathscr{L}_{Yukawa}$) encompasses the SM's Yukawa interactions and introduces an additional term. This term, after spontaneous symmetry breaking, allows for the generation of neutrino masses (of the Majorana type) without requiring right-handed neutrino states. The electric charge (Q) is defined using isospin (I) and

hypercharge (Y) as $Q = I_3 + \frac{Y}{2}$. The two Higgs multiplets, H and Δ, can be expressed in terms of their component fields:

$$\Delta = \frac{1}{2}\begin{pmatrix} \delta^0 & \sqrt{2}\delta^+ \\ \sqrt{2}\delta^- & -\delta^0 \end{pmatrix}, \quad H = \begin{pmatrix} \phi^+ \\ \phi^0 \end{pmatrix}. \tag{2.5}$$

Here, ϕ^0 and δ^0 represent the vevs of the neutral components in the doublet (H) and triplet (Δ), respectively. We will assume these vevs to be positive for now. Assuming spontaneous EWSB occurs at a point with zero electric charge, the vevs of the Higgs fields take on specific values:

$$\langle\Delta\rangle = \begin{pmatrix} v_t & 0 \\ 0 & -v_t \end{pmatrix}, \quad \langle\mathcal{H}\rangle = \begin{pmatrix} 0 \\ v_d/\sqrt{2} \end{pmatrix}. \tag{2.6}$$

Minimising the scalar potential (Equation 2.4) with respect to these vevs leads to two key conditions:

$$\mathcal{M}_\Delta^2 = \frac{\lambda_a}{2}v_d^2 - \frac{\mu v_d^2}{4v_t} + \lambda_b v_t^2, \tag{2.7}$$

$$m_\mathcal{H}^2 = \frac{\lambda}{4}v_d^2 - \frac{\mu v_t}{2} + \frac{\lambda_a}{2}v_t^2. \tag{2.8}$$

The Equation 2.7 relates the mass parameter (M_Δ^2) of the Higgs Triplet to the vevs ($v_d,\ v_t$), the coupling constants ($\lambda_a,\ \lambda_b$), and the μ term. Equation 2.8 relates the mass parameter (m_H^2) of the Higgs doublet to the vevs ($v_d,\ v_t$), the coupling constant (λ), and the μ term. The complete squared mass matrix ($\mathcal{M}$) for all the scalar fields can be constructed by taking the second derivative of the potential with respect to the Higgs field components. Due to the specific VEVs and the conditions derived from minimisation (Equation 2.7, Equation 2.8), this mass matrix can be reorganised into a block diagonal form:

$$\mathcal{M} = \frac{\partial^2 V}{2\partial\eta_i^2}|_{\Delta=\langle\Delta\rangle,\mathcal{H}=\langle\mathcal{H}\rangle}. \tag{2.9}$$

This block diagonal form consists of three 2×2 matrices. The $M_\pm^2$ corresponds to the singly charged Higgs bosons ($H^\pm$). Its specific form is shown in Equation 2.10. The $\mathcal{M}_{CP-even}^2$ block is associated with the CP-even Higgs bosons (h^0 and H^0). A separate term represents the neutral Goldstone boson (G^0). The equation below provided outlines the structure of the $M_\pm^2$ block for the singly charged Higgs bosons:

$$\mathcal{M}_\pm^2 = \begin{pmatrix} v_t & v_d/2 \\ v_d/2 & v_d^2/4v_t \end{pmatrix}. \tag{2.10}$$

To determine the masses of the physical Higgs bosons, we diagonalise the $M_\pm^2$ block using a 2×2 rotation matrix denoted by $\mathcal{R}(\theta\pm)$, where $\theta_\pm$ is the rotation angle. This process essentially separates the Higgs doublet and triplet components that contribute to the singly charged Higgs bosons ($H^\pm$) and neutral Goldstone boson (G^0). Diagonalisation reveals two eigenvalues for $M_\pm^2$. One eigenvalue is zero, confirming the presence of the massless Goldstone boson, which arises due to the breaking of electroweak symmetry. The other eigenvalue corresponds to the mass squared ($m_\pm^2$)

of the singly charged Higgs bosons and is given by the following equation:

$$m_{H^\pm}^2 = \mu \frac{(v_d^2 + 4v_t^2)}{4v_t}. \tag{2.11}$$

After performing the diagonalisation process, we can express the physical Higgs bosons and the Goldstone boson in terms of the original Lagrangian fields ($\phi^\pm$ and $\delta^\pm$) using a rotation. This rotation is described by the angle $\theta_\pm$. The resulting expressions for the mass eigenstates are:

$$\frac{\mu v_d^2}{4v_t} = \cos^2\theta_\pm M_{H^\pm}^2, \tag{2.12}$$

$$\mu \frac{v_d}{2} = -\frac{\sin 2\theta_\pm}{2} M_{H^\pm}^2, \tag{2.13}$$

$$\mu v_t = \sin^2\theta_\pm M_{H^\pm}^2. \tag{2.14}$$

Since the Goldstone boson is massless, the equations obtained from diagonalisation have a unique solution for the rotation angles ($\sin\theta_\pm$ and $\cos\theta_\pm$), with a possible overall sign ambiguity ($\epsilon = \pm 1$). This solution ensures a positive mass squared ($m_{H^\pm}^2$) for the singly charged Higgs bosons ($H^\pm$), as required to avoid hypothetical particles with unphysical properties (tachyons) [87]. One key implication from this solution is that the signs of $\sin\theta_\pm$ and $\cos\theta_\pm$ must be opposite. This leads to the following expressions for the rotation angles:

$$\cos\theta_\pm = \epsilon \frac{v_d}{\sqrt{v_d^2 + 4v_t^2}}, \tag{2.15}$$

$$\sin\theta_\pm = -\epsilon \frac{2v_t}{\sqrt{v_d^2 + 4v_t^2}}, \tag{2.16}$$

where ϵ represents the sign ambiguity and leads to a negative tangent of the angle ($\tan\theta_\pm$). Moving on to the CP-even Higgs bosons, their mass matrix is denoted by $\mathcal{M}_{CP-even}^2$. This matrix is a 2×2 square matrix defined as:

$$\mathcal{M}_{CP-even}^2 = \begin{pmatrix} A & B \\ B & C \end{pmatrix}, \tag{2.17}$$

where the elements of this matrix (A, B, and C) are expressed in terms of the scalar potential parameters, the vacuum expectation values (v_d and v_t), and the coupling constants. The specific definitions for A, B, and C are provided below:

$$A = \frac{\lambda v_d^2}{2}, \quad B = \frac{v_d[-\mu + 2\lambda_a v_t]}{2\sqrt{2}}, \quad C = \frac{\mu v_d^2 + 8\lambda_b v_t^3}{8v_t}. \tag{2.18}$$

Similar to the singly charged Higgs bosons, the CP-even Higgs bosons require diagonalisation to determine their physical masses. This process involves a 2×2

matrix denoted by $\mathcal{R}(\alpha)$, where α is the rotation angle within the CP-even sector. Diagonalisation of the CP-even Higgs mass matrix $\mathcal{M}^2_{CP-even}$ yields two physically relevant states with even parity. These states are denoted by h^0 and H^0 and can be expressed as linear combinations of the original Higgs fields (h_1 and h_2) with coefficients determined by the rotation angle (α). The specific combinations are shown in the following equations:

$$h^0 = +c_\alpha h_1 + s_\alpha h_2, \tag{2.19}$$

$$H^0 = +c_\alpha h_2 - s_\alpha h_1, \tag{2.20}$$

where c_α and s_α represent the cosine and sine of the rotation angle (α), respectively. The diagonalisation process also provides the masses ($m^2_{h^0}$ and $m^2_{H^0}$) of the physical Higgs bosons, which are the eigenvalues of the $\mathcal{M}^2_{CP-even}$ matrix. These masses are expressed in the following equations:

$$m^2_{h^0} = \frac{A + C - \sqrt{(A-C)^2 + 4B^2}}{2}, \tag{2.21}$$

$$m^2_{H^0} = \frac{A + C + \sqrt{(A-C)^2 + 4B^2}}{2}. \tag{2.22}$$

Within the model, it's crucial to consider that the lighter CP-even Higgs boson (h^0) might not be the absolute lightest Higgs boson. This highlights the importance of a more comprehensive analysis. Diagonalisation, a mathematical technique, confirms the existence of a massless Goldstone boson. This particle arises due to the broken CP-even symmetry within the model. The z_1 field is identified with this massless Goldstone boson.

Once the masses of the CP-even Higgs bosons are established, we can proceed to solve for the rotation angle. This specific angle plays a crucial role in determining the degree of mixing between the initial Higgs field and the physical states that emerge. The relationships between the elements of the mass matrix (A, B and C), the rotation angle, and the masses of the physical Higgs bosons can be expressed through the following equations:

$$A = c^2_\alpha m^2_{h^0} + s^2_\alpha m^2_{H^0}, \tag{2.23}$$

$$B = (m^2_{h^0} - m^2_{H^0})\frac{sin2\alpha}{2}, \tag{2.24}$$

$$C = s^2_\alpha m^2_{h^0} + c^2_\alpha m^2_{H^0}. \tag{2.25}$$

We can solve for the rotation angle (α) using Equation 2.23 and Equation 2.25. Additionally, we utilise the trigonometric identity $\sin^2(\alpha) + \cos^2(\alpha) = 1$ and the mass eigenvalues for the Higgs bosons ($m^2_{h^0}$ and $m^2_{H^0}$) obtained through diagonalisation (Equation 2.21 and Equation 2.22). While both equations provide solutions for α, the signs of $\sin(\alpha)$ and $\cos(\alpha)$ depend on the value of element B in the mass matrix.

The specific value of the μ term within the scalar potential plays a crucial role in determining the relative signs of $\sin(\alpha)$ and $\cos(\alpha)$. This relationship is evident in Equation 2.18 and Equation 2.24. Under typical conditions, a positive μ term combined with common ranges for coupling constants (λ_1 and λ_2) often leads to a

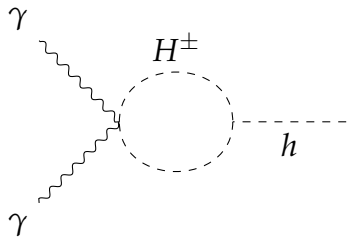

FIGURE 2.1: Feynman diagram showing di-photon decay.

positive tangent of the rotation angle (tanα). However, there's a noteworthy exception: a specific region within the parameter space exists where the μ term becomes very small. Tan (α) can take on a negative value in this unique scenario.

By combining Equation 2.23 and Equation 2.25 and utilising the definitions for the elements of the mass matrix (Equation 2.18), we can arrive at a convenient form for expressing both sine and cosine of the double angle as:

$$\sin 2\alpha = \frac{2B}{\sqrt{(A-C)^2+4B^2}} \ , \ \cos 2\alpha = \frac{2B}{\sqrt{(A-C)^2+4B^2}}. \tag{2.26}$$

2.2 Examining SM and BSM Signal Strengths in Connection with the Di-photon Excess

Experimental data on the properties of the SM Higgs boson (h) has been extensively collected at the LHC. This data, particularly measurements of the Higgs decaying into two photons ($h \to \gamma\gamma$), as shown in Figure 2.1, offers valuable constraints on the allowed values for the parameters within the Higgs Triplet Model. The di-photon signal strength is typically denoted by $\mu_{\gamma\gamma}$ and is expressed as:

$$\mu_{\gamma\gamma} = \frac{\Gamma_{h\to\gamma\gamma}}{\Gamma^{SM}_{h\to\gamma\gamma}} \times \frac{\Gamma^{SM}_{h_{tot}}}{\Gamma_{h_{tot}}}, \tag{2.27}$$

where $\Gamma^{SM}_{h_{tot}} = 4.07$ MeV. Modifying the $h\gamma\gamma$ coupling, we are able to determine the scaling factor as:

$$\kappa_\gamma = \frac{g_{h\gamma\gamma}}{g^{SM}_{h\gamma\gamma}}. \tag{2.28}$$

Within the SM, the decay of the Higgs boson into two photons involves loops containing either fermions or W bosons. Introducing a new charged scalar particle associated with the triplet scalar modifies the SM Higgs boson's di-photon decay rate. This modification reduces in value as the mass of the charged scalar increases. The effect is directly proportional to the square of this mass.

The resulting couplings are defined as [75]:

$$g_{h\gamma\gamma} = \sum_f N_c Q_f^2 g^h_{f\bar{f}} \beta_H^{1/2}\left(\frac{4m_f^2}{m_h^2}\right) + g^h_{WW}\beta^1_H\left(\frac{4m_W^2}{m_h^2}\right) + \frac{\lambda_{hH^+H^-} - v_{SM}}{2m^2_{H^+}}\beta^0_H\left(\frac{4m^2_{H^+}}{m_h^2}\right), \tag{2.29}$$

$$g^{\mathrm{SM}}_{h\gamma\gamma} = \sum_f N_c Q_f^2 \beta_H^{1/2}\left(\frac{4m_f^2}{m_h^2}\right) + \beta_H^1\left(\frac{4m_W^2}{m_h^2}\right), \tag{2.30}$$

where Q_f is the electric charge of fermion f, N_c is the colour factor (3 for quarks, and 1 for leptons), the normalised couplings g^h_{ff} and g^h_{WW} are defined as:

$$g^h_{f\bar{f}} = \cos\alpha, \quad g^H_{f\bar{f}} = -\sin\alpha, \tag{2.31}$$

$$g^h_{WW} = \frac{4v_t \sin\alpha + v_{\mathrm{SM}}\cos\alpha}{v_{\mathrm{SM}}}, \quad g^H_{WW} = \frac{4v_t\cos\alpha - v_{\mathrm{SM}}\sin\alpha}{v_{\mathrm{SM}}}, \tag{2.32}$$

where specific loop functions employed in calculating the di-photon decay rate are detailed in Ref. [88]:

$$\beta(x,y) = (1-x-y)^2 - 4xy, \tag{2.33}$$

$$\beta_{ff'}(x,y) = [(x+y)(1-x-y) - 4xy]\sqrt{\beta(x,y)}, \tag{2.34}$$

$$\beta_S(x) = (x-1)\left(2 - \frac{1}{2}\log x\right) + \frac{1-5x}{\sqrt{4x-1}}\left[\tan^{-1}\frac{2x-1}{\sqrt{4x-1}} - \tan^{-1}\frac{1}{\sqrt{4x-1}}\right], \tag{2.35}$$

$$\begin{aligned}\beta_t(x,y) = {} & \frac{y^2}{x^3}(4xy+3x-4y)\log\frac{y(x-1)}{x-y} + (3x^2-4x-3y^2+1)\times\log\frac{x-1}{x-y} \\ & -\frac{5}{2} + \frac{1-y}{x^2}(3x^3 - xy - 2xy^2 + 4y^2) + y\left(4 - \frac{3}{2}y\right),\end{aligned} \tag{2.36}$$

$$\beta_H^0(x) = -x\left[1 - xf(x)\right], \tag{2.37}$$

$$\beta_H^{1/2}(x) = 2x\left[1 + (1-x)f(x)\right], \tag{2.38}$$

$$\beta_H^1(x) = -\left[2 + 3x + 3x(2-x)f(x)\right], \tag{2.39}$$

$$\beta_{HZ}^0(x,y) = I_1(x,y), \tag{2.40}$$

$$\beta_{HZ}^{1/2}(x,y) = I_1(x,y) - I_2(x,y), \tag{2.41}$$

$$\beta^1_{HZ}(x,y) = \cos\theta_w \left[\left(1+\frac{2}{x}\right)\tan^2\theta_w - \left(5+\frac{2}{x}\right)\right] I_1(x,y) + 4\cos\theta_w(3-\tan^2\theta_w) I_2(x,y). \tag{2.42}$$

The di-photon decay width is expressed as:

$$\Gamma_{h\to\gamma\gamma} = \frac{\alpha^2_{em} g_2^2 m_h^3}{1024\pi^3 m_W^2} \left|g_{h\gamma\gamma}\right|^2. \tag{2.43}$$

We can express the signal strength in terms of the scaling factor κ_γ as:

$$\mu_{\gamma\gamma} \approx \frac{|\kappa_\gamma|^2}{0.9977 + 0.0023|\kappa_\gamma|^2}. \tag{2.44}$$

Recent measurements from CMS [89] and ATLAS [90] on the signal strength of the Higgs boson decaying into two photons is:

$$\mu^{CMS}_{\gamma\gamma} = 1.12^{+0.09}_{-0.09},\ \mu^{ATLAS}_{\gamma\gamma} = 1.04^{+0.10}_{-0.09}. \tag{2.45}$$

Combining these measurements, we obtain a weighted average of:

$$\mu^{exp}_{\gamma\gamma} = 1.08^{+0.07}_{-0.06}. \tag{2.46}$$

The Figure 2.2 illustrates the allowed parameter space for the model at the 1σ and 2σ confidence levels. While the measurement of the Higgs decaying into two photons is remarkably precise, its interpretation can be complex. This complexity arises from the interplay between the SM Higgs, the mixing with the Higgs Triplet states, and potential loop contributions from the singly charged Higgs bosons ($H^\pm$). These effects can sometimes cancel each other out, making it challenging to draw definitive conclusions solely from this channel.

Therefore, to obtain a more comprehensive picture, we consider the second most precisely measured decay channel for the SM Higgs boson: $h \to ZZ^*$. References [91, 92] report an experimentally measured signal strength, $\mu^{exp}_{h,ZZ^*} = 1.02 \pm 0.08$ for this channel. This decay channel is primarily sensitive to the mixing angle within the model. The right section of Figure 2.2, beyond the solid vertical line, represents the parameter consistent with the measured $h \to ZZ^*$ signal strength at the 1σ confidence level.

In Ref. [75], it was found that the decay modes of the H with a mass of 95 GeV are determined by rescaling the widths of a SM-like Higgs using $\sin^2\alpha$. The process $H \to WW^*$ takes place at tree-level via the triplet vev (v_t), while the decay of the decay of the photons ($H \to \gamma\gamma$) involves contributions from charged Higgs and W

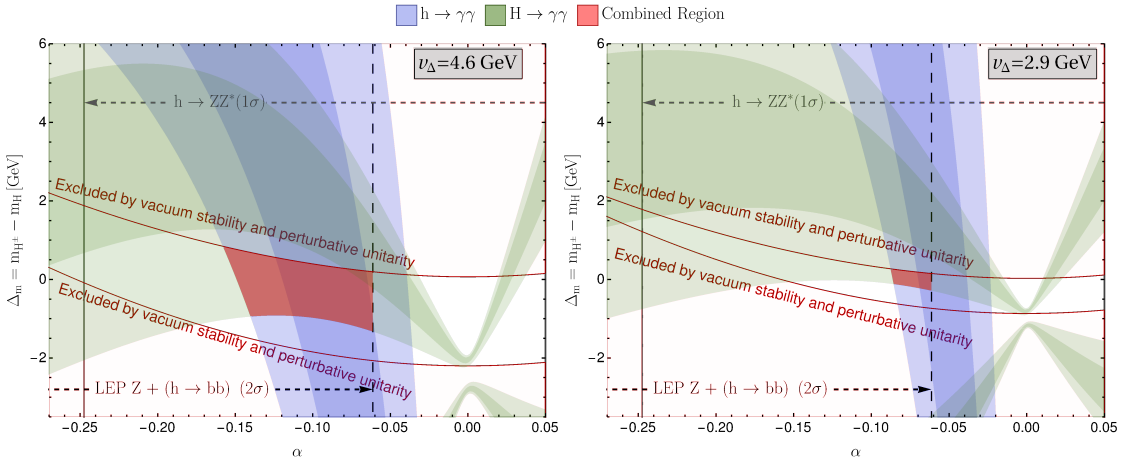

FIGURE 2.2: The 1σ and 2σ preferred regions for the $h \to \gamma\gamma$ and 95 GeV ($H \to \gamma\gamma$) signal strengths in the $\alpha - \Delta m$ plane for two values of triplet vev are shown here [75].

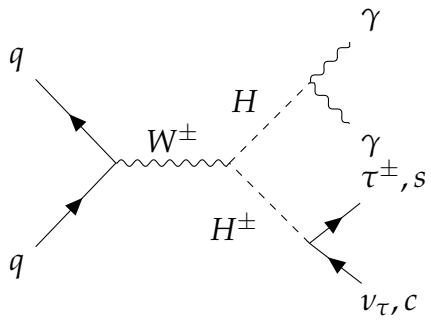

FIGURE 2.3: The Drell-Yan process of $pp \to W^* \to H^\pm H^0$.

loops. The numerical approximation of α_{em} at $q^2 = 0$ is effective for Next-To-Leading-Order (NLO) QED corrections:

$$\Gamma(H \to \gamma\gamma) \approx \frac{\alpha_{em}^2 g_2^2 m_H^3}{1024\pi^3 m_W^2} \left| -\frac{4}{3}\sin\alpha\beta_H^{1/2}\left(\frac{4m_t^2}{m_H^2}\right) + \left(-\sin\alpha + \frac{4v_t}{v}\cos\alpha\right)\beta_H^1\left(\frac{4m_W^2}{m_H^2}\right) + \frac{A_{HH^\pm H^\mp} v}{2m_{H^\pm}^2}\beta_H^0\left(\frac{4m_{H^\pm}^2}{m_H^2}\right)\right|^2. \tag{2.47}$$

Disregarding the **VBF** contribution (since it is subdominant), and using the cross-section for the Higgs at 95 GeV, $\sigma[pp \to h_{95}] \approx 68$ pb [93–96], we have:

$$\sigma[pp \to H \to \gamma\gamma] \approx Br[H \to \gamma\gamma] \times (2 + 68\alpha^2) pb. \tag{2.48}$$

Normalising the signal strength to the one of a hypothetical SM-like Higgs with the same mass, we find numerically:

$$\mu_{H,\gamma\gamma} \approx (21.5 + 719\alpha^2) \times Br[H \to \gamma\gamma]. \tag{2.49}$$

This should be contrasted with the amalgamation of the low-mass $\gamma\gamma$ searches conducted by ATLAS and CMS analyses:

$$\mu^{exp}_{H,\gamma\gamma} = 0.27^{+0.10}_{-0.09}. \tag{2.50}$$

The resulting preferred regions are shown in green in Figure 2.2. The Higgs Triplet model with a hypercharge of 0, shares similarities with the Two-Higgs Doublet Model where a 95 GeV excess was outlined in Ref. [81]. In the fermiophobic limit described there, the dominant production mode is $pp \to W^{\pm *} \to H^{\pm}H$. However, it's crucial to note distinctions; Ref. [81] predicts an additional pseudoscalar with a mass of approximately 80 GeV, and the Higgs potential in that scenario allows for more flexibility than our current setup.

If the neutral component of the $SU(2)_L$ triplet with hypercharge 0 is the origin of the 95 GeV excess observed at the LHC, it would have significant consequences for particle physics. Confirmation would likely come from two sources: a stau-like excess observed in LHC Run 3 data, which aligns with the predicted decay of this new Higgs boson, and a positive shift in the measured W boson mass caused by interactions with this new particle. Additionally, the predicted production of this Higgs boson in association with jets and tau leptons provides a specific signature for researchers to target.

Furthermore, the theory suggests the existence of a charged partner to this Higgs boson with a mass below 100 GeV. This particle would be ideally suited for study at future electron-positron colliders, machines designed for precise measurements. Detecting this charged Higgs would be a strong confirmation of an extended Higgs sector beyond the Standard Model. In conclusion, this scenario not only explains the 95 GeV excess but opens doors for a deeper understanding of the Higgs mechanism and the potential existence of new particles.

Chapter 3

W-boson Mass and Muon $g-2$ in 2HDM+S

The precise measurement of the W boson mass is a crucial topic in particle physics. Recent findings, particularly a 7σ deviation from the experiment, suggest potential new physics beyond the SM might be at play [97]. One promising approach to explore these discrepancies involves the impact of BSM models on Electroweak Precision Observables, specifically the Peskin-Takeuchi oblique parameters [98, 99].

Motivated by these anomalies and recent findings of excesses around 95 GeV at CMS, we aim to investigate a BSM model's parameter space to explain the W boson mass discrepancy. Additionally, discrepancies observed in multi-lepton channels during the decay of SM Higgs boson by the CMS and ATLAS experiments have been linked to the possible existence of a low-mass scalar particle. This work focuses on a 2HDM+S model and analyses the primary decays of $H \to Sh$ and SS^*. This analysis paves the way for further exploration of potential new decay channels for the additional scalar (S), including $S \to \gamma\gamma,\ Z\gamma$, potentially accompanied by missing transverse energy, light jets, or b-jets.

Our analysis of the 2HDM+S model's parameter space prioritises physically realistic scenarios. We ensure the electroweak minimum is either stable or meta-stable for a given set of parameters. A meta-stable state has a very long lifetime, much longer than the age of the universe. To achieve this, we impose restrictions on the couplings between the scalars in the model. These restrictions prevent situations where the potential energy of the system could become infinitely negative. To assess the stability of the electroweak minimum for various parameter configurations, we utilise a software tool called ScannerS [47].

To ensure our chosen parameter points are compatible with existing measurements of the 95 GeV Higgs boson, we leverage publicly available software tools. The ScannerS tool plays a central role in our analysis. It incorporates constraints from various theoretical requirements to identify physically viable parameter space regions within the 2HDM+S model. To ensure the stability or meta-stability of the electroweak minimum for a chosen set of parameters, one important constraint is implemented. This constraint is enforced using HiggsTools [100] software, which is integrated within ScannerS. This tool allows us to compare our model's predictions for the Higgs boson's properties (such as branching ratios and total widths) with current experimental data around 95 GeV. It includes the latest advancements in theoretical calculations, including QCD corrections and off-shell effects. ScannerS also utilises pre-calculated data (parametrisations) to accurately estimate cross-sections

for various Higgs production processes. These parametrisations incorporate next-to-next-to-leading order (NNLO) calculations in QCD, ensuring high accuracy. The data originates from tools like SusHi [101, 102] and HiggsBounds [103].

HiggsBounds is another valuable tool employed in our analysis. It compares our model's predictions for Higgs Boson production cross-sections with exclusion limits set by collider experiments like LEP, Tevatron, and the LHC. This allows us to identify parameter space regions incompatible with current observations. Conversely, HiggsSignals [100] utilises the same input data as HiggsBounds to calculate a χ^2 value. This value indicates how well our model's predictions for the properties of the 125 GeV Higgs boson (h_{125}) at the LHC agree with experimental measurements. A lower χ^2 value suggests better agreement. HiggsSignals interprets the χ^2 value using a profile likelihood ratio test, comparing our model to the SM as the alternative hypothesis. Based on these various tools and their outputs, ScannerS identifies parameter points that satisfy the theoretical constraints of the 2HDM+S model (such as vacuum stability, perturbative unitarity), points that are consistent with existing measurements of the Higgs boson properties at the 95% confidence level and points that do not violate exclusion limits set by collider experiments searching for Higgs bosons.

ScannerS offers different levels of applying these constraints, namely **Skip**, **Ignore**, and **Apply**. The **Skip** level ignores the constraint entirely. No calculations are performed, and the parameter point is not tested against this constraint. In the **Ignore** level, calculations are performed for the parameter point, but the constraint is not enforced. The results are stored for further analysis. Finally, in the **Apply** level, only parameter points satisfying the constraint are retained. For a detailed explanation of each constraint and its corresponding level in ScannerS, please refer to Appendix A.

Our analysis considers constraints arising from electroweak precision observables (EWPO). These observables are sensitive to the properties of particles involved in electroweak interactions. They provide important checks on the validity of our chosen BSM model (2HDM+S). To ensure our model aligns with EWPO, we focus on the Peskin-Takeuchi parameters (U, S, and T). These parameters quantify potential deviations from the SM in the electroweak sector [104, 105]. For models with extended Higgs sectors, new particles can significantly impact these parameters, particularly if they contribute to gauge boson self-energies. Consequently, the predicted mass of the W boson becomes a function of the U, S, and T parameters in our model. ScannerS calculates one-loop corrections to these parameters specific to the 2HDM+S, allowing us to determine the W boson mass as a function of U, S, and T [106]:

$$M_W^2 = \left(M_W^{\mathrm{SM}}\right)^2 \left(1 + \frac{s_w^2}{c_w^2 - s_w^2}\Delta r'\right), \tag{3.1}$$

with

$$\Delta r' = \frac{\alpha}{s_w^2}\left(-\frac{1}{2}S + c_w^2 T + \frac{c_w^2 - s_w^2}{4 s_w^2}U\right), \tag{3.2}$$

and

$$\sin^2\theta_{\mathrm{eff}} = \sin^2\theta_{\mathrm{eff}}^{\mathrm{SM}} - \alpha\frac{c_w^2 s_w^2}{4(c_w^2 - s_w^2)}T, \tag{3.3}$$

where $M_W^{\rm SM} = 80.537\,\text{GeV}$, $\sin^2\theta_{\rm eff}^{\rm SM} = 0.231532$, $s_w = \sqrt{1-\left(\frac{M_W^{\rm SM}}{M_Z}\right)^2}$, $c_w = \sqrt{1-s_w^2}$ and $M_Z = 91.1876\,\text{GeV}$.

3.1 Performing a fitting procedure for the excesses observed at 95 and 152 GeV

We employ a χ^2 technique to analyse the reported excesses in the di-photon ($\gamma\gamma$), tau lepton ($\tau^+\tau^-$), and bottom quark ($b\bar{b}$) decay channels at around 95 GeV. This analysis aims to assess the compatibility of these excesses with the 2HDM+S. Furthermore, we investigate whether the parameter space of the 2HDM+S model can predict an upward shift in the mass of the W boson compared to the SM prediction. This is of particular interest because recent measurements have hinted at a possible deviation from the expected W boson mass.

It was found that the experimental signal strengths for the three distinct channels at 95 GeV were [58, 107, 108]

$$\mu_{\tau\tau}^{exp} \pm \Delta\mu_{\tau\tau}^{exp} = 0.6 \pm 0.25, \tag{3.4}$$

$$\mu_{\gamma\gamma}^{exp} \pm \Delta\mu_{\gamma\gamma}^{exp} = 0.27^{+0.10}_{-0.09}, \tag{3.5}$$

$$\mu_{bb}^{exp} \pm \Delta\mu_{bb}^{exp} = 0.117 \pm 0.057. \tag{3.6}$$

The signal strength, denoted by μ_{XX}, is a metric used to quantify how well a model's prediction for the production rate of a particle ($X = \gamma,\ \tau,\ b$) through a specific process aligns with experimental observations. It is calculated as the ratio of the predicted production cross-section for the new physics process (σ^{BSM}) to the corresponding production cross-section in the SM (σ^{SM}). Both are multiplied by their respective branching ratios (BR) for the particle X. The equation for the signal strength is defined as:

$$\mu_{XX} = \frac{\sigma^{BSM}(gg \to H) \cdot BR^{BSM}(H \to XX)}{\sigma^{SM}(gg \to H(m_{BSM})) \cdot BR^{SM}(H(m_{BSM}) \to XX)}. \tag{3.7}$$

We leverage ScannerS to perform parameter scans within the 2HDM+S model. This allows us to identify parameter combinations that reproduce the experimentally observed signal strengths for the excesses in the $\gamma\gamma$, $b\bar{b}$, and $\tau^+\tau^-$ decay channels around 95 GeV. For each channel, we can compute a contribution to the χ^2 value. The specific form of these χ^2 contributions depends on the details of the model and the experimental data. We can express them mathematically as:

$$\chi^2_{\gamma\gamma,\tau^+\tau^-,b\bar{b}} = \frac{(\mu_{\gamma\gamma,b\bar{b},\tau\tau} - \mu^{exp}_{\gamma\gamma,b\bar{b},\tau\tau})^2}{(\Delta\mu^{exp}_{\gamma\gamma,b\bar{b},\tau\tau})^2}. \tag{3.8}$$

SCANNERS facilitates the calculation of these χ^2 contributions by providing the predicted signal strengths ($\mu_{\gamma\gamma}$, $\mu_{b\bar{b}}$ and $\mu_{\tau^+\tau^-}$) for each parameter combination. In order to evaluate the full representation of the three detected excesses, we compute the aggregate contribution to the χ^2 value as follows:

$$\chi^2_{\gamma\gamma,\tau^+\tau^-,b\bar{b}} = \chi^2_{\gamma\gamma} + \chi^2_{\tau^+\tau^-} + \chi^2_{b\bar{b}}. \tag{3.9}$$

Since we're analysing three independent channels, a good fit to the data is indicated by a total χ^2 value less than a specific threshold. This threshold is chosen based on the number of degrees of freedom in the fit, which in this case is three. Here, a commonly used criterion for three independent measurements is:

$$\chi^2_{\gamma\gamma,\tau^+\tau^-,b\bar{b}} \leq 4. \tag{3.10}$$

We conduct a haphazard search for a 95 GeV and 152 GeV scalar in the 2HDM+S. The definition of the parameter ranges for a 95 GeV is:

$$\begin{array}{ll} m_{h_1} = 94\text{ GeV} - 98\text{ GeV}, & m_{h_2} = 125.09\text{ GeV}, \\ 200\text{ GeV} \leq m_{h_3} \leq 500\text{ GeV} & 400\text{ GeV} \leq m_A \leq 1000\text{ GeV}, \\ -\pi/2 \leq \alpha_{1,2,3} \leq \pi/2, & 400\text{ GeV} \leq m_{h^\pm} \leq 1500\text{ GeV}, \\ 0.5 \leq tan\beta \leq 4.0, & 0 \leq m^2_{12} \leq 5\times 10^5, \\ 1\text{ GeV} \leq v_S \leq 1500\text{ GeV}. & \end{array} \tag{3.11}$$

The parameter ranges for a 152 GeV scalar is therefore provided by:

$$\begin{array}{ll} m_{h_1} = 125.09\text{ GeV}, & m_{h_2} = 148\text{ GeV} - 153\text{ GeV}, \\ 250\text{ GeV} \leq m_{h_3} \leq 800\text{ GeV}, & 400\text{ GeV} \leq m_A \leq 1500\text{ GeV}, \\ -\pi/2 \leq \alpha_{1,2,3} \leq \pi/2, & 400\text{ GeV} \leq m_{h^\pm} \leq 1500\text{ GeV}, \\ 0.5 \leq tan\beta \leq 1.0, & 0 \leq m^2_{12} \leq 5\times 10^5, \\ 1\text{ GeV} \leq v_S \leq 1500\text{ GeV}. & \end{array} \tag{3.12}$$

Our primary goal is to identify regions within the 2HDM+S model's parameter space where the additional scalar particle (S_{95}) interacts strongly enough with gauge bosons and fermions. This could potentially explain the observed excesses in Higgs boson searches around 95 GeV. We focus on parameter points that satisfy two key criteria: theoretical consistency and agreement with the experiment. The parameter points must adhere to all the theoretical constraints imposed on the 2HDM+S model. The model's predicted signal strengths for three channels must be within the 2σ uncertainty range of the latest experimental measurements. By focusing on parameter points meeting these criteria, we can narrow down the most promising regions in the 2HDM+S model that could explain the observed excesses.

Figure 3.1 shows the predicted W boson mass within our 2HDM+S parameter space compared to various experimental measurements. The coloured contours represent parameter points satisfying our criteria. We find good agreement with the ATLAS experiment, the Particle Data Group (PDG), and the global average W boson mass. This agreement holds for both the 95 GeV and 152 GeV scalar masses. In contrast, the predictions from the CDF and LEP experiments fall outside our viable parameter space. This suggests that the 2HDM+S model with these parameters

cannot explain their W boson mass measurements.

Figure 3.2 explores the relationship between the predicted W boson mass and the effective mixing angle $\sin^2\theta_{\text{eff}}$ within the 2HDM+S. Notably, all parameter points with a negative S value satisfy a χ^2 test ($\chi^2_{M_W^{\text{2HDM+S}}} \leq 4$), indicating good compatibility with W boson mass measurements. Our analysis suggests that the 2HDM+S model with the chosen parameter space can reproduce the W boson mass reported by ATLAS and other experiments but not the measurements for CDF and LEP. Additionally, when the predicted W boson mass aligns with the world average, the corresponding effective mixing angle closely resembles the SM prediction.

3.2 The muon $g-2$ with contributions from Vector-Like Leptons

The anomalous magnetic moment of the muon (a_μ) is a highly sensitive probe for physics beyond the SM. The a_μ is a unique quantity that allows for the high precision test of the SM. A persistent discrepancy of 3.5σ exists between the value of a_μ and the SM prediction. This deviation suggests potential contributions from new particles or interactions not accounted for in the SM [112–118]. We explore the 2HDM+$S+f'$ model's ability to explain the a_μ anomaly. This model extends the 2HDM+S scenario by introducing additional BSM fermions. These new fermions can contribute to the a_μ value through one-loop diagrams (Equation 3.13). The equation for this BSM contribution ($\Delta a_\mu^{f'}$) is defined as [24]:

$$\Delta a_\mu^{f'} = \frac{1}{16\pi^2}\sum_i (y_{f'}^i)^2 r_\mu^i F_i(r_{f'}^i), \tag{3.13}$$

where $i = h, S, H, A$, $r_{f'}^i = m_{f'}^2/M_i^2$, and $r_\mu^i = m_\mu^2/M_i^2$. The function F_i is defined as:

$$F_i(r) = \frac{r^3 - 6r^2 + 3r + 6\ln(r) + 2}{6(1-r)^4}. \tag{3.14}$$

By incorporating this additional contribution from BSM fermions, we aim to assess whether the 2HDM+$S+f'$ model can provide a better explanation for the observed a_μ compared to the SM.

To gain insights into the 2HDM+$S+f'$ model, the numerical analysis examines a specific region of its parameter space. This choice ensures our calculations remain theoretically sound and consistent with existing experimental constraints. We fix the masses of the scalar bosons (h, S, H, A, and $H^\pm$) at specific values (125 GeV, 150 GeV, 270 GeV, and 400 GeV, respectively). We limit the value of $\tan\beta$ to lie between 0.5 and 1.0. This parameter space aligns with the one in Ref. [47] which considers:

- Chosen parameters satisfy requirements for perturbative unitarity (avoiding calculations that become unreliable at high energies) and vacuum stability (ensuring the model predicts a stable lowest energy state).

- The model's predictions for the S, T and U parameters (quantifying deviations from the Standard Model in the electroweak sector) are compatible with current experimental measurements.

By carefully selecting the parameter space, we can ensure the validity and relevance of our numerical calculations within the context of the 2HDM+S + f' model.

This analysis suggests that the CP-odd scalar particle (S) within the 2HDM+S + f' model has a limited impact on explaining the observed difference in the muons's magnetic moment. One-loop contributions from the newly introduced fermions (f') in this model are found to be more significant than the contributions arising from the existing CP-even scalars (h, $H^{\pm}$, A) within the base 2HDM+S model. The inclusion of these extra fermionic particles, interacting with the particles of the 2HDM+S model, substantially enhances the contribution of one-loop diagrams to the muon's $g-2$ anomaly compared to contributions from two-loop diagrams. Notably, the presence of these fermions, with masses ranging from 50 GeV to 300 GeV, can potentially explain the observed discrepancy in the muon's magnetic moment.

Figure 3.3 (A, B) and Figure 3.4 (A) illustrate the Δa_μ contributions from various coupling scenarios using Equation 3.13. We concentrate exclusively on the one-loop terms, disregarding the minor contributions from the 2HDM+S model without BSM fermions, as well as the two-loop diagrams involving SM fermions. The BSM fermions interact with the muon through the Lagrangian described in Ref. [119]. These interactions can potentially alter the muon's mass. However, specific flavour symmetries within the model help suppress quantum corrections to the masses of other Standard Model leptons from these new Vector-Like Leptons.

The strength between the muon and the BSM fermion (f') is mediated by a Yukawa coupling. Loop corrections usually lead to a suppression factor of approximately for this coupling. Consequently, we select coupling values ($|y^i_{f'}|$) that adhere to both perturbativity limits and allowable mass corrections for the muon, as shown in Figure 3.4 (B).

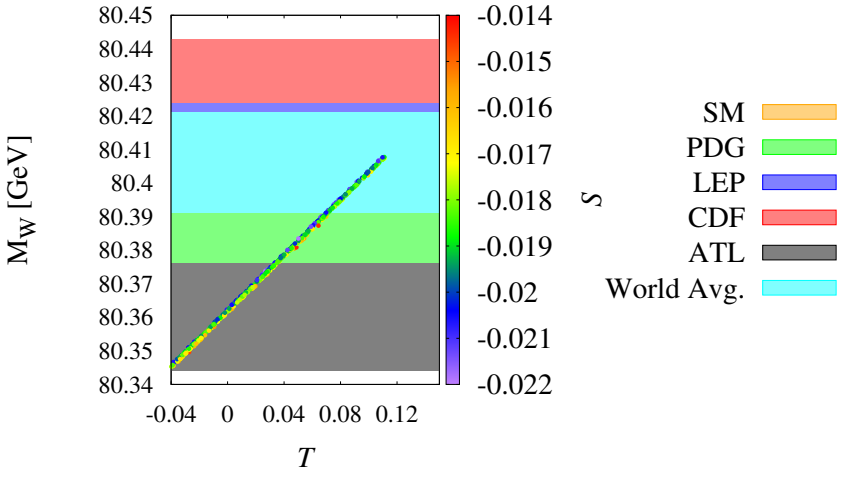

(A)

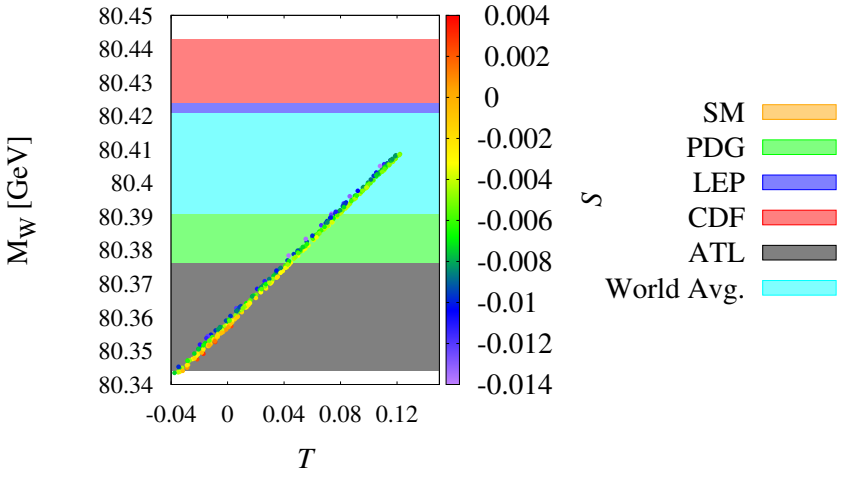

(B)

FIGURE 3.1: The 2HDM+S model's predicted W boson mass for two scalar masses (95 GeV (A) and 152 GeV (B)) versus the Peskin-Takeuchi parameters (T and S) are shown here. Shaded bands indicate the global W boson mass average [75], the SM prediction and individual experimental measurements [85, 109–111].

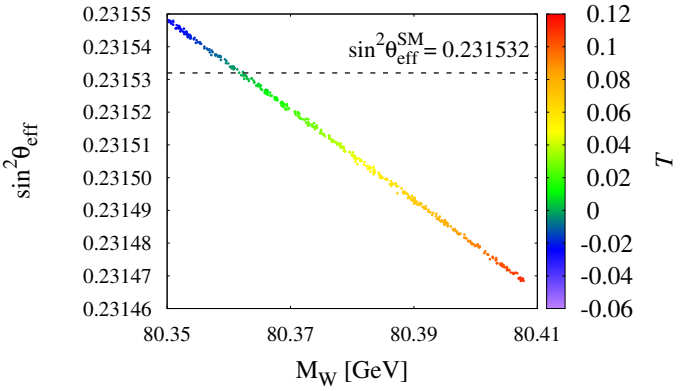

(A)

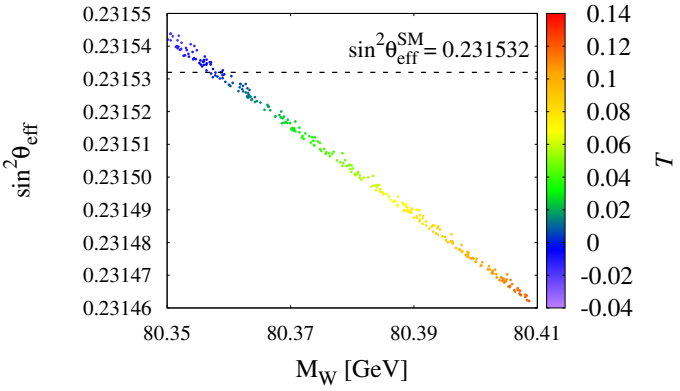

(B)

FIGURE 3.2: These figures depict how the predicted W boson mass and effective mixing angle $\sin^2\theta_{\text{eff}}$ vary within the 2HDM+S model for two scalar masses (95 GeV (A) and 152 GeV (B)). The variations are shown as a function of the Peskin-Takeuchi parameters (T). A dashed line indicates the SM prediction for $\sin^2\theta_{\text{eff}}$.

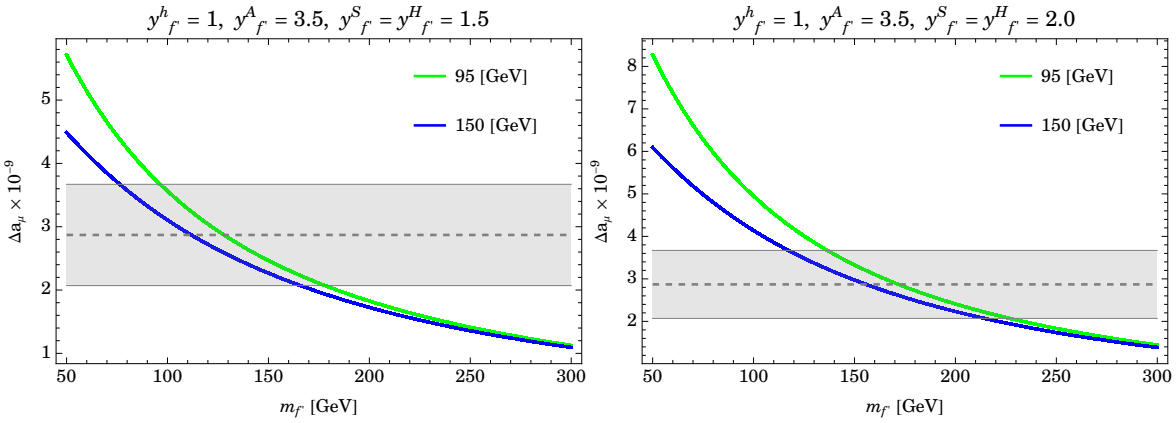

(A) (B)

FIGURE 3.3: Figures (A) and (B) depict the contributions to Δa_μ arising from one-loop diagrams involving BSM fermions with varying masses. The dotted line represents the measured Δa_μ anomaly, and the shaded grey area indicates the 1σ uncertainty range. Each diagram shows the specific coupling strength between the muon and the corresponding BSM fermion.

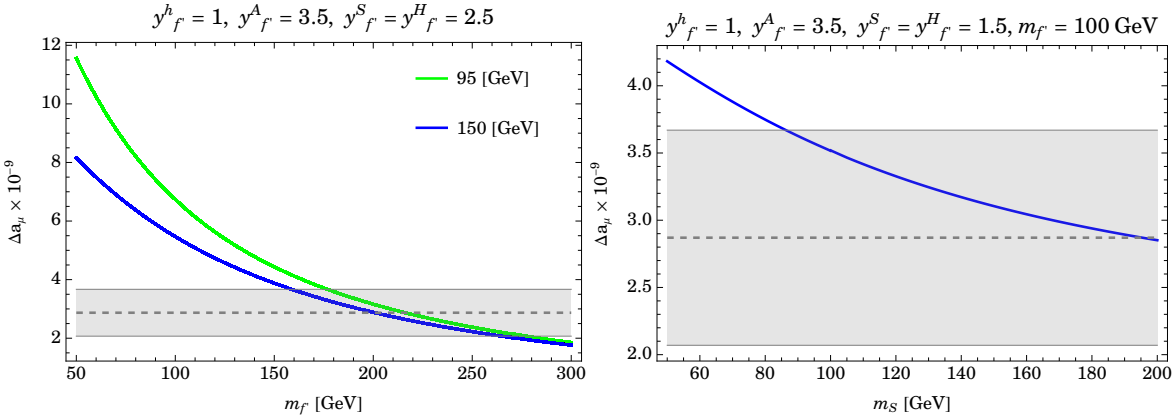

(A) (B)

FIGURE 3.4: Figure (A) explores how Δa_μ is affected by the mass of a BSM fermion within one-loop diagrams. Figure (B) shows the same for the scalar S (assuming a one-loop contribution). The dotted line represents the measured Δa_μ anomaly, and the shaded grey area indicates the 1σ uncertainty range. Each diagram shows the specific coupling strength relevant to the contribution.

Chapter 4

Additional Scalars at Future e^+e^- Colliders

4.1 Future e^+e^- Colliders

The hint of new scalars (at ≈95 GeV) [60, 107, 120–136] directly at the electroweak scale gives further motivation to build e^+e^- accelerators in the future. Numerous e^+e^- accelerators have made substantial progress towards practically and are considered promising candidates for a future accelerator. The CERN-based Circular Electron-Positron Collider (CEPC) [16, 17], the International Linear Collider (ILC) [137, 138], the Compact Linear Collider (CLIC) [139], and the Future Circular Collider (FCC)-*ee* [140, 141] are a few of these.

The comparatively simple final states produced by the collision of electrons and positrons at the e^+e^- colliders provide an ideal experimental environment for accurate measurements and a deeper understanding of the physics involved. Exact measurements of fundamental parameters in the SM, including the masses, lifetimes, and couplings of particles like the Higgs boson, W and Z bosons, and the top quark, are made possible by the simplicity of e^+e^- colliders. Figure 4.1 shows the various production cross-sections for the for the Higgs boson.

When compared to proton-proton colliders, e^+e^- have certain significant advantages, particularly when it comes to the in-depth investigation of the Higgs boson's properties. Accurate evaluations of the Higgs boson's characteristics, such as its coupling to other particles, are made possible by the environment. Moreover, the collision energies of these colliders are flexible, allowing experimenters to work at different energy scales. As a result, weak interactions can be examined at these accelerators, advancing our understanding of the breaking of electroweak symmetry.

Circular Electron-Positron Collider (CEPC)

A particle accelerator called CEPC is being developed with the goal of serving as a factory for Higgs bosons. Operating at a centre-of-mass energy of ≈ 240 GeV, which coincides with the peak of Higgs boson synthesis via electron-positron collision, the tunnel will span around 100 km [143]. With the recoil mass approach, the CEPC can detect Higgs bosons without observing their decay, enabling a model-independent disentanglement of Higgs boson synthesis from its decay [144]. The CEPC can effectively probe Higgs boson properties because of its pristine environment, which allows for exact measurements of Higgs boson decay channels. It is anticipated that the CEPC will yield more than a million Higgs bosons, which will enable precise

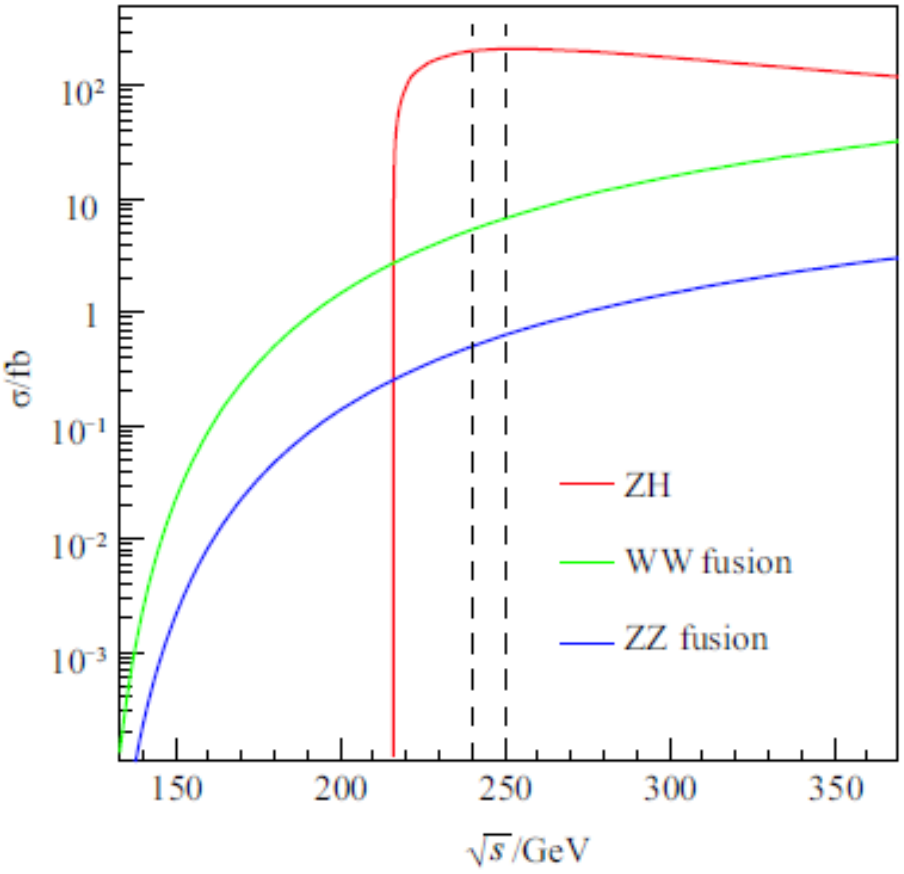

FIGURE 4.1: This graph illustrates the production cross-sections for three key Higgs boson production processes: Higgstrahlung, WW fusion, and ZZ fusion. The processes are plotted as functions of the centre-of-mass energy. The dashed black line indicates the possible working energy range of the Circular Electron-Positron Collider (CEPC) [142].

measurements of the Higgs boson coupling to the Z boson. A schematic view of the CEPC is shown in Figure 4.2.

Moreover, the CEPC has a high sensitivity down to 0.3% for the detection of the Higgs boson decays that are not immediately observable.

Compact Linear Collider (CLIC)

A high luminosity e^+e^- collider with a multi-TeV capacity is called the CLIC. Its goal is to reach very high centre-of-mass energies, well above what is presently possible. High energies are essential for creating heavy particles and investigating novel physics phenomena. It is anticipated that the CLIC will function at three different energy levels: $\sqrt{s} = 380$ GeV, 1.5 TeV, and 3 TeV [139]. Phase one will enable measurements of the Higgs couplings and Higgs widths with previously unheard-of accuracy, as well as investigations on the characteristics of Higgs bosons through phenomena like Higgstrahlung and WW-fusion [145]. High-precision research on top-quark physics [146] is also made possible at this energy level. A threshold scan to top-quark pair production at approximately 350 GeV will occupy a segment of the operational period.

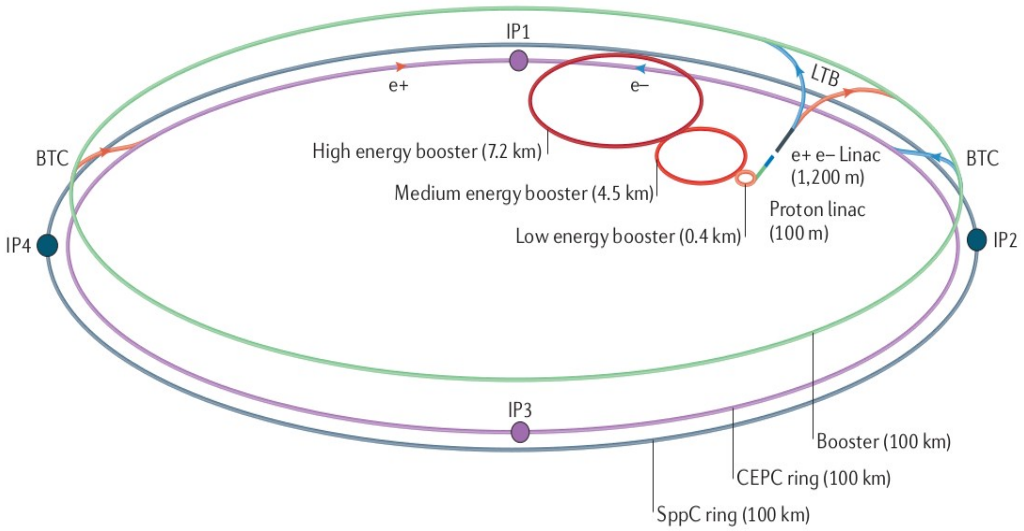

FIGURE 4.2: A diagram depicting the configuration of the Super Proton-Proton Collider (SppC) and the CEPC [143].

New physics phenomena can be discovered in the second stage when a new energy frontier is opened [146]. It is possible to identify the $e^+e^- \to ZHH$ process and to obtain new information about top-quark and Higgs features, such as the unusual Higgs branching ratios and the Higgs self-coupling. The physics potential of CLIC is greatly increased by stage three at 3 TeV, where new electroweak particles or dark matter candidates may be discovered. These particles may be more detectable at CLIC than they are at the HL-LHC. Furthermore, through indirect searches, this stage offers ideal sensitivity to new physics processes at even higher energy scales. The schematic overview of the CLIC is shown in Figure 4.3.

Future Circular Collider (FCC)-*ee*

With the help of the FCC programme, it will be possible to distinguish between the properties of the electroweak and Higgs bosons and determine their interactions with a precision that is orders of magnitude more than what is currently possible. By increasing sensitivity to activities that took place between 10^{-12} and 10^{-10} seconds after the Big Bang, this effort seeks to clarify the circumstances that led to the creation of the modern Higgs vacuum field [147]. The FCC is expected to significantly advance our understanding of rare phenomena at or below the electroweak scale, including dark matter, WIMPs, and neutrino mass creation, as well as our ability to find new particles.

As a key tool for particle physics research, the FCC-*ee*, as part of the FCC project, is anticipated to create significant quantities of various particles, including Z boson pairs, Higgs bosons, and top quark pairs. The FCC-*ee* schematic arrangement is displayed in Figure 4.4.

International Linear Collider (ILC)

The International Linear Collider (ILC) is a next-generation particle accelerator specifically designed to shed light on the intricacies of the Higgs boson. Its primary focus

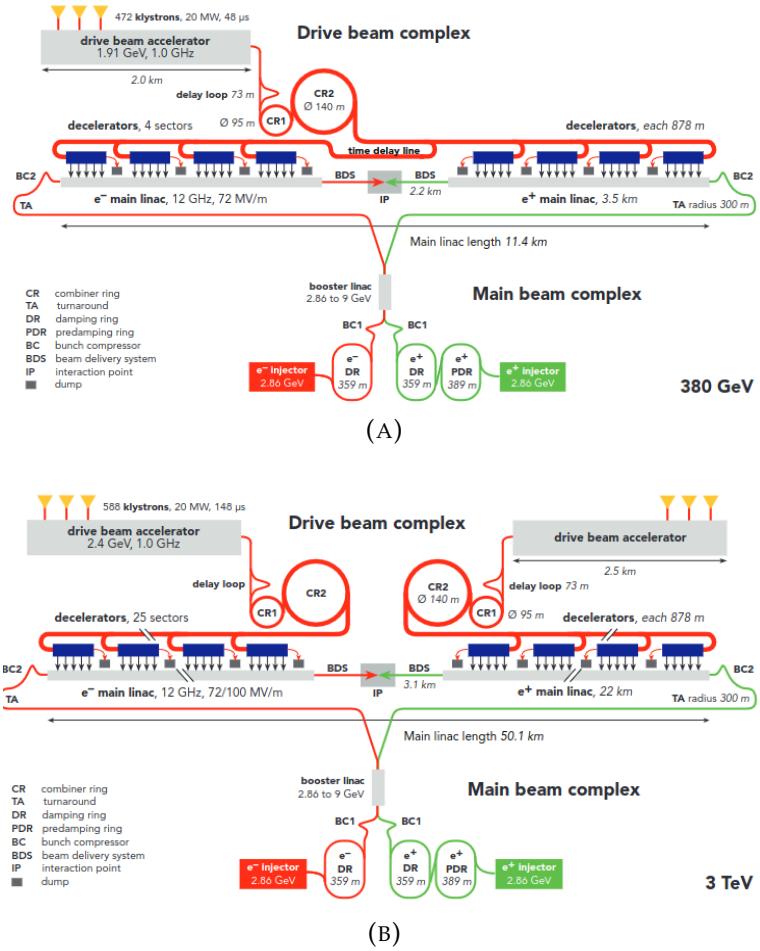

(A)

(B)

FIGURE 4.3: A schematic overview of the CLIC complex at 380 GeV (A) and at 3 TeV (B) [146].

is to characterise the Higgs boson and its interactions with exceptional precision and minimal assumptions about underlying theoretical models [148]. While the LHC has already made significant contributions to our understanding of the Higgs boson, the ILC offers several advantages. Unlike the LHC, which relies on proton-proton collisions, the ILC utilises electron-positron collisions. This approach allows for cleaner and more controlled interactions, leading to more precise measurements of the Higgs boson's properties.

Furthermore, the ILC's high luminosity and energy capabilities are expected to make it highly sensitive to rare or weakly interacting decays of the Higgs boson. This sensitivity could potentially unveil new weakly interacting massive particles or shed light on alternative dark matter models that might be difficult to detect at other colliders.

The centre-of-mass energy of the ILC is exactly specified and modifiable [149, 150]. Compared with Higgs signal processes, SM events are created at a similar intensity and do not significantly exceed in size. This property makes the simple selection of Higgs boson occurrences easier. A recoil Z boson uniquely identifies Higgs boson occurrences in its first stages at $\sqrt{s} = 250\,\text{GeV}$. Since order-1 parity violation is present in all electroweak processes at energies above the Z resonance,

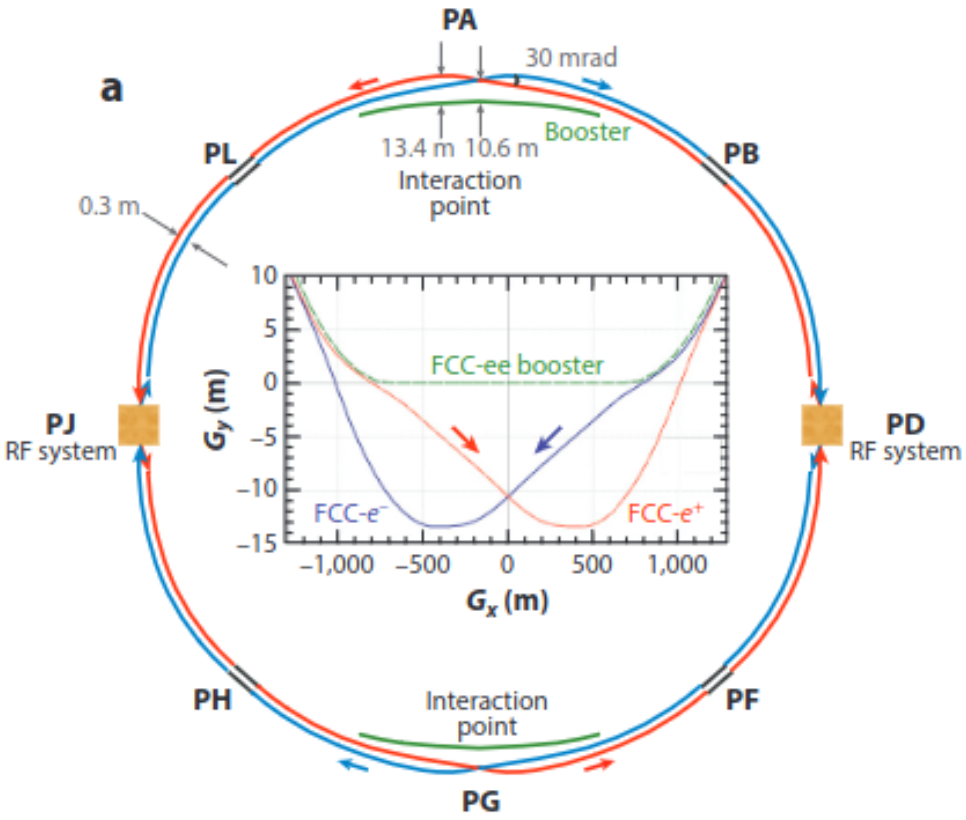

FIGURE 4.4: The overall layout of the FCC-*ee*. [147].

the significant effects of beam polarisation provide access to important physics data.

For accurate research using polarised beams, the ILC is a versatile particle accelerator that can be upgraded to greater energies. It investigates Higgs boson couplings, precisely monitors top quark properties, and closely examines important reactions, which may lead to the discovery of novel physics. It also makes searches for weakly linked particles easier, which makes it an innovative tool for future discoveries in particle physics. Figure 4.5 depicts the ILC's layout schematically.

4.2 Additional Scalars at Future e^+e^- Colliders

Recent excesses detected at the LHC that point to a 95 GeV mass for a possible scalar have piqued the interest of physicists. We thus perform a detailed analysis of possible signals in a 2HDM+S model [47, 48] and start working on a feasibility study for a future e^+e^- collider. We investigate a range of model-independent parameters in the context of the 2HDM+S framework through comprehensive parameter scans and statistical analysis in order to identify locations that may be responsible for the excesses seen in the $S \to \gamma\gamma$, $b\bar{b}$, W^+W^-, $\tau^+\tau^-$ decay channels.

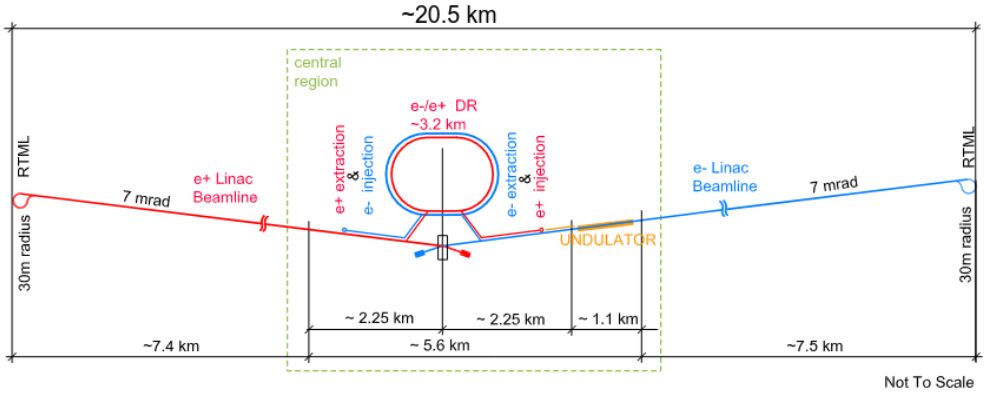

FIGURE 4.5: A schematic view of the International Linear Collider (ILC) [148].

4.2.1 Statistical analysis in the 2HDM+S parameter space

In our research, we impose a number of theoretical preconditions on the parameter space of the 2HDM+S. In order to ensure the physical feasibility of the electroweak minimum for the parameter configuration under consideration, the electroweak vacuum needs to be stable or meta-stable, which implies that its lifetime is significantly longer than the age of the universe. To be more precise, we impose constraints on the scalar couplings in order to exclude parameter combinations in which the scalar potential is not lower-bound restricted. To assess the electroweak vacuum's lifetime, we utilise the SCANNERS tool [47].

Appendix A contains an overview of the experimental constraints. The degree of concordance between experimental data and theoretical signal rate predictions is evaluated using a χ^2 analysis. The experimental findings suggest that taking into account signal rates connected to a scalar resonance of 95 GeV is the most appropriate way to explain the excesses at that energy [58, 59, 107, 151]:

$$\mu^{exp}_{\gamma\gamma} \pm \Delta\mu^{exp}_{\gamma\gamma} = 0.27^{+0.10}_{-0.09}, \tag{4.1}$$

$$\mu^{exp}_{bb} \pm \Delta\mu^{exp}_{bb} = 0.117 \pm 0.057, \tag{4.2}$$

$$\mu^{exp}_{\tau\tau} \pm \Delta\mu^{exp}_{\tau\tau} = 0.6 \pm 0.25, \tag{4.3}$$

$$\mu^{exp}_{WW} \pm \Delta\mu^{exp}_{WW} = 14.6 \pm 6.8. \tag{4.4}$$

The cross-sections and branching ratios are multiplied, and the resulting product is divided by the corresponding predictions for the SM Higgs boson at the same mass to determine the signal strength, which can be represented as follows:

$$\mu_{XX} = \frac{\sigma^{\mathrm{BSM}}(gg \to h_i) \times \mathrm{BR}^{\mathrm{BSM}}(h_i \to XX)}{\sigma^{\mathrm{SM}}(gg \to H(m_{h_i})) \times \mathrm{BR}^{\mathrm{SM}}(H(m_{h_i}) \to XX)}, \tag{4.5}$$

where $X = \gamma,\ b,\ \tau,\ W$, and $i = h_1, h_2, h_3, A, H^\pm$.

The branching ratios for a 95 GeV scalar were obtained using N2HDECAY [152], and the cross-sections were taken from the CERN Yellow reports. The 1σ variations are used to report experiment uncertainty. Using parameter scans from ScannerS, the values $\mu_{\gamma\gamma}$, μ_{bb}, and $\mu_{\tau\tau}$ corresponding to the experimentally observed signal strengths were obtained. Using ScannerS, the branching ratios of the Higgs-like bosons were also calculated. This allowed for the construction of χ^2 contributions for each observed excess, which are given as follows:

$$\chi^2_{XX} = \frac{\left(\mu_{XX} - \mu^{\text{exp}}_{XX}\right)^2}{\left(\Delta\mu^{\text{exp}}_{XX}\right)^2}. \tag{4.6}$$

We determine the cumulative χ^2 contribution as follows in order to assess the complete representation of the three excesses as well as an additional excess in the WW channel (where the signal rates were derived from ScannerS and observed results from experiments were obtained from Ref. [59]):

$$\chi^2_{95} = \chi^2_{\gamma\gamma} + \chi^2_{\tau^+\tau^-} + \chi^2_{b\bar{b}} + \chi^2_{WW}, \tag{4.7}$$

where we can sum the four distinct χ^2 contributions by treating the data for the four channels where the excesses were recorded as independent measurements. In the following quantitative analysis, we will consider parameter points to be appropriate models of the excess phenomenon if they are able to satisfactorily describe the combined effect of the four individual excesses at a confidence level of 1σ or above. When four measurements are taken into consideration separately, this criterion is equivalent to the requirement that $\chi^2_{95} \leq 12$.

We see an apparent mismatch between the signal levels from the LEP and LHC experiments when we look at Figure 4.6. In addition to being caused by $S(95) \to WW$, the excess in WW events also results from a coincidence involving $S(152) \to WW$, in which one lepton is produced by the WW decay and another by the decay of $S(95)$. This shows that WW processes are not the only cause of most of this excess. This is because $H \to SS'$, which are di-boson signatures, are the source of it. This clarifies that the 95 GeV signal originates from di-boson signatures, as well as the enhanced signal intensity of the WW excess.

4.2.2 Discovery Potential of a 95 GeV Scalar at Future e^+e^- Collider

A comprehensive set of benchmark investigations is used to evaluate the CEPC's capability for accurate Higgs measurements [153]. By using Geant4 [154, 155] simulations based on CLID SiD and CLIC ILD detector concepts [156, 157], which are derived from the ILC, the studies take into account the beam spectrum and initial state radiation of CEPC while taking into account $\gamma\gamma \to$ hadron backgrounds and pertinent SM processes from e^+e^- collisions. Through the study of the Higgstrahlung process $e^+e^- \to ZH$ at centre-of-mass energies around $\sqrt{s} = 250$ GeV, these simulations enable accurate evaluations of the interaction between the Higgs boson and the Z boson, as well as the consequences that arise. The coupling g_{HZZ} can be

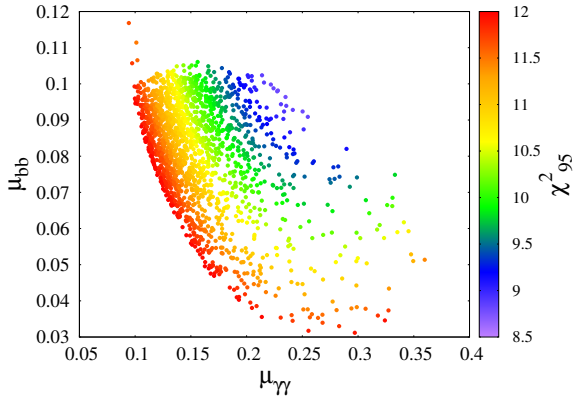

(A)

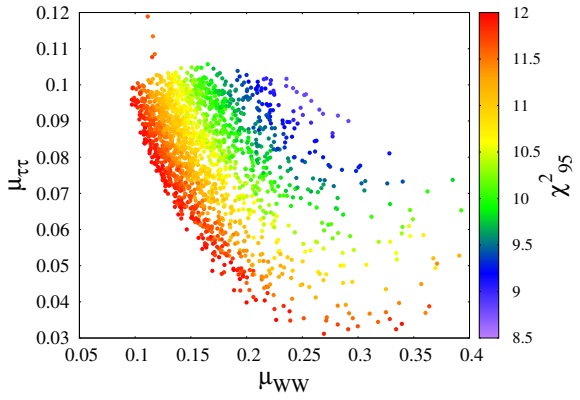

(B)

FIGURE 4.6: For the 95,GeV scalar, signal strengths for various final states are plotted against the total χ^2_{96}. (A) Depicts the $\gamma\gamma$ and $b\bar{b}$ signal strengths. (B) Displays the WW and $\tau\tau$ signal strengths.

found model-independently through the reconstruction of the Z recoil mass, which is defined as follows:

$$M_{recoil} = \sqrt{s + M^2_{\mu^+\mu^-} - 2(E_{\mu^+} + E_{\mu^-})\sqrt{s}}, \tag{4.8}$$

where the muons' energies are E_{μ^+}, E_{μ^-}, and their invariant mass is $M_{\mu^+\mu^-}$.

For a given centre-of-mass, e^+e^- beams with 80% left- and right-handed polarisation and an integrated luminosity of 500 fb^{-1} are used to construct the SM backgrounds and signals from BSM models. Applying cuts on the leading and subleading jets and muons improves signal events. These comprise extra cuts made to:

$$E_{b,\mu} > 5\,GeV,\ M^{recoil}_{\mu^+\mu^-} < 120\,GeV, M_{b\bar{b}} < 100\,GeV. \tag{4.9}$$

A significant dilution effect results from several background events surviving the initial cuts, necessitating the employment of additional event selection criteria. In order to train the Deep Neural Network (DNN) model and achieve the best possible discrimination between the signal and the background, a second event selection criterion is therefore necessary. Key factors like the energy of the b-tagged jets

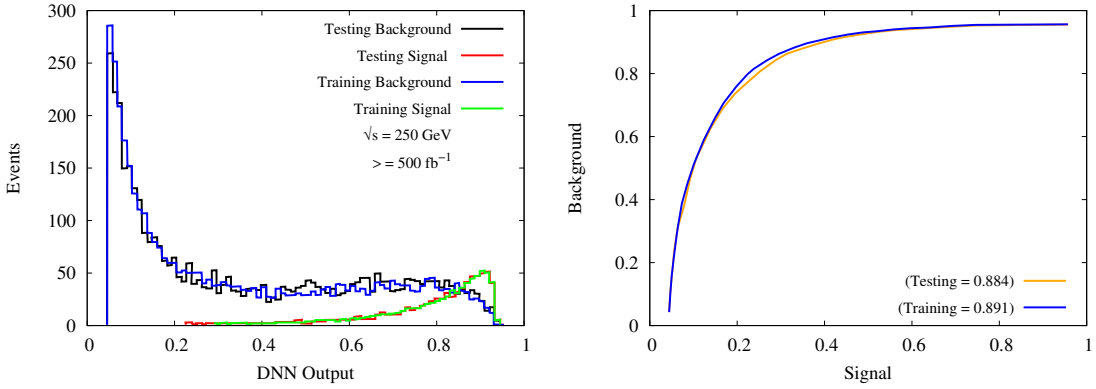

(A) (B)

FIGURE 4.7: The output of the DNN after testing and training the recoil mass is included (left), and the corresponding ROC curve (right) for $\sqrt{s} = 250\,\text{GeV}$ are included.

and muons, their azimuthal and polar angles, their invariant mass, and their recoil mass were highlighted throughout the DNN model's training process using physical objects. Using a grid technique for hyperparameter search, the ideal DNN structure was found, yielding a model with four completely connected hidden layers. Certain hyperparameters were used in the training, including the learning rate and batch size, to name a couple. The output distributions for specific class labels were analysed on both training and test samples in order to resolve overfitting problems. Even though the network is very tiny, regular assessment makes sure overfitting doesn't occur.

The normalised DNN model output distributions for the recoil mass and signal background events in the training and testing datasets are shown in Figure 4.7 (A). For both background and signal events, significant variations are found in the distributions between the training and validation datasets. The performance of the model is visualised by a Receiver Operating Characteristic (ROC) curve, located on the right side of Figure 4.7 (B). This curve compares the model's ability to identify positive and negative cases correctly. To summarise the model's overall performance, we calculate the Area Under the Curve (AUC) for the training and testing datasets. Training AUC score are 0.884 and the testing AUC score is 0.891.

The significance of the signal over the background is calculated by:

$$\sigma(\delta_{sys}) = \frac{S}{\sqrt{B + (\delta_{sys} \cdot B)^2}}, \tag{4.10}$$

where the SM background cross-section is $B = \sigma_{bkg} \times \mathcal{L}$, σ_{bkg}, and the BSM signal cross-section at 10% SM Higgs is $S = \sigma_{sig} \times \mathcal{L}$, σ_{sig}. Since it is specific to Lepton colliders, the recoil mass approach may be used to tag $e^+e^- \to ZS$ events regardless of the Higgs boson decay, making it a powerful tool for model-independent observations. These include the branching ratios of the Higgs boson and the inclusive $e^+e^- \to ZS$ with $Z \to \mu^+\mu^-$ and $S \to b\bar{b}$ production cross-section, which we refer to as $\sigma_{ZS,\, S\to b\bar{b}}$. We give an anticipated recoil mass at both $\sqrt{s} = 200\,(A),\ 250\,(B)\,\text{GeV}$ at $\mathcal{L} = 40\,\text{fb}^{-1}$ at CEPC in Figure 4.8. As supported by the Chinese high-energy community, the

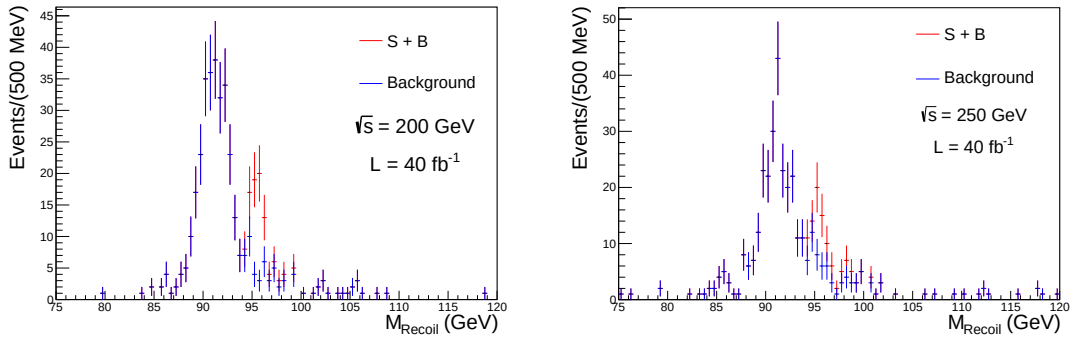

(A) (B)

FIGURE 4.8: Recoil-mass distributions illustrating the anticipated signal events with $m_S = 95.5\,\text{GeV}$ and pertinent background events, assessed post DNN classification output for (A) $\sqrt{s} = 200\,\text{GeV}$ and (B) $\sqrt{s} = 250\,\text{GeV}$ at an integrated luminosity of $\mathcal{L} = 40\,\text{fb}^{-1}$.

proposed CEPC will run for 10 years at 24-250 GeV with the goal of accumulating one million Higgs events at $5\,\text{ab}^{-1}$ integrated luminosity [158, 159].

From the recoil mass analysis, a statistical accuracy of 1.36% is found for $\sigma_{ZS,\,S\to b\bar{b}}$ at an integrated luminosity of $5\,\text{ab}^{-1}$ and a centre-of-mass of $s = 250\,\text{GeV}$; this corresponds to a relative precision of 0.46%. The main source of uncertainty in the measurement of scalar mass is the beam energy spread, which is 0.16% at CEPC. A low-mass tail from radiation (8.31 GeV width, 8.75 GeV relative mass resolution) and a Gaussian core are included in the fit of the recoil mass distribution. Estimated statistical accuracy of m_S is 6.9 MeV, which could be enhanced with knowledge of scalar decay [142].

Chapter 5

Conclusions

Particle physics has witnessed significant strides in understanding subatomic particle behaviour. A key area of focus is the 95 GeV excess observed in experimental data. This anomaly aligns with the theoretical prediction of a neutral component within an $SU(2)_L$ triplet with hypercharge $Y = 0$. Previously, the CDF II experiment reported a deviation in the W boson mass from the SM predictions, and this resulted in a world average of $m_W^{World\ avg.} = 80.406 \pm 0.015$. However, recent ATLAS measurements align more closely with the SM. This discrepancy highlights the need for a deeper understanding of electroweak interactions.

Studying the Higgs boson's production with jets and tau leptons provides valuable insights into Brout-Englert-Higgs mechanisms and their interactions. This is crucial for validating the SM and exploring extensions like the Type II Two Higgs Doublet (2HDM). The possibility of a charged Higgs boson below 100 GeV adds a layer of complexity, potentially impacting the Higgs sector and electroweak symmetry breaking. This thesis focused on the 2HDM+S model. It investigated its compatibility with electroweak precision observables via the Peskin-Takeuchi parameters (S, T and U). We incorporated one-loop corrections to these parameters, allowing us to calculate the W boson mass dependence. We employed a χ^2 analysis to explore the observed enhancements at 95 GeV and 152 GeV across various channels. This allowed us to assess the model's prediction of an upward shift in the W boson mass.

Furthermore, we extended our study to the muon anomalous magnetic moment (Δa_μ) by introducing Vector-Like Leptons into the 2HDM+S model. This enabled the evaluation of one-loop contributions to Δa_μ, potentially explaining the discrepancy between the measured and predicted values of the muon's anomalous magnetic moment. Our analysis demonstrates that the 2HDM+S parameter space aligns well with various experimental measurements, including the global W boson mass average. However, deviations from some specific measurements, like those from CDF II and LEP, exist. Additionally, our results highlight the importance of Vector-Like Leptons in enhancing the one-loop contributions to Δa_μ, potentially resolving the observed discrepancy.

We also conducted an extensive analysis of the 2HDM+S model, showcasing its ability to reconcile experimental findings with theoretical constraints. We demonstrated the model's potential to explain the observed excesses around 95 GeV in various channels ($\gamma\gamma$, $\tau^+\tau^-$, $b\bar{b}$ and WW). Tools like HIGGSBOUNDS and HIGGSSIGNALS were employed to assess the model against collider search exclusion limits and to quantify its agreement with observed Higgs properties using χ^2 analysis.

The observed discrepancy between LHC and LEP experiments in WW events, interpreted as di-boson signatures involving both $S(95)$ and $S(152)$, highlights the intricate dynamics within the model and suggests avenues for further investigation. A recent paper [136] studied a model, the Scale Invariant Scotogenic model, to explain anomalies in W boson mass measurements and the observed 95 GeV excess. This model allows for light neutrino masses and a dark matter candidate. They found a parameter space where the model could explain both the W boson mass anomaly and the 95 GeV excess. However, this required the dilaton particle ($m_D \approx 95\,\text{GeV}$) to decay invisibly. While LHC di-Higgs production wouldn't be affected, future e^+e^- colliders could see significant changes (20% decrease to 70% increase) in double Higgstrahlung compared to the SM. Future research could involve a more detailed analysis of these discrepancies and their implications for the model's parameter space.

This research adds to the ongoing search for physics beyond the Standard Model. Our findings highlight the potential of the 2HDM+S model to explain a range of experimental observations.

Appendix A

ScannerS

In particle physics extensions beyond the Standard Model (SM), adhering to parameter ranges consistent with existing data is crucial. SCANNERS [160] is a tool designed for generating and verifying parameter sets in various beyond-SM models. It performs systematic scans across a model's parameter space on a point-by-point basis, rather than providing broad model-wide conclusions.

SCANNERS applies individual constraints to each randomly generated parameter point, selecting those that comply. This method does not offer a definitive best-fit point or a complete likelihood distribution, making it unsuitable for drawing broad conclusions about a model's overall fit. However, it's effective for creating phenomenological benchmarks and focusing on specific areas within the parameter space.

The strength of SCANNERS lies in its simplicity and ability to conduct targeted scans, even in areas not encompassing the model's optimal fit point. Its design allows for easy re-evaluation of parameter points when constraints are updated without the need for new scans.

A.1 Constraints

The tool SCANNERS operates by enforcing experimental constraints at a 95% confidence level, approximately equivalent to 2 standard deviations. Unlike these experimental constraints, the theoretical ones are mere exclusions and do not carry a statistical interpretation. As a result, SCANNERS identifies points that conform to the theoretical framework, yet these points are not necessarily excluded based on observational data at around a 95% confidence level. SCANNERS incorporates these constraints at three distinct operational levels. The first level, labeled **skip**, completely disregards the specific constraint, omitting any associated computations and consequently not subjecting any parameter points to this constraint. The second level, **ignore**, involves performing all relevant calculations and retaining the results, but without enforcing the constraint on the parameter points. The most stringent level, **apply**, is where only those points that meet the specific constraint are accepted.

A.1.1 Theoretical constraints

Theoretical constraints in particle physics models serve to maintain internal coherence and self-consistency. These constraints are binary, meaning a parameter point either

satisfies them and is considered valid, or fails to meet them, leading to its exclusion. SCANNERS enforces several key theoretical constraints:

- **Perturbative Unitarity**: This principle ensures the consistency of scattering amplitudes at high energies, demanding that the sum of probabilities for all outcomes of a scattering process equals 1. In SCANNERS, perturbative unitarity is validated by ensuring the eigenvalues $\mathcal{M}^{i}_{2\to 2}$ of the $2 \to 2$ scattering matrix do not exceed 8π. This constraint, particularly relevant in extended Higgs frameworks, is subject to potential modifications due to loop corrections [161] or finite-energy effects [162–164].

- **Vacuum Stability**: This pertains to the potential of the vacuum transitioning to a lower energy state, which could lead to vacuum decay. For models where EW vacuum stability is unproven or lacks analytical solutions, SCANNERS links to the EVADE [165] library.

- **Boundedness from below**: This condition ensures the stability of a quantum field theory by requiring the potential energy to be bounded as field values increase indefinitely. It's essential for the stability of the vacuum state and the definition of a well-grounded state in the theory. SCANNERS incorporates analytical solutions to enforce this constraint.

Overall, SCANNERS implements these constraints to maintain the physical validity of parameter points within theoretical models, focusing on principles like unitarity, vacuum stability, and boundedness.

A.1.2 Constraints on Electroweak Precision Observables

The Electroweak Precision Observables (EWPO) consist of a collection of both theoretical predictions and experimental measurements that are linked to the electroweak force. This force represents the unification of electromagnetic and weak nuclear interactions in the realm of particle physics. These observables play a pivotal role in assessing the consistency and precision of the SM. SCANNERS incorporates fit results for Electroweak Precision Observables (EWPOs), specifically the oblique parameters U, T and S. The obtained results are employed to create a correlation matrix for these parameters. SCANNERS utilises findings from Refs. [106, 166] to compute model predictions for the oblique parameters, applicable to any number of scalar $SU(2)_L$ doublets and singlets.

Observational measurements are vital for evaluating the reliability and precision of the Standard Model (SM). The tool SCANNERS is designed to incorporate fit outcomes for Electroweak Precision Observables (EWPOs), with a specific focus on the oblique parameters, denoted as S, T, and U. These fit results are instrumental in creating a correlation matrix for these parameters. Moreover, SCANNERS utilises methodologies from specific references [106, 166] to compute predictions for the oblique parameters. This computation applies to any number of scalar $SU(2)_L$ doublets and singlets, providing a broad range of modelling capabilities within the tool.

A.1.3 Flavour Physics

Flavour physics investigates phenomena related to transforming quarks and leptons from one type to another, a process known as flavour changing. This can occur through weak interactions, which are responsible for processes like beta decay. Given that, every model presently employed in ScannerS is inherently flavour-conserving [167], charged Higgs exchange is the primary source of contributions to the majority of flavour observables. In the Two Higgs Doublet Model (2HDM), there is a charged Higgs sector which either does not exist or reflects the characteristics of the model itself. For flavour constraints, our approach is similar to how we handle Electroweak (EW) precision constraints, and we base it on fit outcomes from specific references [104]. These fit results provide constraints at the 2 standard deviations (2σ) level within the $m_{H^\pm} - \tan\beta$ parameter space of 2HDM. Notably, these constraints are also applicable to extended models that include additional singlets, such as in the Two Higgs Doublet Model with an Additional Scalar (2HDM+S), demonstrating their broader relevance in theoretical physics modelling.

A.1.4 Higgs constraints

One of the key challenges in exploring models with extended Higgs sectors is ensuring compatibility with the established properties of the 125 GeV Higgs boson observed at the LHC and other experiments. The ScannerS program tackles this challenge by leveraging functionalities within the HiggsTools framework [100].

ScannerS utilises HiggsBounds, a component of HiggsTools, to assess the theoretical compatibility of a model's Higgs sector with experimental data. This tool takes a theoretical model as input, typically defined by parameters governing the Higgs boson's properties and interactions with other particles. Additionally, it requires a set of benchmark scenarios - specific parameter configurations of particular interest within the model. HiggsBounds performs several key tasks. It calculates the masses of the Higgs bosons in the model and their couplings to other particles. This involves solving the equations related to the Higgs potential and diagonalising the mass matrix. Using the benchmark scenarios, the derived Higgs properties are compared with data from experiments like the LHC, LEP, and others. HiggsBounds also performs a statistical analysis to determine if the model's predictions are consistent with experimental observations. This considers uncertainties in measurements and the overall compatibility of predictions with the data.

Similar to HiggsBounds, ScannerS employs HiggsSignals, another component of HiggsTools. HiggsSignals also takes a theoretical model as input, defined by parameters affecting the Higgs sector. These parameters influence characteristics like Higgs boson masses, production rates, and decay modes. Using benchmark scenarios, HiggsSignals calculates various properties of the Higgs boson, including masses, branching ratios for different decay modes, and production cross-sections for various processes. Similar to HiggsBounds, it compares the calculated Higgs properties with experimental data and performs a statistical analysis to assess the compatibility of the model's predictions with the observations.

To ensure accurate predictions of Higgs boson branching ratios and total decay widths, ScannerS incorporates a modified version of the HDECAY code [47, 168–170]. This modified version allows for model-specific forecasts while incorporating

the latest Quantum Chromodynamics (QCD) corrections and accounting for off-shell effects, which are crucial for precise calculations. For reliable cross-sections, SCANNERS utilises a detailed parametrisation of Next-to-Next-to-Leading Order (NNLO) QCD calculations key processes like gluon fusion and bottom quark pair ($b\bar{b}$) associated Higgs production. These parametrisation are derived from tools such as SUSHI-1.6.1 [101, 102].

Additionally, SCANNERS utilises cross-section parametrisations incorporated within the HIGGSBOUNDS framework [103]. These parametrisations encompass diverse cross-section calculations, including those associated with W/Z boson associated production ($VH@NNLO$) and Next-to-Leading Order (NLO) QCD processes for top quark associated charged Higgs production. By combining these tools and functionalities, SCANNERS provides a comprehensive framework for exploring extended scalar sectors while ensuring compatibility with established experimental data on the Higgs boson.

Appendix B

Deep Neural Network

We simulated the Higgs-strahlung process at a future electron-positron collider with a center-of-mass energy of $\sqrt{s} = 250\,\text{GeV}$. This process is illustrated in Figure B.1 and involves the production of a Higgs boson (assumed to have a mass of 95.5 GeV) alongside a Z boson. The simulation employed a suite of software tools: `MadGraph5` [171] generated the initial particle interactions, `Pythia8` [172] simulated the decay of these particles into more fundamental ones, `Delphes`, tuned for the CEPC detector [173–175], modelled the detector's response, and `FastJet` [176] with the anti-k_T algorithm [177] identified jets of particles using a cone size parameter of $R = 0.4$. Both signal (Higgs boson) and background processes used dynamic scales for a more accurate simulation. The processes that were generated are $e^+e^- \to ZS,\ S \to b\bar{b},\ Z \to \mu^+\mu^-$ for the background and $e^+e^- \to Zb\bar{b},\ Z \to \mu^+\mu^-$ for the signal.

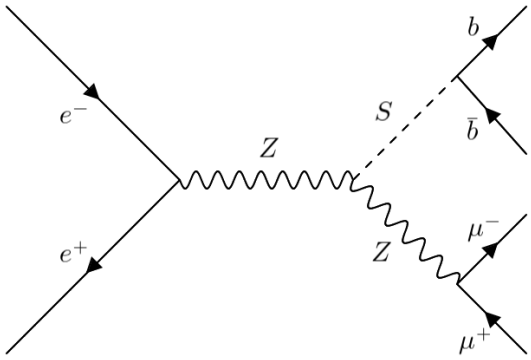

(A)

FIGURE B.1: This is an illustration of the signal process $e^+e^- \to ZS, Z \to \mu^+\mu^-, S \to b\bar{b}$ with $m_S = 95\,\text{GeV}$.

B.1 Signal and Background discrimination

We applied specific selection criteria to distinguish the Higgs boson signal from background noise. The analysis required the detection of exactly two muons and the identification of two jets originating from b-quarks. Additionally, minimum energy thresholds were set for the leading and sub-leading b-tagged jets and muons (all above 5 GeV). Furthermore, we analyzed the recoil mass distribution (produced using the Equation 4.8 function) for both signal and background (shown in Figure 4.7

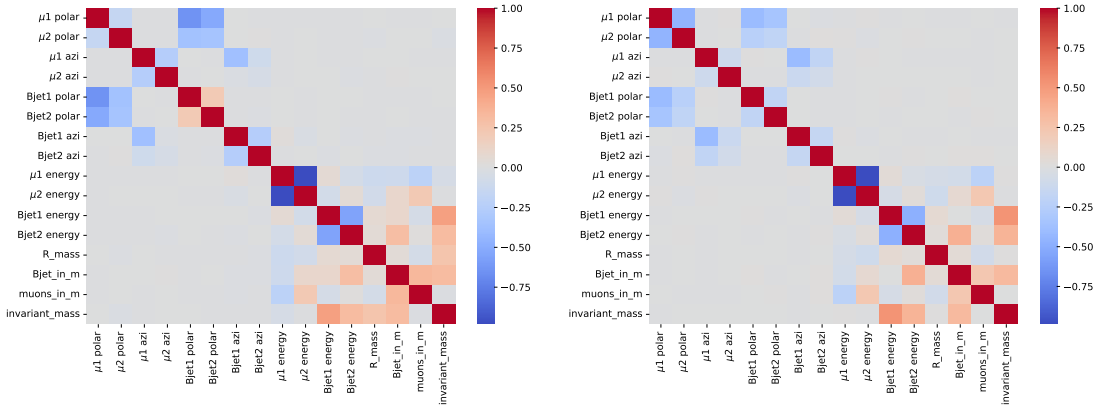

(A) (B)

FIGURE B.2: The correlation matrices for the background (A) and signal (B) at a mass of $m_S = 95\,\text{GeV}$. These are for both the leading and sub-leading muons and b-tagged jets to determine the most sensitive features that will be used in the dataset for the DNN model.

A). We imposed further cuts on the recoil mass ($M_{\text{recoil}} < 120\,\text{GeV}$) and the invariant mass of the b-quark pair ($m_{b\bar{b}} < 100\,\text{GeV}$) to enhance the signal.

The chosen machine learning model is the Deep Neural Network (DNN) because of its effectiveness in event classification. We used 16 input variables such as energy of b-tagged jets (E_b) and muons (E_μ), azimuthal angle of the b-tagged jets (ϕ_b) and muons (ϕ_μ), polar angle of the b-tagged jets (θ_b) and muons (θ_μ), invariant mass of the b-tagged jets ($m_{b\bar{b}}$) and the recoil mass for muons (M_{recoil}) as motivated in Figure B.2. The dataset is split into training and testing with 70% of the events being for used training and the 30% for testing.

The DNN is constructed from 12 input layers, each having 39 neurons. The batch size is set to 30, and the number of epochs is 100. The chosen optimiser is Adam, and the learning rate is 0.0003253. In order to achieve optimal performance for the DNN, a hyperparameter optimisation algorithm is deployed to find the best possible hyperparameters that will maximise the accuracy of the DNN. These hyperparameters were optimised using Weights & Biases [178]. Weights & Biases is the machine learning platform that allows developers to build better models faster. It provides for iteration on datasets, evaluates model performance, reproduces models, visualises results (Figure B.3) and spots regressions.

Although the chosen network is relatively small, ensuring it doesn't overfit the training data is crucial. Overfitting occurs when a model memorizes the training data too well and performs poorly on unseen data. To investigate this, we will analyze the model's output distributions for each class label, comparing the results from both the training and test datasets. This comparison will help us identify potential overfitting issues.

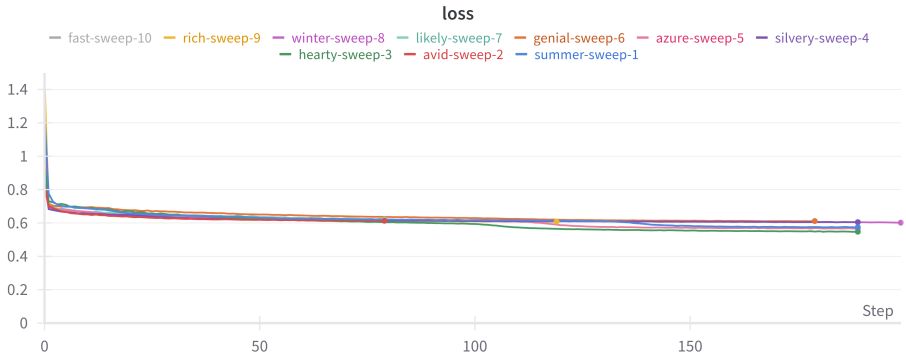

(A)

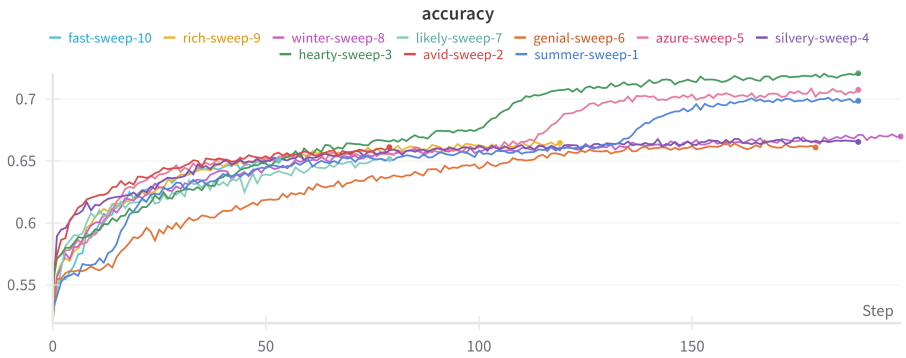

(B)

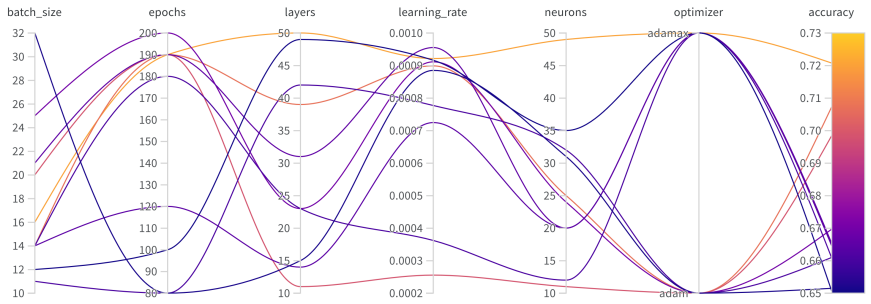

(C)

FIGURE B.3: The loss function (A), Accuracy (B) and Sweeps (C) from the hyperparameter optimisation are illustrated here. This is just one of the many runs that were deployed to tune the hyperparameters of the DNN.

Bibliography

[1] Mary K. Gaillard, Paul D. Grannis, and Frank J. Sciulli. "The Standard model of particle physics". In: *Rev. Mod. Phys.* 71 (1999), S96–S111. DOI: 10.1103/RevModPhys.71.S96. arXiv: hep-ph/9812285.

[2] Serguei Chatrchyan et al. "Observation of a New Boson at a Mass of 125 GeV with the CMS Experiment at the LHC". In: *Phys. Lett. B* 716 (2012), pp. 30–61. DOI: 10.1016/j.physletb.2012.08.021. arXiv: 1207.7235 [hep-ex].

[3] Serguei Chatrchyan et al. "Observation of a New Boson with Mass Near 125 GeV in pp Collisions at $\sqrt{s}$ = 7 and 8 TeV". In: *JHEP* 06 (2013), p. 081. DOI: 10.1007/JHEP06(2013)081. arXiv: 1303.4571 [hep-ex].

[4] Georges Aad et al. "Observation of a new particle in the search for the Standard Model Higgs boson with the ATLAS detector at the LHC". In: *Phys.Lett.B* 716 (2012), pp. 1–29. DOI: 10.1016/j.physletb.2012.08.020. arXiv: 1207.7214 [hep-ex].

[5] Peter W. Higgs. "Broken Symmetries and the Masses of Gauge Bosons". In: *Phys. Rev. Lett.* 13 (1964). Ed. by J. C. Taylor, pp. 508–509. DOI: 10.1103/PhysRevLett.13.508.

[6] F. Englert and R. Brout. "Broken Symmetry and the Mass of Gauge Vector Mesons". In: *Phys. Rev. Lett.* 13 (1964). Ed. by J. C. Taylor, pp. 321–323. DOI: 10.1103/PhysRevLett.13.321.

[7] Nikita Blinov and Anson Hook. "Solving the Wrong Hierarchy Problem". In: *JHEP* 06 (2016), p. 176. DOI: 10.1007/JHEP06(2016)176. arXiv: 1605.03178 [hep-ph].

[8] Jaco de Swart, Gianfranco Bertone, and Jeroen van Dongen. "How Dark Matter Came to Matter". In: *Nature Astron.* 1 (2017), p. 0059. DOI: 10.1038/s41550017-0059. arXiv: 1703.00013 [astro-ph.CO].

[9] Carlo Rovelli. *Quantum gravity*. Cambridge university press, 2004.

[10] Paul Langacker. *The standard model and beyond*. Taylor & Francis, 2017.

[11] O. Bruning, H. Burkhardt, and S. Myers. "The Large Hadron Collider". In: *Prog. Part. Nucl. Phys.* 67 (2012), pp. 705–734. DOI: 10.1016/j.ppnp.2012.03.001.

[12] Evgeny K. Akhmedov. "Neutrino physics". In: *ICTP Summer School in Particle Physics*. June 1999, pp. 103–164. arXiv: hep-ph/0001264.

[13] R. D. Blandford and R. Narayan. "Cosmological applications of gravitational lensing". In: *Ann. Rev. Astron. Astrophys.* 30 (1992), pp. 311–358. DOI: 10.1146/annurev.aa.30.090192.001523.

[14] David Griffiths. *Introduction to elementary particles*. John Wiley & Sons, 2020.

[15] R. Assmann, M. Lamont, and S. Myers. "A brief history of the LEP collider". In: *Nucl. Phys. B Proc. Suppl.* 109 (2002). Ed. by F. L. Navarria, M. Paganoni, and P. G. Pelfer, pp. 17–31. DOI: 10.1016/S0920-5632(02)90005-8.

[16] Mingyi Dong et al. "CEPC Conceptual Design Report: Volume 2 - Physics & Detector". In: (Nov. 2018). Ed. by João Barreiro Guimarães da Costa et al. arXiv: 1811.10545 [hep-ex].

[17] Fenfen An et al. "Precision Higgs physics at the CEPC". In: *Chin. Phys. C* 43.4 (2019), p. 043002. DOI: 10.1088/1674-1137/43/4/043002. arXiv: 1810.09037 [hep-ex].

[18] Christopher T. Hill and Elizabeth H. Simmons. "Strong Dynamics and Electroweak Symmetry Breaking". In: *Phys. Rept.* 381 (2003). [Erratum: Phys.Rept. 390, 553–554 (2004)], pp. 235–402. DOI: 10.1016/S0370-1573(03)00140-6. arXiv: hep-ph/0203079.

[19] Stephen P. Martin. "A Supersymmetry primer". In: *Adv. Ser. Direct. High Energy Phys.* 18 (1998). Ed. by Gordon L. Kane, pp. 1–98. DOI: 10.1142/9789812839657_0001. arXiv: hep-ph/9709356.

[20] Anne M. Green. "Determining the WIMP mass using direct detection experiments". In: *JCAP* 08 (2007), p. 022. DOI: 10.1088/1475-7516/2007/08/022. arXiv: hep-ph/0703217.

[21] Csaba Csaki. "The Minimal supersymmetric standard model (MSSM)". In: *Mod. Phys. Lett. A* 11 (1996), p. 599. DOI: 10.1142/S021773239600062X. arXiv: hep-ph/9606414.

[22] Edward W. Kolb and Michael S. Turner. "Grand Unified Theories and the Origin of the Baryon Asymmetry". In: *Ann. Rev. Nucl. Part. Sci.* 33 (1983), pp. 645–696. DOI: 10.1146/annurev.ns.33.120183.003241.

[23] D. S. Gorbunov, G. G. Raffelt, and D. V. Semikoz. "Axion - like particles as ultrahigh-energy cosmic rays?" In: *Phys. Rev. D* 64 (2001), p. 096005. DOI: 10.1103/PhysRevD.64.096005. arXiv: hep-ph/0103175.

[24] Danielle Sabatta et al. "Connecting muon anomalous magnetic moment and multi-lepton anomalies at LHC". In: *Chin. Phys. C* 44.6 (2020). DOI: 10.1088/1674-1137/44/6/063103. arXiv: 1909.03969 [hep-ph].

[25] T. Aaltonen et al. "Precision Top-Quark Mass Measurements at CDF". In: *Phys. Rev. Lett.* 109 (2012), p. 152003. DOI: 10.1103/PhysRevLett.109.152003. arXiv: 1207.6758 [hep-ex].

[26] G. Abbiendi et al. "Measurement of the mass and width of the W boson". In: *Eur. Phys. J. C* 45 (2006), pp. 307–335. DOI: 10.1140/epjc/s2005-02440-5. arXiv: hep-ex/0508060.

[27] P. Aarnio et al. "Measurement of the Mass and Width of the Z^0 Particle from Multi - Hadronic Final States Produced in e^+e^- Annihilations". In: *Phys. Lett. B* 231 (1989), pp. 539–547. DOI: 10.1016/0370-2693(89)90706-5.

[28] Nima Arkani-Hamed et al. "Selfbreaking of the standard model gauge symmetry". In: *Phys. Rev. D* 62 (2000), p. 096006. DOI: 10.1103/PhysRevD.62.096006. arXiv: hep-ph/0006238.

[29] O. W. Greenberg. "The Color charge degree of freedom in particle physics". In: May 2008. arXiv: 0805.0289 [physics.hist-ph].

[30] O. Pooley. "Handedness, parity violation, and the reality of space". In: (2003). Ed. by Katherine Brading and Elena Castellani, pp. 250–280.

[31] D. B. Fairlie. "Two Consistent Calculations of the Weinberg Angle". In: *J. Phys. G* 5 (1979), p. L55. DOI: 10.1088/0305-4616/5/4/002.

[32] ShaoXu Ren et al. "The Origins of Bosons and Fermions". In: *Journal of Modern Physics* 5.17 (2014), pp. 1848–1879.

[33] Institute of Particle Physics and Accelerator Technologies. *Standard Model*. URL: https://www.rtu.lv/en/hep/particle-physics/standard-model.

[34] Deepak Kar. *Experimental particle physics: understanding the measurements and searches at the Large Hadron Collider*. IOP Publishing, 2019.

[35] R. L. Workman et al. "Review of Particle Physics". In: *PTEP* 2022 (2022), p. 083C01. DOI: 10.1093/ptep/ptac097.

[36] Pavel Fileviez Perez and Mark B. Wise. "On the Origin of Neutrino Masses". In: *Phys. Rev. D* 80 (2009), p. 053006. DOI: 10.1103/PhysRevD.80.053006. arXiv: 0906.2950 [hep-ph].

[37] O. W. Greenberg. "The origin of quark color". In: *Phys. Today* 68.1 (2015), pp. 33–37. DOI: 10.1063/pt.3.2655.

[38] R. P. Feynman and Steven Weinberg. *ELEMENTARY PARTICLES AND THE LAWS OF PHYSICS. THE 1986 DIRAC MEMORIAL LECTURES*. Cambridge University Press, Sept. 1999. ISBN: 978-0-521-65862-1, 978-0-511-25165-8.

[39] Joseph John Thomson. *Cathode rays*. 4. Academic Reprints, 1897.

[40] Carl D Anderson. "The positive electron". In: *Physical Review* 43.6 (1933), p. 491.

[41] J. Beringer et al. "Review of Particle Physics (RPP)". In: *Phys. Rev. D* 86 (2012), p. 010001. DOI: 10.1103/PhysRevD.86.010001.

[42] John Ellis, Mary K Gaillard, and Dimitri V Nanopoulos. "A historical profile of the Higgs boson". In: *The standard theory of particle physics* (2016), pp. 255–274.

[43] Simone Marzani et al. "Higgs production via gluon-gluon fusion with finite top mass beyond next-to-leading order". In: *Nucl. Phys. B* 800 (2008), pp. 127–145. DOI: 10.1016/j.nuclphysb.2008.03.016. arXiv: 0801.2544 [hep-ph].

[44] Paolo Bolzoni et al. "Higgs production via vector-boson fusion at NNLO in QCD". In: *Phys. Rev. Lett.* 105 (2010), p. 011801. DOI: 10.1103/PhysRevLett.105.011801. arXiv: 1003.4451 [hep-ph].

[45] Heribertus B. Hartanto et al. "Higgs boson production in association with top quarks in the POWHEG BOX". In: *Phys. Rev. D* 91.9 (2015), p. 094003. DOI: 10.1103/PhysRevD.91.094003. arXiv: 1501.04498 [hep-ph].

[46] M. Y. Hussein. "Higgs Boson Production at the LHC". In: (Mar. 2017). arXiv: 1703.03952 [hep-ph].

[47] Margarete Muhlleitner et al. "The N2HDM under Theoretical and Experimental Scrutiny". In: *JHEP* 03 (2017), p. 094. DOI: 10.1007/JHEP03(2017)094. arXiv: 1612.01309 [hep-ph].

[48] Igor P Ivanov. "Building and testing models with extended Higgs sectors". In: *Progress in Particle and Nuclear Physics* 95 (2017).

[49] Stefan von Buddenbrock et al. "The compatibility of LHC Run 1 data with a heavy scalar of mass around 270 GeV". In: (June 2015). arXiv: 1506.00612 [hep-ph].

[50] Stefan von Buddenbrock et al. "Phenomenological signatures of additional scalar bosons at the LHC". In: *Eur. Phys. J. C* 76.10 (2016), p. 580. DOI: 10.1140/epjc/s10052-016-4435-8. arXiv: 1606.01674 [hep-ph].

[51] Stefan von Buddenbrock et al. "The Madala hypothesis with Run 1 and 2 data at the LHC". In: *J. Phys. Conf. Ser.* 889.1 (2017), p. 012020. DOI: 10.1088/1742-6596/889/1/012020. arXiv: 1709.09419 [hep-ph].

[52] Stefan von Buddenbrock et al. "Multi-lepton signatures of additional scalar bosons beyond the Standard Model at the LHC". In: *J. Phys. G* 45.11 (2018), p. 115003. DOI: 10.1088/1361-6471/aae3d6. arXiv: 1711.07874 [hep-ph].

[53] Stefan von Buddenbrock et al. "Constraints on a 2HDM with a singlet scalar and implications in the search for heavy bosons at the LHC". In: *J. Phys. G* 46.11 (2019), p. 115001. DOI: 10.1088/1361-6471/ab3cf6. arXiv: 1809.06344 [hep-ph].

[54] Stefan Buddenbrock et al. "The emergence of multi-lepton anomalies at the LHC and their compatibility with new physics at the EW scale". In: *JHEP* 10 (2019), p. 157. DOI: 10.1007/JHEP10(2019)157. arXiv: 1901.05300 [hep-ph].

[55] Yesenia Hernandez et al. "The anomalous production of multi-lepton and its impact on the measurement of Wh production at the LHC". In: *Eur. Phys. J. C* 81.4 (2021), p. 365. DOI: 10.1140/epjc/s10052-021-09137-1. arXiv: 1912.00699 [hep-ph].

[56] Stefan von Buddenbrock, Richard Ruiz, and Bruce Mellado. "Anatomy of inclusive $t\bar{t}W$ production at hadron colliders". In: *Phys. Lett. B* 811 (2020), p. 135964. DOI: 10.1016/j.physletb.2020.135964. arXiv: 2009.00032 [hep-ph].

[57] Andreas Crivellin et al. "Accumulating evidence for the associated production of a new Higgs boson at the LHC". In: *Phys. Rev. D* (). DOI: 10.1103/PhysRevD.108.115031. arXiv: 2109.02650 [hep-ph].

[58] Srimoy Bhattacharya et al. "Growing Excesses of New Scalars at the Electroweak Scale". In: (June 2023). arXiv: 2306.17209 [hep-ph].

[59] Guglielmo Coloretti et al. "Searching for low-mass resonances decaying into W bosons". In: *Phys. Rev. D* 108.3 (2023), p. 035026. DOI: 10.1103/PhysRevD.108.035026. arXiv: 2302.07276 [hep-ph].

[60] Sumit Banik et al. "Uncovering New Higgses in the LHC Analyses of Differential $t\bar{t}$ Cross Sections". In: (Aug. 2023). arXiv: 2308.07953 [hep-ph].

[61] Oliver Fischer et al. "Unveiling hidden physics at the LHC". In: *Eur. Phys. J. C* 82.8 (2022), p. 665. DOI: 10.1140/epjc/s10052-022-10541-4. arXiv: 2109.06065 [hep-ph].

[62] Georges Aad et al. "Inclusive and differential cross-sections for dilepton $t\bar{t}$ production measured in $\sqrt{s} = 13$ TeV pp collisions with the ATLAS detector". In: *JHEP* 07 (2023), p. 141. DOI: 10.1007/JHEP07(2023)141. arXiv: 2303.15340 [hep-ex].

[63] "Measurement of Higgs boson production in association with a W or Z boson in the H $\rightarrow$ WW decay channel". In: (2021).

[64] G. Aad et al. "Observation of WWW Production in pp Collisions at $\sqrt{s}$ =13 TeV with the ATLAS Detector". In: *Phys. Rev. Lett.* 129.6 (2022), p. 061803. DOI: 10.1103/PhysRevLett.129.061803. arXiv: 2201.13045 [hep-ex].

[65] Morad Aaboud et al. "Measurement of fiducial and differential W^+W^- production cross-sections at $\sqrt{s} = 13$ TeV with the ATLAS detector". In: *Eur.Phys.J.C* 79.10 (2019), p. 884. DOI: 10.1140/epjc/s10052-019-7371-6. arXiv: 1905.04242 [hep-ex].

[66] Georges Aad et al. "Observation of four-top-quark production in the multilepton final state with the ATLAS detector". In: *Eur. Phys. J. C* 83.6 (2023), p. 496. DOI: 10.1140/epjc/s10052-023-11573-0. arXiv: 2303.15061 [hep-ex].

[67] Aram Hayrapetyan et al. "Observation of four top quark production in proton-proton collisions at $\sqrt{s} = 13$TeV". In: *Phys. Lett. B* 847 (2023), p. 138290. DOI: 10.1016/j.physletb.2023.138290. arXiv: 2305.13439 [hep-ex].

[68] Armen Tumasyan et al. "Measurements of the Higgs boson production cross section and couplings in the W boson pair decay channel in proton-proton collisions at $\sqrt{s} = 13$ TeV". In: *Eur. Phys. J. C* 83.7 (2023), p. 667. DOI: 10.1140/epjc/s10052-023-11632-6. arXiv: 2206.09466 [hep-ex].

[69] Andreas Crivellin and Bruce Mellado. "Anomalies in Particle Physics". In: (Sept. 2023). arXiv: 2309.03870 [hep-ph].

[70] The LEP Working Group for Higgs et al. "Search for the standard model Higgs boson at LEP". In: *Physics Letters B* 565 (2003), pp. 61–75.

[71] Albert M Sirunyan et al. "Search for a standard model-like Higgs boson in the mass range between 70 and 110 GeV in the diphoton final state in proton-proton collisions at $\sqrt{s} = 8$ and 13 TeV". In: *Phys. Lett. B* 793 (2019), pp. 320–347. DOI: 10.1016/j.physletb.2019.03.064. arXiv: 1811.08459 [hep-ex].

[72] "Search for a standard model-like Higgs boson in the mass range between 70 and 110 GeV in the diphoton final state in proton-proton collisions at $\sqrt{s} = 13$ TeV". In: (2023).

[73] "Search for diphoton resonances in the 66 to 110 GeV mass range using 140 fb^{-1} of 13 TeV pp collisions collected with the ATLAS detector". In: (2023).

[74] Ronald Fisher. "Statistical methods and scientific induction". In: *Journal of the Royal Statistical Society Series B: Statistical Methodology* 17.1 (1955), pp. 69–78.

[75] Saiyad Ashanujjaman et al. "$SU(2)_L$ triplet scalar as the origin of the 95 GeV excess?" In: *Phys. Rev. D* 108.9 (2023), p. L091704. DOI: 10.1103/PhysRevD.108.L091704. arXiv: 2306.15722 [hep-ph].

[76] Vanda Silveira and A Zee. "Scalar phantoms". In: *Physics Letters B* 161.1-3 (1985), pp. 136–140.

[77] John McDonald. "Gauge singlet scalars as cold dark matter". In: *PRD* 50.6 (1994), p. 3637.

[78] CMS collaboration et al. "Searches for additional Higgs bosons and for vector leptoquarks in $\tau\tau$ final states in proton-proton collisions at $\sqrt{s} = 13$ TeV". In: *arXiv preprint arXiv:2208.02717* (2022).

[79] CMS collaboration et al. "Measurements of the Higgs boson production cross section and couplings in the W boson pair decay channel in proton-proton collisions at $\sqrt{s} = 13$ TeV". In: *arXiv:2206.09466* (2022).

[80] Junjie Cao et al. "Diphoton signal of the light Higgs boson in natural NMSSM". In: *Physical Review D* (2017).

[81] Ulrich Haisch and Augustinas Malinauskas. "Let there be light from a second light Higgs doublet". In: *Journal of High Energy Physics* 2018.3 (2018), pp. 1–24.

[82] Kaoru Hagiwara et al. "Review of particle physics. Particle Data Group". In: *Phys. Rev. D* 66 (2002), p. 010001. DOI: 10.1103/PhysRevD.66.010001.

[83] J. de Blas et al. "Impact of the Recent Measurements of the Top-Quark and W-Boson Masses on Electroweak Precision Fits". In: *Phys. Rev. Lett.* 129.27 (2022), p. 271801. DOI: 10.1103/PhysRevLett.129.271801. arXiv: 2204.04204 [hep-ph].

[84] Emanuele Bagnaschi et al. "SMEFT analysis of m_W". In: *JHEP* 08 (2022), p. 308. DOI: 10.1007/JHEP08(2022)308. arXiv: 2204.05260 [hep-ph].

[85] T. Aaltonen et al. "High-precision measurement of the W boson mass with the CDF II detector". In: *Science* 376.6589 (2022), pp. 170–176. DOI: 10.1126/science.abk1781.

[86] M Chabab, MC Peyranère, and L Rahili. "Probing the Higgs sector of Y= 0 Y= 0 Higgs triplet model at LHC". In: *The Eur. Phys. J. C* 78 (2018), pp. 1–16.

[87] M. Chabab, M. C. Peyranère, and L. Rahili. "Probing the Higgs sector of $Y = 0$ Higgs Triplet Model at LHC". In: *Eur. Phys. J. C* 78.10 (2018), p. 873. DOI: 10.1140/epjc/s10052-018-6339-2. arXiv: 1805.00286 [hep-ph].

[88] Nicole F. Bell et al. "Two-Step Electroweak Symmetry-Breaking: Theory Meets Experiment". In: *JHEP* 05 (2020), p. 050. DOI: 10.1007/JHEP05(2020)050. arXiv: 2001.05335 [hep-ph].

[89] Albert M Sirunyan et al. "Measurements of Higgs boson production cross sections and couplings in the diphoton decay channel at $\sqrt{s}$ = 13 TeV". In: *JHEP* 07 (2021), p. 027. DOI: 10.1007/JHEP07(2021)027. arXiv: 2103.06956 [hep-ex].

[90] Georges Aad et al. "Measurement of the properties of Higgs boson production at $\sqrt{s} = 13$ TeV in the $H \to \gamma\gamma$ channel using 139 fb^{-1} of pp collision data with the ATLAS experiment". In: *JHEP* 07 (2023), p. 088. DOI: 10.1007/JHEP07(2023)088. arXiv: 2207.00348 [hep-ex].

[91] "A portrait of the Higgs boson by the CMS experiment ten years after the discovery". In: *Nature* 607.7917 (2022), pp. 60–68.

[92] Georges Aad et al. "Higgs boson production cross-section measurements and their EFT interpretation in the 4ℓ decay channel at $\sqrt{s}$ =13 TeV with the ATLAS detector". In: *Eur. Phys. J. C* 80.10 (2020), p. 957. DOI: 10.1140/epjc/s10052-020-8227-9. arXiv: 2004.03447 [hep-ex].

[93] Stefan Dittmaier et al. "Handbook of LHC Higgs cross sections: 2. Differential distributions". In: *arXiv preprint arXiv:1201.3084* (2012).

[94] Dirk Graudenz, Michael Spira, and Peter M Zerwas. "QCD corrections to Higgs-boson production at proton-proton colliders". In: *Phys.Rev.L* ().

[95] M. Spira et al. "Higgs boson production at the LHC". In: *Nucl. Phys. B* 453 (1995), pp. 17–82. DOI: 10.1016/0550-3213(95)00379-7. arXiv: hep-ph/9504378.

[96] Robert V Harlander and William B Kilgore. "Next-to-next-to-leading order Higgs production at hadron colliders". In: *Phys.Rev.L* 88.20 (2002), p. 201801.

[97] CDF Collaboration†‡ et al. "High-precision measurement of the W boson mass with the CDF II detector". In: *Science* 376.6589 (2022), pp. 170–176.

[98] Michael E Peskin and Tatsu Takeuchi. "New constraint on a strongly interacting Higgs sector". In: *Phys.Rev.L* 65.8 (1990), p. 964.

[99] KS Kumar et al. "Low-energy measurements of the weak mixing angle". In: *Annual Rev. of Nuclear and Particle Science* 63 (2013), pp. 237–267.

[100] Henning Bahl et al. "HiggsTools: BSM scalar phenomenology with new versions of HiggsBounds and HiggsSignals". In: *Com. Phys. Commun.* (2023). DOI: 10.1016/j.cpc.2023.108803. arXiv: 2210.09332 [hep-ph].

[101] Robert V. Harlander, Stefan Liebler, and Hendrik Mantler. "SusHi: A program for the calculation of Higgs production in gluon fusion and bottom-quark annihilation in the Standard Model and the MSSM". In: *C.P.C.* 184 (2013), pp. 1605–1617. DOI: 10.1016/j.cpc.2013.02.006. arXiv: 1212.3249 [hep-ph].

[102] Robert V. Harlander, Stefan Liebler, and Hendrik Mantler. "SusHi Bento: Beyond NNLO and the heavy-top limit". In: *Comput. Phys. Commun.* 212 (2017), pp. 239–257. DOI: 10.1016/j.cpc.2016.10.015. arXiv: 1605.03190 [hep-ph].

[103] Philip Bechtle et al. "HiggsBounds-5: Testing Higgs Sectors in the LHC 13 TeV Era". In: *Eur. Phys. J. C* 80.12 (2020), p. 1211. DOI: 10.1140/epjc/s10052-020-08557-9. arXiv: 2006.06007 [hep-ph].

[104] Johannes Haller et al. "Update of the global electroweak fit and constraints on two-Higgs-doublet models". In: *Eur. Phys. J. C* 78.8 (2018), p. 675. DOI: 10.1140/epjc/s10052-018-6131-3. arXiv: 1803.01853 [hep-ph].

[105] Michael E Peskin and Tatsu Takeuchi. "Estimation of oblique electroweak corrections". In: *Physical Review D* 46.1 (1992), p. 381.

[106] W. Grimus et al. "The Oblique parameters in multi-Higgs-doublet models". In: *Nucl. Phys. B* 801 (2008), pp. 81–96. DOI: 10.1016/j.nuclphysb.2008.04.019. arXiv: 0802.4353 [hep-ph].

[107] T. Biekötter, S. Heinemeyer, and G. Weiglein. "The 95.4 GeV di-photon excess at ATLAS and CMS". In: (June 2023). arXiv: 2306.03889 [hep-ph].

[108] G. Abbiendi et al. "Decay mode independent searches for new scalar bosons with the OPAL detector at LEP". In: *Eur. Phys. J. C* 27 (2003), pp. 311–329. DOI: 10.1140/epjc/s2002-01115-1. arXiv: hep-ex/0206022.

[109] Chih-Ting Lu et al. "Electroweak precision fit and new physics in light of the W boson mass". In: *Phys. Rev. D* 106.3 (2022), p. 035034. DOI: 10.1103/PhysRevD.106.035034. arXiv: 2204.03796 [hep-ph].

[110] P. Achard et al. "Measurement of the mass and the width of the W boson at LEP". In: *Eur. Phys. J. C* 45 (2006), pp. 569–587. DOI: 10.1140/epjc/s2005-02459-6. arXiv: hep-ex/0511049.

[111] "Improved W boson Mass Measurement using 7 TeV Proton-Proton Collisions with the ATLAS Detector". In: (2023).

[112] G. W. Bennett et al. "Final Report of the Muon E821 Anomalous Magnetic Moment Measurement at BNL". In: *Phys. Rev. D* 73 (2006), p. 072003. DOI: 10.1103/PhysRevD.73.072003. arXiv: hep-ex/0602035.

[113] G. W. Bennett et al. "Measurement of the negative muon anomalous magnetic moment to 0.7 ppm". In: *Phys. Rev. Lett.* 92 (2004), p. 161802. DOI: 10.1103/PhysRevLett.92.161802. arXiv: hep-ex/0401008.

[114] H. N. Brown et al. "Precise measurement of the positive muon anomalous magnetic moment". In: *Phys. Rev. Lett.* 86 (2001), pp. 2227–2231. DOI: 10.1103/PhysRevLett.86.2227. arXiv: hep-ex/0102017.

[115] Fred Jegerlehner and Andreas Nyffeler. "The Muon g-2". In: *Phys. Rept.* 477 (2009), pp. 1–110. DOI: 10.1016/j.physrep.2009.04.003. arXiv: 0902.3360 [hep-ph].

[116] Kaoru Hagiwara et al. "$(g-2)_\mu$ and $\alpha(M_Z^2)$ re-evaluated using new precise data". In: *J. Phys. G* 38 (2011), p. 085003. DOI: 10.1088/0954-3899/38/8/085003. arXiv: 1105.3149 [hep-ph].

[117] Michel Davier et al. "Reevaluation of the Hadronic Contributions to the Muon g-2 and to alpha(MZ)". In: *Eur. Phys. J. C* 71 (2011), p. 1515. DOI: 10.1140/epjc/s10052-012-1874-8. arXiv: 1010.4180 [hep-ph].

[118] Thomas Blum et al. "The muon (g-2) theory value: present and future". In: *arXiv preprint arXiv:1311.2198* (2013).

[119] Ayres Freitas et al. "Testing the Muon g-2 Anomaly at the LHC". In: *JHEP* 05 (2014). [Erratum: JHEP 09, 155 (2014)]. DOI: 10.1007/JHEP09(2014)155. arXiv: 1402.7065 [hep-ph].

[120] Junjie Cao et al. "Diphoton signal of the light Higgs boson in natural NMSSM". In: *Phys. Rev. D* 95.11 (2017), p. 116001. DOI: 10.1103/PhysRevD.95.116001. arXiv: 1612.08522 [hep-ph].

[121] Andreas Crivellin, Julian Heeck, and Dario Müller. "Large $h \to bs$ in generic two-Higgs-doublet models". In: *Phys. Rev. D* 97.3 (2018), p. 035008. DOI: 10.1103/PhysRevD.97.035008. arXiv: 1710.04663 [hep-ph].

[122] Ulrich Haisch and Augustinas Malinauskas. "Let there be light from a second light Higgs doublet". In: *JHEP* 03 (2018), p. 135. DOI: 10.1007/JHEP03(2018)135. arXiv: 1712.06599 [hep-ph].

[123] Patrick J. Fox and Neal Weiner. "Light Signals from a Lighter Higgs". In: *JHEP* 08 (2018), p. 025. DOI: 10.1007/JHEP08(2018)025. arXiv: 1710.07649 [hep-ph].

[124] Da Liu et al. "A Light Higgs at the LHC and the B-Anomalies". In: *JHEP* 06 (2018), p. 150. DOI: 10.1007/JHEP06(2018)150. arXiv: 1805.01476 [hep-ph].

[125] Kun Wang et al. "The semi-constrained NMSSM in light of muon g-2, LHC, and dark matter constraints". In: *Chin. Phys. C* 42.10 (2018), pp. 103109–103109. DOI: 10.1088/1674-1137/42/10/103109. arXiv: 1811.04435 [hep-ph].

[126] T. Biekötter, M. Chakraborti, and S. Heinemeyer. "A 96 GeV Higgs boson in the N2HDM". In: *Eur. Phys. J. C* 80.1 (2020), p. 2. DOI: 10.1140/epjc/s10052-019-7561-2. arXiv: 1903.11661 [hep-ph].

[127] James M. Cline and Takashi Toma. "Pseudo-Goldstone dark matter confronts cosmic ray and collider anomalies". In: *Phys. Rev. D* 100.3 (2019), p. 035023. DOI: 10.1103/PhysRevD.100.035023. arXiv: 1906.02175 [hep-ph].

[128] Kiwoon Choi et al. "Light Higgs bosons in the general NMSSM". In: *Eur. Phys. J. C* 79.11 (2019), p. 956. DOI: 10.1140/epjc/s10052-019-7473-1. arXiv: 1906.03389 [hep-ph].

[129] Anirban Kundu, Suvam Maharana, and Poulami Mondal. "A 96 GeV scalar tagged to dark matter models". In: *Nucl. Phys. B* 955 (2020), p. 115057. DOI: 10.1016/j.nuclphysb.2020.115057. arXiv: 1907.12808 [hep-ph].

[130] Junjie Cao et al. "96 GeV diphoton excess in seesaw extensions of the natural NMSSM". In: *Phys. Rev. D* 101.5 (2020), p. 055008. DOI: 10.1103/PhysRevD.101.055008. arXiv: 1908.07206 [hep-ph].

[131] T. Biekötter, M. Chakraborti, and S. Heinemeyer. "The "96 GeV excess" at the LHC". In: *Int. J. Mod. Phys. A* 36.22 (2021), p. 2142018. DOI: 10.1142/S0217751X21420185. arXiv: 2003.05422 [hep-ph].

[132] Ahmed Ali Abdelalim et al. "Di-photon decay of a light Higgs state in the BLSSM". In: *Nucl. Phys. B* 985 (2022), p. 116013. DOI: 10.1016/j.nuclphysb.2022.116013. arXiv: 2012.04952 [hep-ph].

[133] S. Heinemeyer et al. "Phenomenology of a 96 GeV Higgs boson in the 2HDM with an additional singlet". In: *Phys. Rev. D* 106.7 (2022), p. 075003. DOI: 10.1103/PhysRevD.106.075003. arXiv: 2112.11958 [hep-ph].

[134] Thomas Biekötter, Sven Heinemeyer, and Georg Weiglein. "Mounting evidence for a 95 GeV Higgs boson". In: *JHEP* 08 (2022), p. 201. DOI: 10.1007/JHEP08(2022)201. arXiv: 2203.13180 [hep-ph].

[135] Syuhei Iguro, Teppei Kitahara, and Yuji Omura. "Scrutinizing the 95–100 GeV di-tau excess in the top associated process". In: *Eur. Phys. J. C* 82.11 (2022), p. 1053. DOI: 10.1140/epjc/s10052-022-11028-y. arXiv: 2205.03187 [hep-ph].

[136] Amine Ahriche et al. "The scale invariant scotogenic model: CDF-II *W*-boson mass and the 95~GeV excesses". In: (Nov. 2023). arXiv: 2311.08297 [hep-ph].

[137] "The International Linear Collider Technical Design Report-Volume 2:Physics". In: (June 2013). Ed. by Howard Baer et al. arXiv: 1306.6352 [hep-ph].

[138] "The International Linear Collider Technical Design Report - Volume 3.I: Accelerator & in the Technical Design Phase". In: (June 2013). Ed. by Chris Adolphsen et al. arXiv: 1306.6353 [physics.acc-ph].

[139] T. K. Charles et al. "The Compact Linear Collider (CLIC) - 2018 Summary Report". In: (). Ed. by P. N. Burrows et al. DOI: 10.23731/CYRM-2018-002. arXiv: 1812.06018 [physics.acc-ph].

[140] A. Abada et al. "FCC Physics Opportunities: Future Circular Collider Conceptual Design Report Volume 1". In: *Eur. Phys. J. C* 79.6 (2019), p. 474. DOI: 10.1140/epjc/s10052-019-6904-3.

[141] A. Abada et al. "FCC-ee: The Lepton Collider: Future Circular Collider Conceptual Design Report Volume 2". In: *Eur. Phys. J. ST* 228.2 (2019). DOI: 10.1140/epjst/e2019-900045-4.

[142] Zhenxing Chen et al. "Cross Section and Higgs Mass Measurement with Higgsstrahlung at the CEPC". In: *Chin. Phys. C* 41.2 (2017), p. 023003. DOI: 10.1088/1674-1137/41/2/023003. arXiv: 1601.05352 [hep-ex].

[143] Yilang Shao. "CEPC's Features and Expectation for the Future". In: *J. Phys.: Conf. Ser.* 2005.1 (Aug. 2021), p. 012025. DOI: 10.1088/1742-6596/2005/1/012025. URL: https://dx.doi.org/10.1088/1742-6596/2005/1/012025.

[144] MANQI RUAN. "The Circular Electron Positron Collider (CEPC) Project: The Physics Reach and Reference Detector Design." In: *AAPPS Bulletin* 27.6 (2017).

[145] H. Abramowicz et al. "Higgs physics at the CLIC electron–positron linear collider". In: *Eur. Phys. J. C* 77.7 (2017), p. 475. DOI: 10.1140/epjc/s10052-017-4968-5. arXiv: 1608.07538 [hep-ex].

[146] H. Abramowicz et al. "Top-Quark Physics at the CLIC Electron-Positron Linear Collider". In: *JHEP* 11 (2019), p. 003. DOI: 10.1007/JHEP11(2019)003. arXiv: 1807.02441 [hep-ex].

[147] Michael Benedikt et al. "Future Circular Colliders succeeding the LHC". In: *Nature Phys.* 16.4 (2020), pp. 402–407. DOI: 10.1038/s41567-020-0856-2.

[148] Philip Bambade et al. "The International Linear Collider: A Global Project". In: (Mar. 2019). arXiv: 1903.01629 [hep-ex].

[149] Barry Barish and James E Brau. "The international linear collider". In: *International Journal of Modern Physics A* 28.27 (2013), p. 1330039.

[150] T. Barklow et al. "ILC Operating Scenarios". In: (June 2015). arXiv: 1506.07830 [hep-ex].

[151] OPAL collaboration and G Abbiendi. "Decay-mode independent searches for new scalar bosons with the OPAL detector at LEP". In: *The Eur. Phys. J. C* 27.3 (2003), pp. 311–329.

[152] M. Krause and M. Mühlleitner. "ewN2HDECAY - A program for the Calculation of Electroweak One-Loop Corrections to Higgs Decays in the Next-to-Minimal Two-Higgs-Doublet Model Including State-of-the-Art QCD Corrections". In: (Apr. 2019). DOI: 10.1016/j.cpc.2019.106924. arXiv: 1904.02103 [hep-ph].

[153] H. Abramowicz et al. "Physics at the CLIC e+e- Linear Collider – Input to the Snowmass process 2013". In: *Snowmass 2013: Snowmass on the Mississippi*. July 2013. arXiv: 1307.5288 [hep-ex].

[154] Susanna Guatelli et al. "Introduction to the Geant4 Simulation toolkit". In: *AIP Conference Proceedings*. Vol. 1345. 1. American Institute of Physics. 2011, pp. 303–322.

[155] J. Allison et al. "Recent developments in Geant4". In: *Nucl. Instrum. Meth. A* 835 (2016), pp. 186–225. DOI: 10.1016/j.nima.2016.06.125.

[156] "Physics and Detectors at CLIC: CLIC Conceptual Design Report". In: (Feb. 2012). Ed. by Lucie Linssen et al. DOI: 10.5170/CERN-2012-003. arXiv: 1202.5940 [physics.ins-det].

[157] P. Lebrun et al. "The CLIC Programme: Towards a Staged e+e- Linear Collider Exploring the Terascale : CLIC Conceptual Design Report". In: (Sept. 2012). DOI: 10.5170/CERN-2012-005. arXiv: 1209.2543 [physics.ins-det].

[158] Fenfen An et al. "Precision Higgs physics at the CEPC". In: *Chinese Physics C* 43.4 (2019), p. 043002.

[159] Yaquan Fang and Shuiting Xin. "Physics Highlights at CEPC". In: *Nuclear and Particle Physics Proceedings* 330 (2023), pp. 15–19.

[160] Rita Coimbra, Marco O. P. Sampaio, and Rui Santos. "ScannerS: Constraining the phase diagram of a complex scalar singlet at the LHC". In: *Eur. Phys. J. C* 73 (2013), p. 2428. DOI: 10.1140/epjc/s10052-013-2428-4. arXiv: 1301.2599 [hep-ph].

[161] William J. Marciano, G. Valencia, and S. Willenbrock. "Renormalization Group Improved Unitarity Bounds on the Higgs Boson and Top Quark Masses". In: *Phys. Rev. D* 40 (1989), p. 1725. DOI: 10.1103/PhysRevD.40.1725.

[162] Mark D. Goodsell and Florian Staub. "Unitarity constraints on general scalar couplings with SARAH". In: *Eur. Phys. J. C* 78.8 (2018), p. 649. DOI: 10.1140/epjc/s10052-018-6127-z. arXiv: 1805.07306 [hep-ph].

[163] Mark D. Goodsell and Florian Staub. "Improved unitarity constraints in Two-Higgs-Doublet-Models". In: *Phys. Lett. B* 788 (2019), pp. 206–212. DOI: 10.1016/j.physletb.2018.11.030. arXiv: 1805.07310 [hep-ph].

[164] Manuel E. Krauss and Florian Staub. "Unitarity constraints in triplet extensions beyond the large s limit". In: *Phys. Rev. D* 98.1 (2018), p. 015041. DOI: 10.1103/PhysRevD.98.015041. arXiv: 1805.07309 [hep-ph].

[165] Wolfgang G. Hollik, Georg Weiglein, and Jonas Wittbrodt. "Impact of Vacuum Stability Constraints on the Phenomenology of Supersymmetric Models". In: *JHEP* 03 (2019), p. 109. DOI: 10.1007/JHEP03(2019)109. arXiv: 1812.04644 [hep-ph].

[166] W. Grimus et al. "A Precision constraint on multi-Higgs-doublet models". In: *J. Phys. G* 35 (2008), p. 075001. DOI: 10.1088/0954-3899/35/7/075001. arXiv: 0711.4022 [hep-ph].

[167] Andrzej J. Buras et al. "Higgs-mediated FCNCs: Natural Flavour Conservation vs. Minimal Flavour Violation". In: *JHEP* 10 (2010), p. 009. DOI: 10.1007/JHEP10(2010)009. arXiv: 1005.5310 [hep-ph].

[168] Georges Aad et al. "Measurements of Higgs boson production and couplings in diboson final states with the ATLAS detector at the LHC". In: *Phys. Lett. B* (). DOI: 10.1016/j.physletb.2014.05.011. arXiv: 1307.1427 [hep-ex].

[169] J. M. Butterworth et al. "THE TOOLS AND MONTE CARLO WORKING GROUP Summary Report from the Les Houches 2009 Workshop on TeV Colliders". In: arXiv: 1003.1643 [hep-ph].

[170] Isabell Engeln, Margarete Mühlleitner, and Jonas Wittbrodt. "N2HDECAY: Higgs Boson Decays in the Different Phases of the N2HDM". In: *C.P.C.* 234 (2019), pp. 256–262. DOI: 10.1016/j.cpc.2018.07.020. arXiv: 1805.00966 [hep-ph].

[171] Johan Alwall et al. "MadGraph 5 : Going Beyond". In: *JHEP* 06 (2011), p. 128. DOI: 10.1007/JHEP06(2011)128. arXiv: 1106.0522 [hep-ph].

[172] Christian Bierlich et al. "A comprehensive guide to the physics and usage of PYTHIA 8.3". In: *SciPost Phys. Codeb.* 2022 (2022), p. 8. DOI: 10.21468/SciPostPhysCodeb.8. arXiv: 2203.11601 [hep-ph].

[173] J. de Favereau et al. "DELPHES 3, A modular framework for fast simulation of a generic collider experiment". In: *JHEP* 02 (2014), p. 057. DOI: 10.1007/JHEP02(2014)057. arXiv: 1307.6346 [hep-ex].

[174] Cheng Chen et al. "Fast simulation of the CEPC detector with Delphes". In: (Dec. 2017). arXiv: 1712.09517 [hep-ex].

[175] Waleed Abdallah et al. "CEPC Technical Design Report – Accelerator (v2)". In: (Dec. 2023). arXiv: 2312.14363 [physics.acc-ph].

[176] Matteo Cacciari, Gavin P. Salam, and Gregory Soyez. "FastJet User Manual". In: *Eur. Phys. J. C* 72 (2012), p. 1896. DOI: 10.1140/epjc/s10052-012-1896-2. arXiv: 1111.6097 [hep-ph].

[177] Matteo Cacciari, Gavin P. Salam, and Gregory Soyez. "The anti-k_t jet clustering algorithm". In: *JHEP* 04 (2008), p. 063. DOI: 10.1088/1126-6708/2008/04/063. arXiv: 0802.1189 [hep-ph].

[178] Weights Biases. *Weights Biases*. URL: https://wandb.ai/site.